



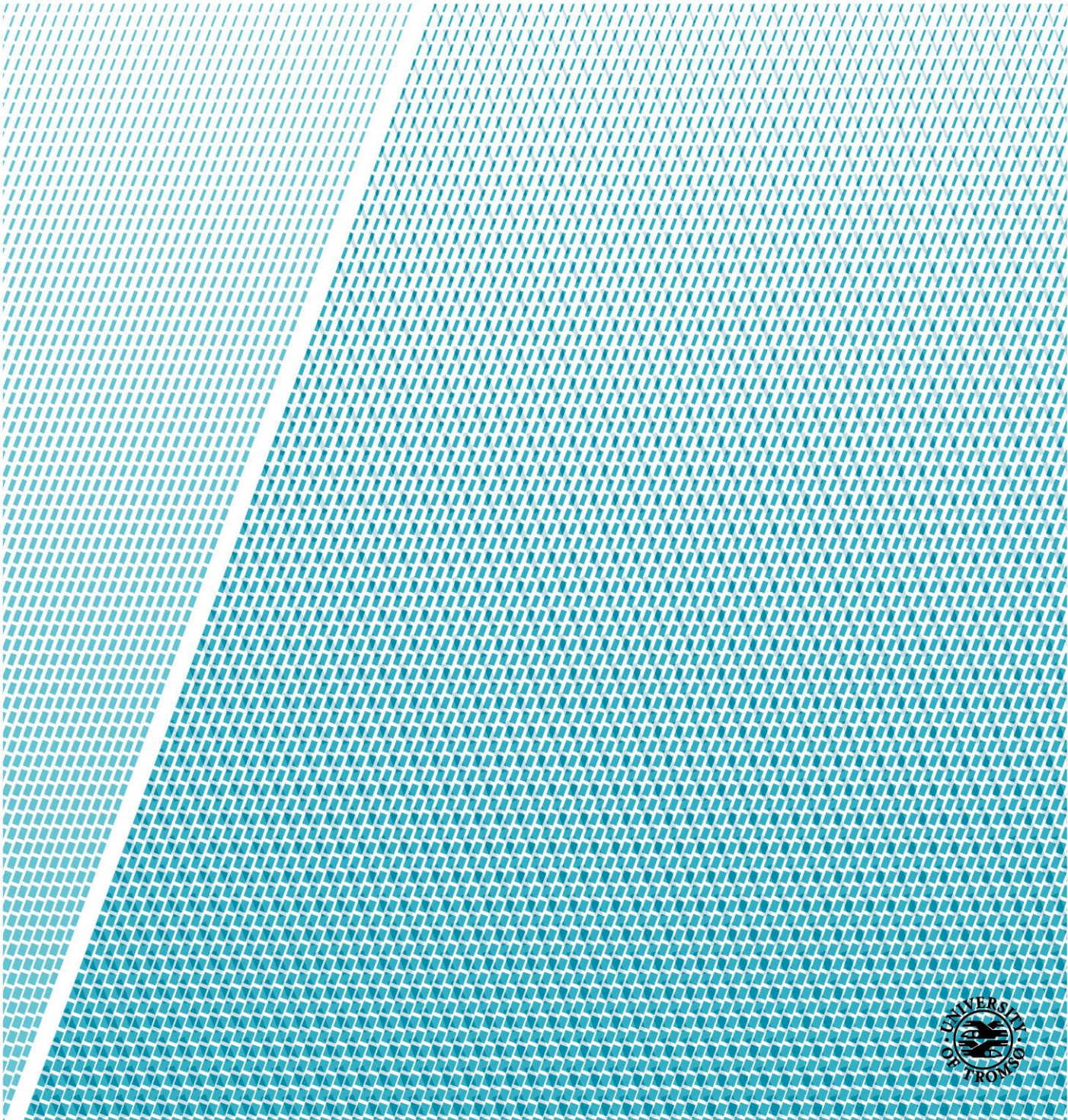
**UiT**

**THE ARCTIC  
UNIVERSITY  
OF NORWAY**

Faculty of Science and Technology  
Department of Geosciences

# **The Late Paleozoic development of the Ottar basin from seismic 3D interpretation**

—  
**Sigurd A. Tonstad**  
*Master's thesis in Geology, GEO-3900*  
*May 2018*







## Abstract

The Late Paleozoic sedimentary environments of the Ottar basin in the SW Barents Sea was studied using five 3D seismic surveys. By the use of seismic stratigraphic analysis and correlation to wells located in close proximity to the study area, the Paleozoic succession has been subdivided into 4 main units: Billefjorden Group (Late Devonian – Mid Carboniferous), Gipsdalen Group (Mid Carboniferous – Early Permian), Bjarmeland Group (Early Permian), Tempelfjorden Group (Mid- to Late Permian) and one from the Triassic: the Havert Formation (Early Triassic). All five groups have been described and discussed with emphasis on their appearance and internal seismic facies with the purpose of recreating the sedimentary processes and the paleoenvironment at time of their deposition.

The Paleozoic represents a period of large scale tectonics influencing the regional environment and depositional patterns. The five defined units are heavily influenced by multiple regression- and transgression events, as well as temperature fluctuations. The cyclic shifts in environmental conditions resulted in a transition from siliciclastic deposition, to large scale evaporite precipitation and continued carbonate production before a transgression shifted the depositional trends towards spiculites, shales and suspension material by the Late Permian – Early Triassic. The Early Triassic signified the development of the stable Bjarmeland Platform.

The study area comprises two salt pillows, named the Norvarg- and Samson Dome, that have a conformable Paleozoic succession acting as a folded seal. The evolution of the two domes display the differences in tectonic development of the study area compared to the surrounding evaporite basins (e.g. Nordkapp- and Maud Basin). Due to a later tectonic activation and a rigid overburden, the Norvarg- and Samson Dome developed as salt pillows, as the evaporite bodies failed to penetrate the overburden, reaching the final stage of diapir evolution. This has resulted in a succession that is not influenced by diapirs and large-scale tectonic events within the Ottar basin.





## Acknowledgement

Da var det tid for innlevering noe som betyr at 5 års studietid er over. En spennende, men også en svært krevende prosess. Det er mange som er ansvarlige for at denne oppgaven blir ferdigstilt og som fortjener en stor takk.

Først og fremst vil jeg rette en stor takk til min dyktige hovedveileder, Stig-Morten Knutsen, og mine to biveilederne Iver Martens og Rune Mattingdal. Tusen takk for all hjelp og for at dere bestandig svarer på henvendelser, både i tide og utide. Jeg setter utrolig stor pris på all den tiden dere har satt til side for å komme med gode råd og innspill.

En stor takk rettes til familie og venner som har bidratt med korrekturlesning. Vil også rette en spesielt stor takk til min far Kjetil Tonstad, for gode råd og for å ha delt av sin enorme kunnskap.

Hjertelig takk til min kjære samboer, Stine Bjordal Olsen. Takk for gode diskusjoner og støttende ord i tyngre perioder. Dine bidrag har vært uvurderlige.

Tusen takk til alle som har gjort studietiden morsom, spennende og lærerik. Dere vet hvem dere er.

Sigurd A. Tonstad

Tromsø, Mai 2018



# Contents

- 1. Introduction ..... 1
  - 1.1 Objective..... 1
  - 1.2 Study Area..... 1
- 2. Geological Background ..... 3
  - 2.1 Tectonic Development ..... 3
    - 2.1.1 Paleozoic ..... 3
    - 2.1.2 Mesozoic ..... 7
    - 2.1.3. Cenozoic ..... 8
  - 2.2 Stratigraphy and Depositional Environments ..... 11
    - 2.2.1 Paleozoic ..... 11
    - 2.2.2 Mesozoic ..... 18
    - 2.2.3. Cenozoic ..... 19
  - 2.3 Structural Setting..... 21
    - 2.3.1 Loppa High..... 21
    - 2.3.2 Nordkapp Basin ..... 21
    - 2.3.3 Hammerfest Basin ..... 22
    - 2.3.4 Bjarmeland Platform ..... 22
    - 2.3.5 Norsel High ..... 22
    - 2.3.6 Norvarg Dome ..... 23
    - 2.3.7 Samson Dome ..... 23
- 3. Data and Method ..... 25
  - 3.1 Dataset..... 25
    - 3.1.1 3D - Seismic Survey..... 27
  - 3.2 Seismic Reflection Theory ..... 27
    - 3.2.1 Wavelet Processing..... 28
  - 3.3 Seismic Resolution ..... 29
    - 3.3.1 Vertical Resolution ..... 30
    - 3.3.2 Horizontal Resolution ..... 33
  - 3.4 Artefacts and Noise..... 36
  - 3.5 Well Data ..... 38
    - 3.3.1 Well 7124/3-1 Nysleppen Fault Complex..... 38
    - 3.3.3 Well 7226/11-1 Norsel High..... 38
  - 3.6 Software..... 40
    - 3.6.1 Petrel ..... 40
    - 3.6.2 Seismic Attributes..... 40



3.7 Seismic Interpretation Method.....	41
3.7.1 Seismic Sequence Stratigraphy.....	41
3.7.2 Seismic Facies.....	41
4. Results.....	47
4.1 Horizons .....	50
4.1.1 Base Billefjord .....	50
4.1.2 Top Billefjord.....	52
4.1.3 Top Gipsdalen.....	54
4.1.4 Top Bjarmeland .....	56
4.1.5 Top Tempelfjorden.....	58
4.1.6 Base Triassic .....	60
4.2 Seismic Units .....	62
4.2.1 Billefjorden Group .....	62
4.2.2 Gipsdalen Group.....	66
4.2.3 Bjarmeland Group .....	73
4.2.5 Havert Formation .....	89
5. Discussion.....	95
5.1 Depositional Environments of the Ottar basin .....	95
5.1.1 The Upper Billefjorden Group .....	95
5.1.2 Gipsdalen Group.....	99
5.1.3 Bjarmeland Group .....	104
5.1.4 Tempelfjorden Group.....	107
5.1.5 Havert Formation .....	110
5.2 The Samson & Norvarg Domes – Implications for tectonic movements.....	112
6. Summary & Conclusion .....	117
References.....	119

# 1. Introduction

## 1.1 Objective

The main objective of this thesis is to investigate the Late Paleozoic depositional development in the Ottar basin in terms of depositional processes and their lateral variations. The main data used is released 3D-seismic data supplemented with chronostratigraphic data from exploration wells.

## 1.2 Study Area

The study area, known as the Ottar basin, is not a formally defined structural feature of the Barents Shelf, but it is usually described as representing the southern part of the Bjarmeland Platform, between the Nordkapp Basin to the east and Loppa High to the west (Figure 1.1).

The Ottar basin differs from the surrounding basins in one important aspect, which is the absence of salt movements. Aside from the Samson and Norvarg Domes, the basin has experienced little Mesozoic tectonism which is evident from the horizontal stratigraphy stemming from the Late Paleozoic and the Mesozoic Era (Breivik et al., 1995).

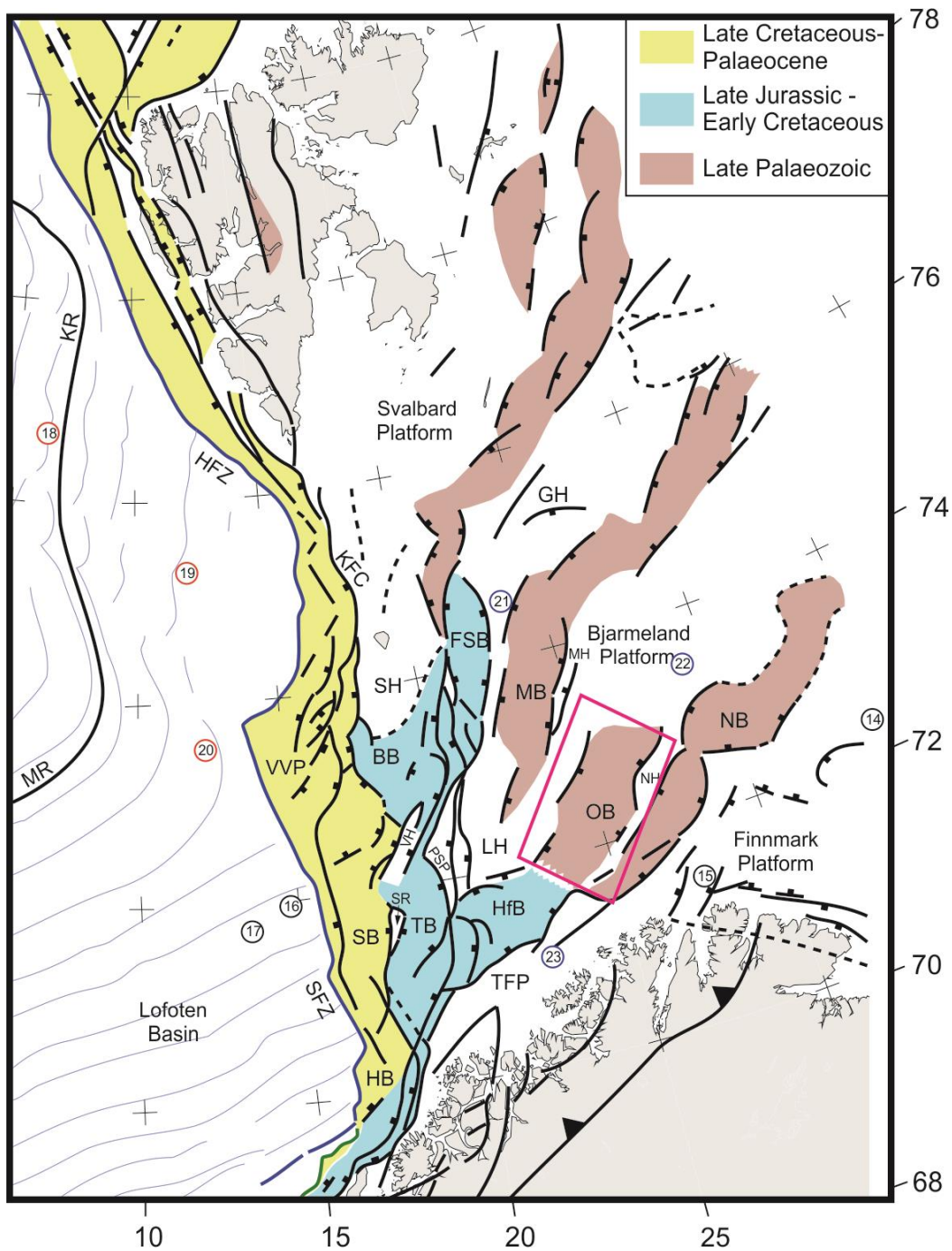


Figure 1.1: The study area is marked by the red square. The Otta basin also contains the Samson- and Norvarg Dome, along with the Swaen Graben. Modified from Faleide et al. (2015). NB = Nordkapp Basin, LH = Loppa High, OB = Otta basin, HfB = Hammerfest Basin.



## 2. Geological Background

The Barents Sea covers the continental Barents Sea Shelf with shallow water depths averaging about 300 meters. The area is bordered by the Svalbard archipelagos and Franz Josef Land to the north and to the south by the coast of Norway and Russia. The western part of the region is bound by the Norwegian-Greenland Sea and the Novaya Zemlya and Kara Sea to the east. This creates an area of approximately 1.3 million km<sup>2</sup> (Doré, 1995; Worsley, 2008).

### 2.1 Tectonic Development

The Barents Sea can be divided into two separate but extensive geological provinces, which are divided by a large monoclinical structure located in the center orientated from north to south (Smelror et al., 2009). The region, divided into east and west, were dominated by different tectonic events. The eastern Barents Sea was influenced by the intricate tectonic histories of Novaya Zemlya, Timian Pechora Basin and the Uralian orogeny. The southwestern Barents Sea was influenced by the large-scale tectonic events known as The Timanian, Caledonian, Ellesmerian and Uralian orogenies. The geological framework has also been influenced by the proto-Atlantic rifting episodes in the west and the subsequent opening and breakup of the northern North Atlantic along the western margin of the shelf (Smelror et al., 2009; Lawver et al., 2011; Gernigon et al., 2014).

#### 2.1.1 Paleozoic

##### *Precambrian*

In the Ediacaran time (635-541 Ma), the Timanian orogeny was formed along the northeastern passive margin of Baltica. This development resulted in a fold-and-thrust belt in the southeastern Barents Sea (Gernigon et al., 2014). The orogeny influenced the configuration of the basement located in the eastern Finnmark Platform, and resulted in the formation of structures that were oriented in a NW-SE direction (Samuelsberg et al., 2003; Siedlecka et al., 2004).

### *Early Paleozoic (Cambrian-Late Devonian)*

The Barents Sea has been involved in two continental collisions and a subsequent continental parting (Doré, 1995). The basement history closely resembles that of the Scandinavian Caledonides (Doré, 1995; Gudlaugsson et al., 1998; Smelror et al., 2009). The Caledonian orogeny culminated in the Late Silurian to Early Devonian era, 400 million years ago. This resulted in the merging of the Laurentian and Baltican plates forming the continent known as Laurussia (Figure 2.1) (Smelror et al., 2009). The collision also represented the closure of the Iapetus Ocean, an important body of water located in a position similar to the present day northeast Atlantic (Doré, 1995). The collision of the two plates occurred in the Scandian phase of the Caledonian orogeny. This created a regional metamorphism that developed the crystalline basement situated below the SW Barents Sea. The Scandian phase concluded with the Emsian collapse and the subsequent Devonian extensional shearing (Cavanagh et al., 2006).

Laurussia altered its direction to a more rapid northward motion during the Middle and Late Devonian (Figure 2.1). This happened simultaneously as Siberia started its slight southward motion. The Ellesmerian orogeny that occurred in the Late Devonian to Carboniferous might have been a result from the collision between Siberia and Laurussia (Lawver et al., 2011).

### *Late Paleozoic (Early Carboniferous – Late Permian)*

The Mid Mississippian (346.7 – 330.9 Ma) marked the beginning of an eastward moving trend for what was to become the Arctic blocks as well as the super continent, Gondwana (Lawver et al., 2011). Siberia also showed an eastward moving trend which subsequently resulted in a collision with Baltica (Figure 2.1). The Middle-Pennsylvanian (306 Ma) marked the final closure of the Rheic Ocean. This led to a reduction in motion of the pieces that were to become the continent Pangea as well as its subsequent consolidation (Figure 2.1) (Lawver et al., 2011). The Permian era marked the beginning of a northward motion which resulted in the re-location of the Barents Sea region to approx. 45° N (Samuelsberg et al., 2003; Stemmerik & Worsley, 2005). The Pangea supercontinent was assembled by the end of the Permian era (Figure 2.1)

In the Late Paleozoic, the Barents Sea region was part of a large E-W oriented continental shelf that extended from the Sverdrup Basin in the west, through the northern Greenland, into the Norwegian and Russian Barents Sea, and Arctic Russia in the east. This large area embodied the northern margin of Pangea. The margin was characterized by subsiding intracratonic basins with a varying degree of magnitude (e.g. Nordkapp Basin & Sverdrup Basin) (Stemmerik, 2000; Worsley, 2008).

The post-Caledonian rifting which was active in the Early Carboniferous through the Mid Carboniferous resulted in wide depressions and the subsequent formation of half-grabens. The developing tectonic setting resulted in partly fault-bonded subsidence across the Barents plate through the Early Carboniferous (Nøttvedt et al., 1990). The increased rifting, a result from oblique sinistral shear, caused the creation of N-S and NE-SW oriented half-grabens. This formation occurred during the Mid Carboniferous. The extensional regime resulted in Svalbard relocating further north (Worsley, 2008; Smelror et al., 2009).

Mid Serpukhovian to Mid Bashkirian (330-315 Ma) marked a period of regional uplift and subsequent erosion as well as a cessation in the sedimentation and the formation of basins (Stemmerik, 2000). The subsidence and basin formation occurred again in the Mid- to Late Bashkirian, following a period of regional uplift. This rifting resulted in the development of two linked rifting zones; the zone between Greenland and Norway, that



stretched across the Barents Sea in a N-E direction, and a zone between Spitsbergen and Greenland which stretched towards the west (Gudlaugsson et al., 1998; Stemmerik & Worsley, 2005). Along the rift axis, subsidence and depocenters with a half-graben geometry developed (Stemmerik & Worsley, 2005; Henriksen et al., 2011). Several phases of compression and rifting resulted in the formation of numerous stable platform areas as well as the development of fault-bounded basins (Stemmerik, 2000).

Rifting was the dominant regime from the Late Bashkirian through the Early Moscovian (323-307 Ma). A period of reduced sedimentation and regional subsidence followed in the later periods of Moscovian to Gzhelian (315-298 Ma) (Stemmerik, 2000). This period of subsidence was detrimental to the development of the regional basins that comprised most of the Barents Shelf (Gudlaugsson et al., 1998; Henriksen et al., 2011). This event was probably related to the closure of the Uralian Ocean that occurred along the margin of Baltica (Henriksen et al., 2011). During the Late Carboniferous through Early Permian the opening of the proto-North Atlantic took place. This occurred between Baltica and East Greenland (Golonka et al., 2003).

During the ending of the Early Permian, cool sea water flooded the Barents Shelf as a result of the formation of a marine seaway between Norway and Greenland. This marine seaway severely influenced the marine circulation systems (Henriksen et al., 2011). Kungurian (283-272 Ma) saw the occurrence of a tectonic event which involved re-activation of previous lineaments. This led to the connection of the Boreal Ocean with sedimentary basins in central East-Greenland (Stemmerik, 2000; Stemmerik & Worsley, 2005).

### 2.1.2 Mesozoic

The border between the Permian and Early Triassic marks the collision between Larussia and Siberia, which created the continent known as Laurasia. This continent later became a part of the supercontinent Pangea (Figure 2.1). The collision between these continents resulted in the Uralian orogeny that greatly influenced larger parts of the Barents Sea (Golonka et al., 2003). Events where tension and stress was released have signified the Permian-Triassic transition. These events stem from a shift in plate tectonics from convergent to divergent. This also led to a crustal uplift, followed by a crustal collapse (Golonka et al., 2003).

Early Triassic was a period dominated by major rifting and subsidence (Henriksen et al., 2011; Gernigon et al., 2014). This phase also contained the preliminary breakup of Pangea which was exacerbated in the Norian (227 – 208 Ma) period along with the creation of rift basins as well as the development of passive margins (Golonka et al., 2003). Regardless of these events, Triassic is still considered as a relatively quiet tectonic period in the western Barents Sea (Figure 2.1) (Henriksen et al., 2011).

The present day structural configuration in the western Barents Sea was a result of the tectonic regime that presided in Mid Jurassic to Early Cretaceous. This was a period of rifting and extension (Henriksen et al., 2011). The rifting initiated in Cretaceous were related to different events, with two phases; Berriasian/Valingian (Early Cretaceous) and Hautervian/Barremian (Early Cretaceous), a result from the propagation of the Atlantic rifting (Faleide et al., 1993). The rifting phase that took place in the Late Cretaceous resulted in the Arctic Eurasia Basin becoming linked to the regional De Greer Zone and the development of the western Barents Sea-Svalbard margin (Faleide et al., 2008).

### 2.1.3. Cenozoic

At the Paleocene – Eocene boundary, seafloor spreading started south of the Greenland-Senja Fracture Zone in the Norwegian – Greenland Sea. This expansion of the Norwegian-Greenland Sea resulted in the formation of a sheared western Barents Sea margin that experienced both transtensional and transpressional deformation during the Eocene era (Faleide et al., 1991; Faleide et al., 1993). The margin was divided by a central rift segment that consisted of two individual segments; the Hornsund Fault Zone and the Senja Fracture Zone (Faleide et al., 2008).

The Senja Fracture Zone comprises several rift-basins, which creates a succession of pull-apart basins located east of the continent-ocean transition. In Eocene, the fault zone was established as a shear zone but as the relative plate movement in Oligocene changed, the shear zone changed with it. As a result of these changes, the shear zone was transformed into a collection of NNW- trending normal faults (Myhre & Eldholm, 1988). As Greenland moved past Svalbard, the Hornsund Fault Zone was developed as a response (Myhre & Eldholm, 1988; Faleide et al., 1991; Faleide et al., 2008).

In Oligocene, the seafloor spreading of the Labrador Sea ended. This caused a change in the direction the plates were moving. The direction changed to a N-W orientation which initiated the spreading of the Greenland Sea seafloor (Eldholm et al., 1987; Myhre & Eldholm, 1988).



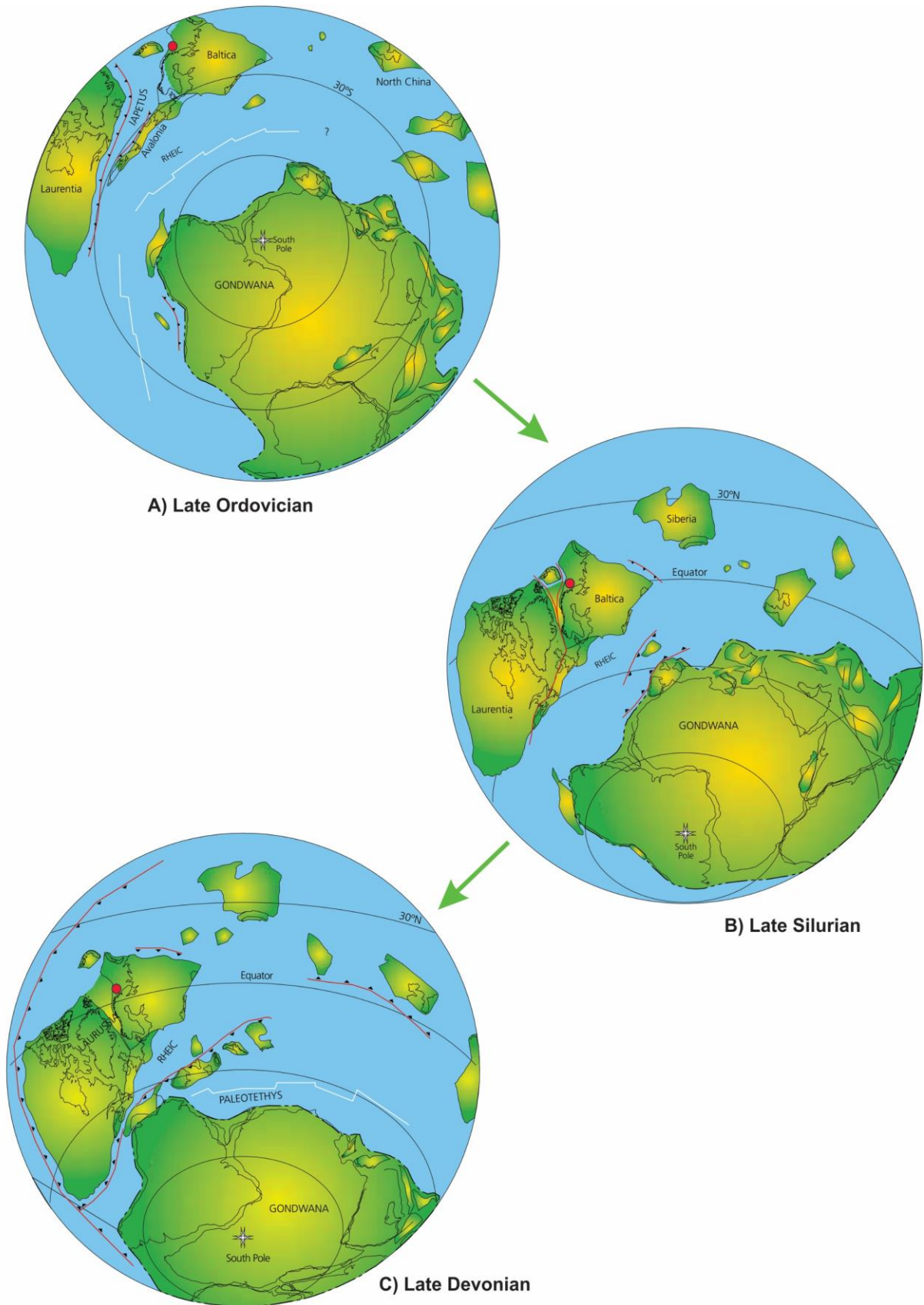
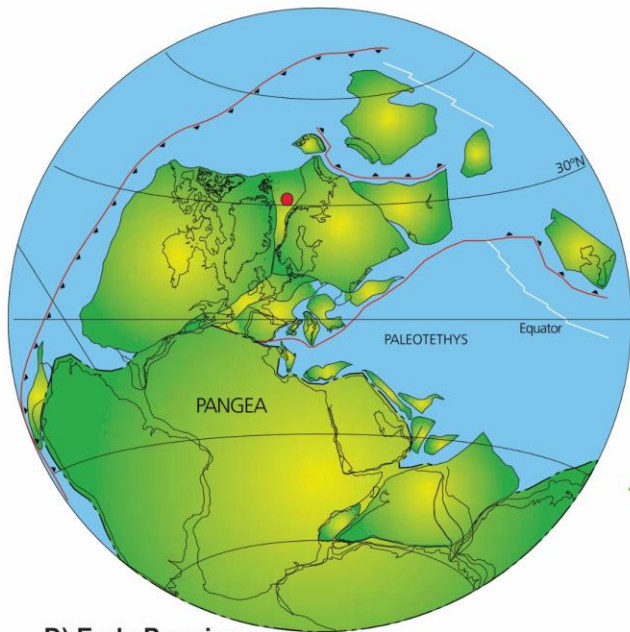
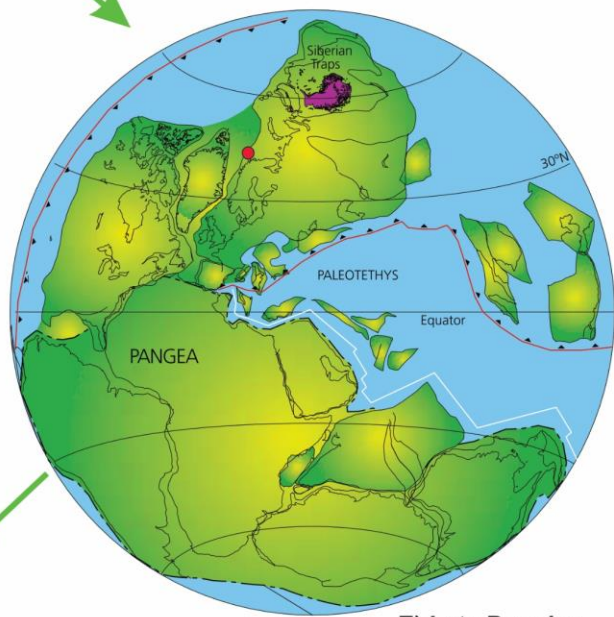


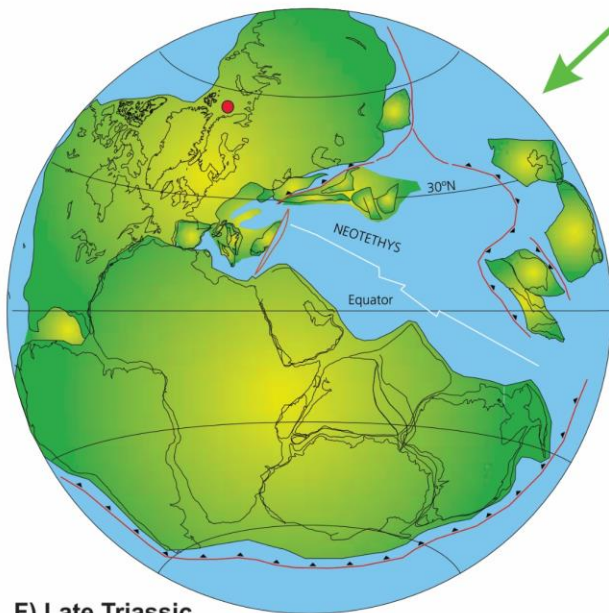
Figure 2.1: A tectonic reconstruction from A) Late-Ordovician to F) Late-Triassic. The red dot marks the approximate position of the study area. Figure is modified from Torsvik et al. (2002).



**D) Early Permian**



**E) Late Permian**



**F) Late Triassic**

*Figure 2.1 Continued*

## 2.2 Stratigraphy and Depositional Environments

The stratigraphy present in the western Barents Sea stretches from Late Paleozoic until Quaternary (Figure 2.3). There is a scarcity of information regarding the underlying basement, but indirect evidence points toward a consolidation during the Caledonian orogeny (Gudlaugsson et al., 1998; Worsley, 2008; Glørstad-Clark et al., 2010).

### 2.2.1 Paleozoic

In Late Devonian, the SW Barents Shelf was located in the central parts of the northern Pangean margin and was relocating further north from equatorial latitudes. Deposits containing coal and plant fossils indicate a humid climate and a non-marine depositional environment. The Billefjorden Group consisting of several different types of clastics was deposited as a rift-infill sequence (Figure 2.3). Influence from marine sources can be found in the uppermost part of the Billefjorden Group in the south-eastern Finnmark Platform, which may indicate the existence of a seaway through the Nordkapp Basin (Worsley, 2008). The humid climate that prevailed in Late Devonian changed to more arid and warmer conditions through Mid Carboniferous - Mid Permian. During this period, the sedimentation changed from continental to shallow-marine siliciclastic and later to carbonate and evaporite deposition. Sabkha evaporites deposited at sea-level lowstand coupled with shallow-marine carbonates are the dominate deposits at the platform areas in the Gipsdalen Group (Worsley, 2008; Duran et al., 2013).

Late Carboniferous marked the establishment of an extensive carbonate platform, where the buildup stretched throughout Early Permian. This was coupled with local basin deposition of evaporites (Worsley, 2008; Smelror et al., 2009; Glørstad-Clark et al., 2010). During the Permian, the biogenic composition changed due to the change in water temperatures from shallow-warm to temperate. This resulted in a change from warm-water carbonates to cool-water carbonates. The period also saw frequent glaciations and deglaciations of the Gondwana continent, which gave rise to rapid sea-level changes. This cyclic exposure of the shelf resulted in extensive dolomitization and karstification (Worsley, 2008). The final disappearance of the ice cap surrounding Gondwana gave rise to a major transgressive event. This marked the end of the rapid sea-level fluctuations (Worsley, 2008).

The end of Permian marked the beginning of a period with colder climate. This is evident from the deposition of cold- and deep-water shales containing lenses of sandstone and limestone that are associated with local highs and platform margins (Worsley, 2008).

The northward motion of the Pangea margin influenced the sedimentary regimes and conditions along the entire shelf (Figure 2.2 A-F). The climate changed from tropical and humid in Early Carboniferous (Figure 2.2-B), subtropical and dry in Bashkirian through Mid Sakmarian (Figure 2.2-C and D), cool temperate in the Late Sakmarian trough Kungurian (Figure 2.2-E and F) and by the end of Permian becoming cold temperate (Stemmerik, 2000; Larssen et al., 2005).

### *Billefjorden Group (Figure 2.3)*

This Late Devonian – Early Carboniferous deposition consists mainly of fluvial and lacustrine sediments that were formed under humid and warm conditions (Stemmerik & Worsley, 2005; Worsley, 2008). The Group is mainly located on the Finnmark Platform and is difficult to map outside this area. It is generally believed to represent thick siliciclastic wedges in Carboniferous half-grabens in the SW Barents Sea (Larssen et al., 2005). The sediments that are assigned to this group are separated from the underlying Precambrian metasandstones by an angular unconformity. The age varies from onshore to offshore, but in the offshore Barents Sea they are often thought of as stemming from Famennian/Viséan to Early Serpukhovian (346.7 – 332 Ma) (Larssen et al., 2005; Worsley, 2008). Non-marine sediments dominate the group even though marine shale and shallow marine sandstone have been found towards the top of the group in some areas (Larssen et al., 2005). This could indicate conditions that reflect a temporary marine environment which could have resulted from a sea-level maximum reached in the Viséan (Figure 2.2-B) or the presence of a seaway through the Nordkapp Basin (Stemmerik & Worsley, 2005). This seaway led to a more open marine environment that dominated the eastern Barents Shelf (Worsley, 2008).

### *Gipsdalen Group (Figure 2.3)*

During the Serpukhovian the northern North Atlantic along with the Arctic experienced a regional uplift (Samuelsberg et al., 2003). This led to the regional unconformity separating the Billefjorden Group (fluvial siliciclastics) from the overlying Gipsdalen Group. This large unconformity is related to a drastic change in climate, changing from warm and humid to warm and arid (Larssen et al., 2005). The controlling deposits in the Group are siliciclastics with a red color and warm-water carbonates which are often karstified and dolomitized. Evaporites also have a major presence within the Group (Larssen et al., 2005; Worsley, 2008). Bashkirian marks the restart of sedimentation in half-grabens and the accumulation of syn-rift siliciclastics stemming from alluvial fans and braided river deposits (Samuelsberg et al., 2003; Larssen et al., 2005). During the transition from Bashkirian to Kasimovian a transgression occurred (Figure 2.2 C-D). This led to the evolution of a shallow-marine setting, characterized by a change in depositional style. The previous style had been dominated by a mixture of siliciclastics and carbonates but was now dominated by pure carbonates (Samuelsberg et al., 2003)

### *Bjarmeland Group (Figure 2.3)*

The warm-water carbonates deposited in the Early Sakmarian (295 Ma) is separated from the overlying cool-water carbonates deposited in Mid Sakmarian through the Late Artinskian (292 – 283 Ma) by an unconformity signifying subaerial exposure. This cool-water carbonate succession is called the Bjarmeland Group (Larssen et al., 2005; Stemmerik & Worsley, 2005). This shift represents a change from a subtropical warm-water carbonate platform (Figure 2.2-C) to a more temperate cool-water platform (Figure 2.2-E). This is due to a large change in the organization of the central parts of the Pangean Shelf (Samuelsberg et al., 2003; Stemmerik & Worsley, 2005). The development of the Uralides resulted in a change in the circulation. This again altered the depth and temperature of the water (Worsley, 2008).

During the mid-Artinskian a major transgression occurred. This created an extensive cold-water carbonate shelf that extended from the Sverdrup Basin and included the central Pangean Shelf (Figure 2.2-E). Carbonate mounds and ridges were developed which were dominated by grainstones and cementstones (Stemmerik & Worsley, 2005).



### *Tempelfjorden Group (Figure 2.3)*

The cool-water carbonates of the Bjarmeland Group were overlain by the Tempelfjorden Group dominated by deep-water spiculites, but also a composition of shales and sandstones (Rafaelsen et al., 2008). There is an abrupt change in lithofacies when moving from Bjarmeland to Tempelfjorden which indicate a rapid flooding and a transgressive event (Figure 2.2-F). The lithofacies being dominated by spiculitic chert and shales (Colpaert et al., 2007).

Late Permian saw a renewed transgressive event, which resulted in the termination of biogenic production and sedimentation (Colpaert et al., 2007). The climate transitioned to a colder environment and the deposits became increasingly more influenced by siliciclastic sediments (Samuelsberg et al., 2003).

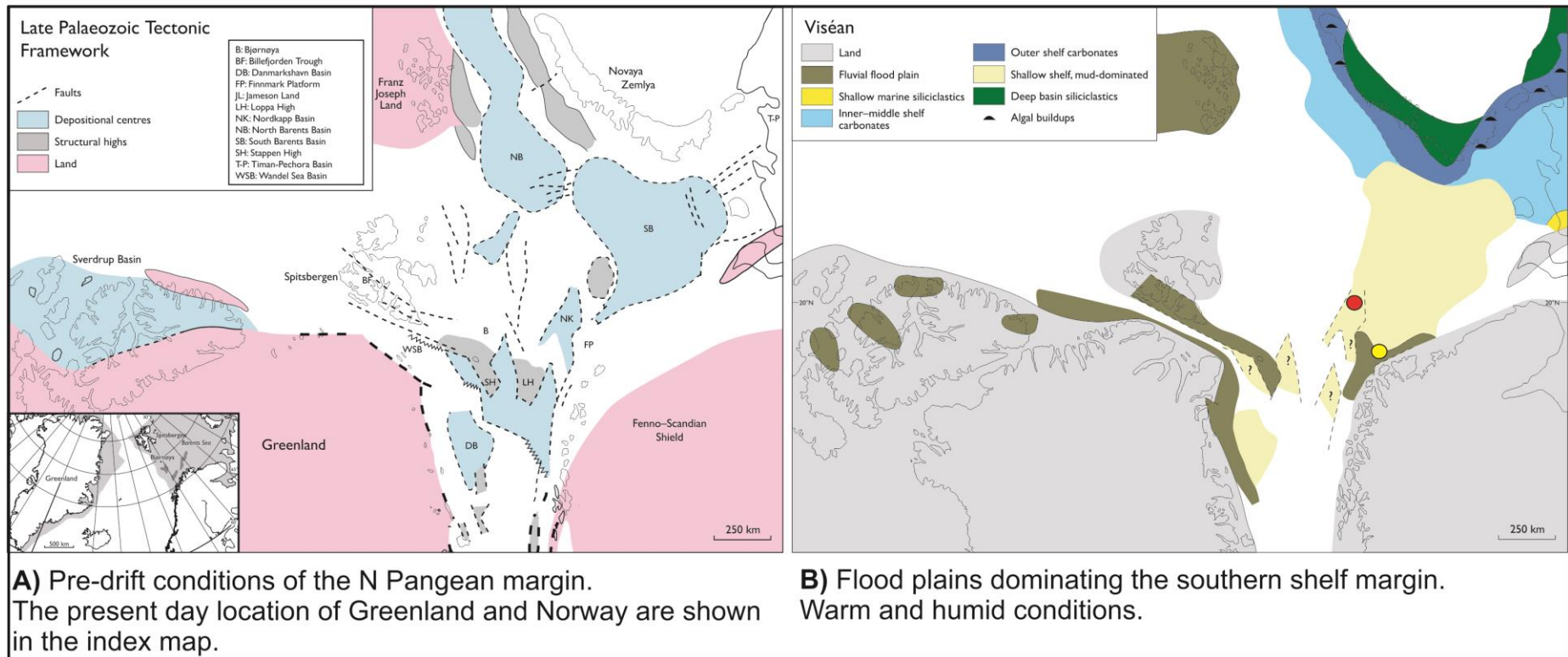


Figure 2.2: A) Reconstruction of the pre-drift elements of the Northern Pangea margin. B) –F) Paleogeographic reconstructions of the northern Pangea margin during the Late Paleozoic. Red circle = Nordkapp Basin, yellow circle = Finnmark Platform. Modified from Stemmerik and Worsley (2005).

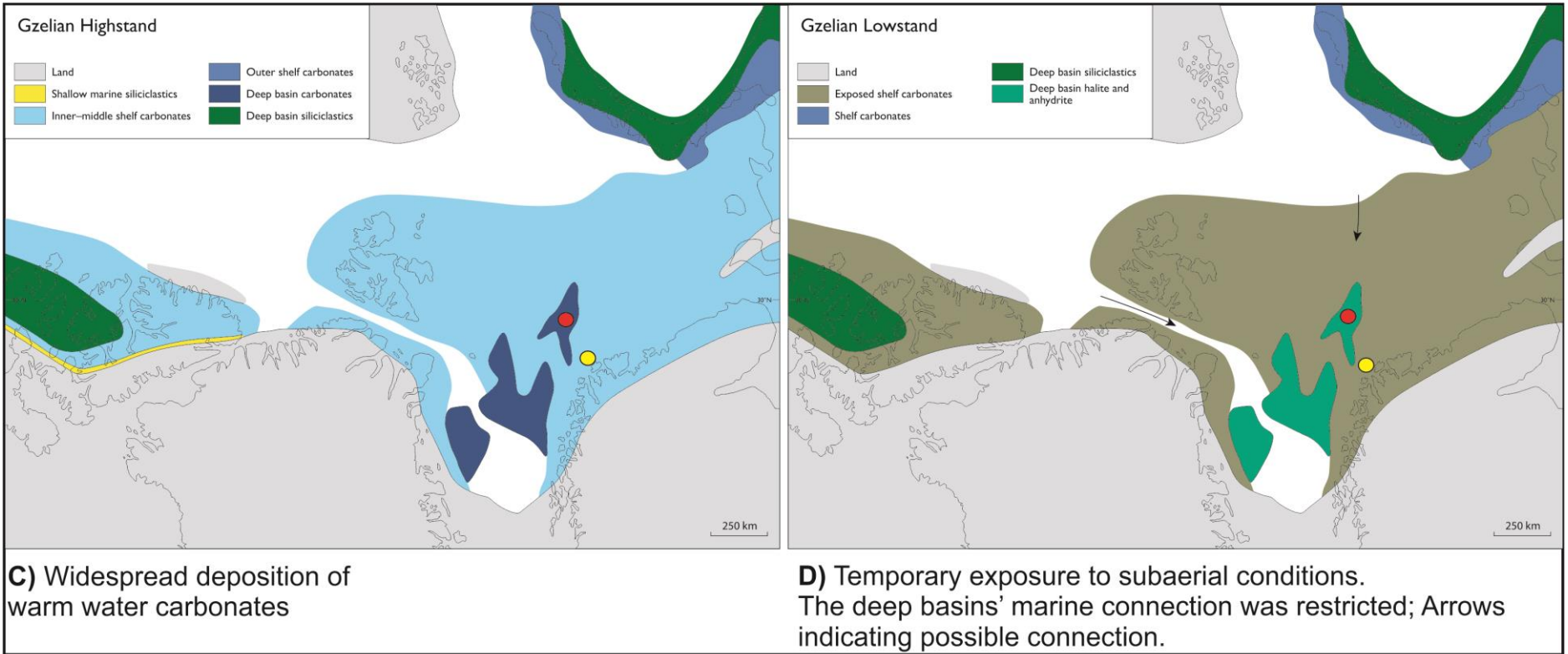


Figure 2.2 continued

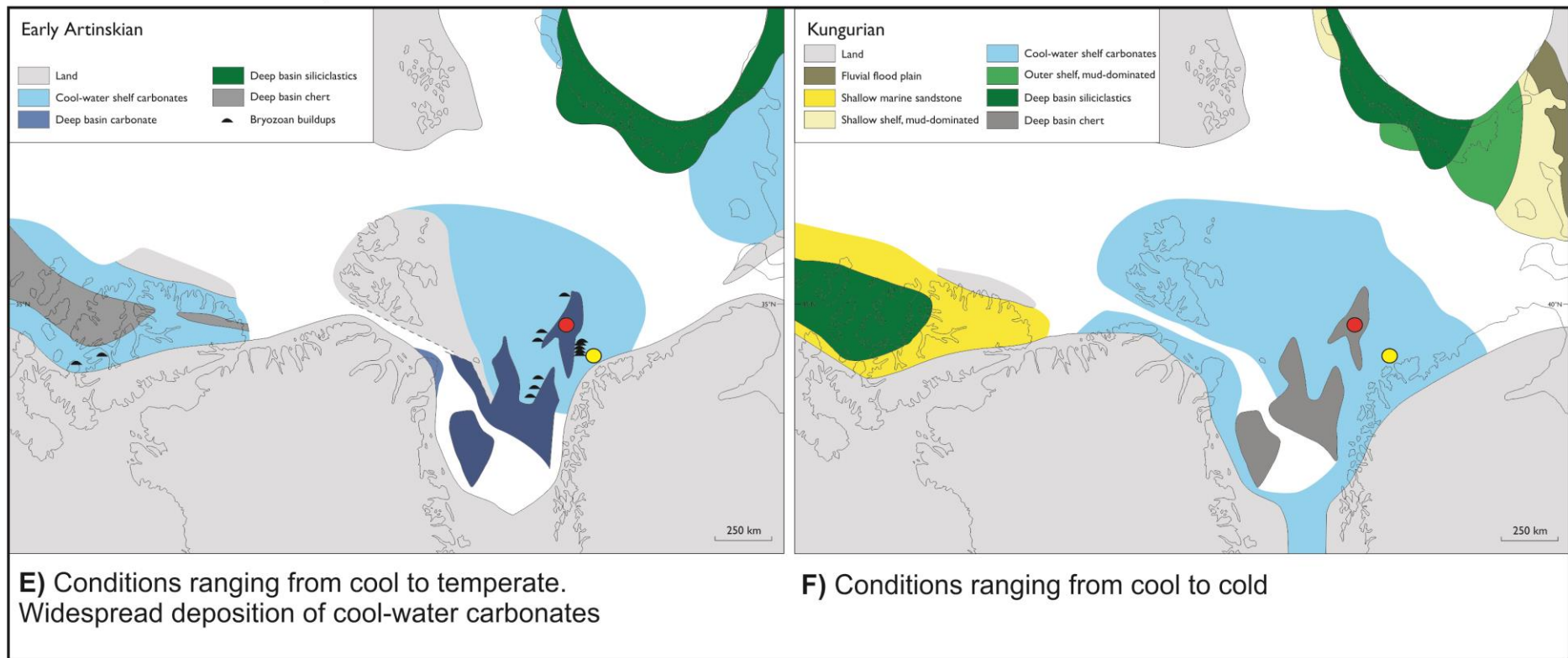


Figure 2.2 continued

### 2.2.2 Mesozoic

A significant hiatus marks the change from Late Permian to Early Triassic. The hiatus can be seen as a marked change from silica-rich shale to non-siliceous shales. This transition is still poorly understood (Worsley, 2008). The sediments deposited during the Triassic are heavily influenced by erosion and transportation mainly from the Baltic shield and later the Urals, which created a coastline that prograded northwesterly (Worsley, 2008; Glørstad-Clark et al., 2010). Organic rich shales belonging to the Kobbe and Snadd subgroups (Figure 2.3) were deposited at the same time, favored by restricted basins (Smelror et al., 2009). A NNE-trending system of clinoforms can be traced over most of the Hammerfest Basin and Bjarmeland Platform which is believed to stem from a sandy deltaic and shoreface environment due to the area being situated close to the paleocoast (Worsley, 2008).

In early Norian (228 mya), the deposition of well-sorted and mature sandstones gave rise to excellent reservoir units like the Nordmela and Stø Formations of the Realgrunnen Subgroup (Kapp Toscana) (Figure 2.3). The deposition followed the formation of shallow marine and coastal marine depositional environments in Early- to Mid Jurassic (Worsley, 2008).

In Bathonian, a regional transgression occurred, which gave rise to the environmental conditions necessary for the deposition of the shale-dominated Adventdalen Group (Figure 2.3), a group with a substantial content of organic carbon, particularly in the Late Jurassic units (e.g. Hekkingen Fm.)(Faleide et al., 1993; Worsley, 2008).

A change in depositional environment marks the transition from Jurassic to Cretaceous. The sea level reached its maximum in Late Jurassic, but transitioned into a regression in Early Cretaceous. Thick units of claystone with interbedded limestone and dolomite (Knurr and Kolje Formations) were deposited in the Hammerfest Basin as a result of continuous sedimentation (Figure 2.3) (Worsley, 2008; Smelror et al., 2009). In Albian times, the Kolmule Formation was deposited as a result of a transgression (Smelror et al., 2009).

In Late Cretaceous two formations were deposited, the Kveite and Kviting Formations, which belong to the Nygrunnen Group (Figure 2.3) (Worsley, 2008; Ostanin et al., 2013).

### 2.2.3. Cenozoic

The opening of the Norwegian-Greenland Sea during the Paleogene subjected the Barents Shelf to transtention and transpression. The western margin was subject to continued tectonic activity. In the western basins and the outer shelf margins, the Torsk Formation (Sotbakken Group) was deposited (Figure 2.3). The formation is characterized by its large content of claystone with a minor constituent of tuff located at its base (Faleide et al., 1993; Ostanin et al., 2013).

Neogene marked a period of repeated glaciations. Subsidence and uplift with subsequent erosion was present during this period. This created large wedges over and off the continental shelf margins, and resulted in the re-deposition of eroded sediments at the continental slope (Vorren et al., 1991; Faleide et al., 1996; Worsley, 2008; Glørstad-Clark et al., 2010; Laberg et al., 2012).



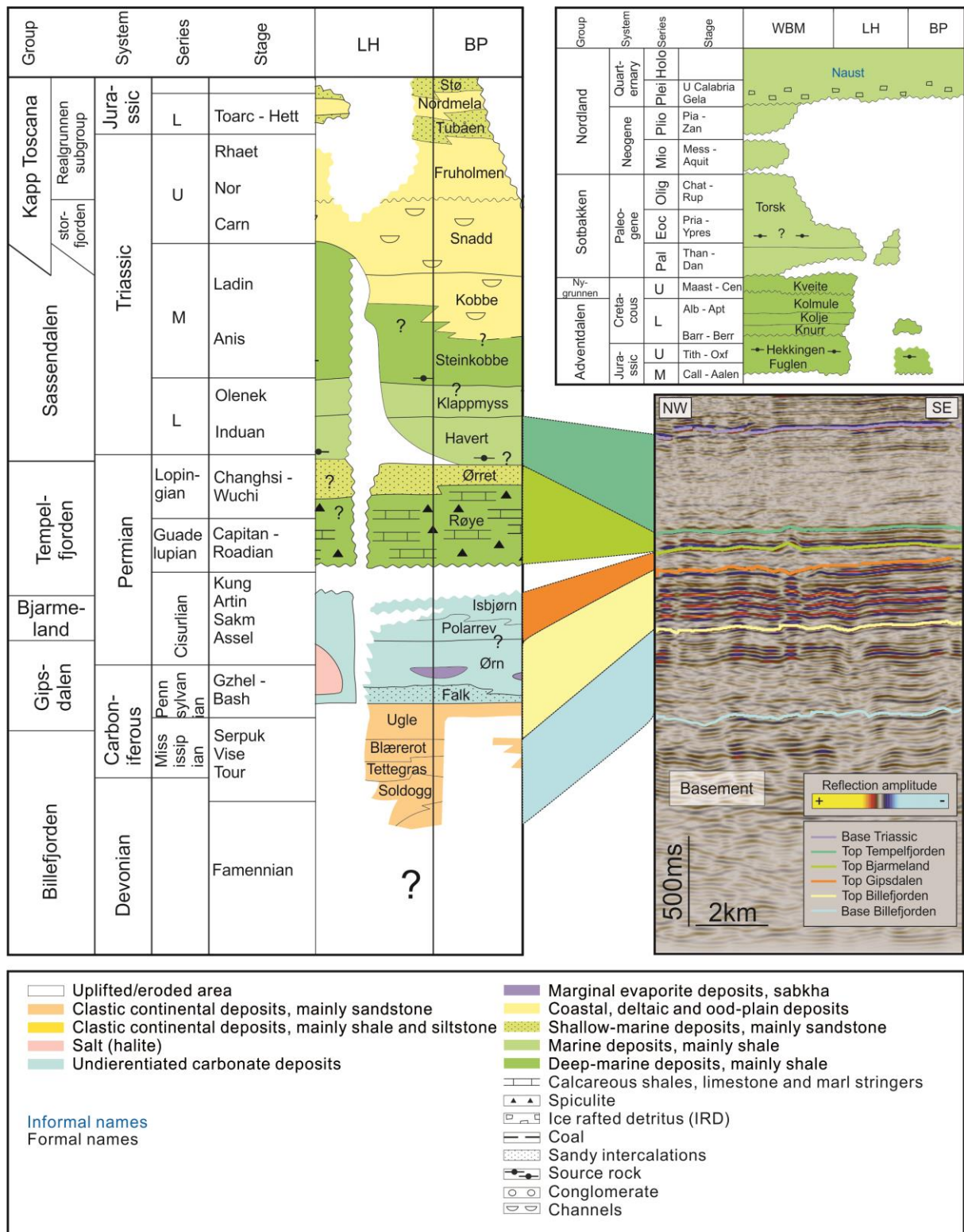


Figure 2.3: Lithostratigraphic chart from the Norwegian Barents Sea and a correlation panel showing the interpreted units. The figure is modified from NPDfactpages (2014). WBM = Western Barents Margin, LH = Loppa High, BP = Bjarmeland Platform.

## 2.3 Structural Setting

Ottar basin is situated among some of the more well-known structural elements of the Barents Sea. Surrounding the basin that will be studied in this thesis is the Loppa High to the west, Nordkapp Basin and Norsel High to the East and the Hammerfest Basin to the south (Figure 2.4). The Ottar basin is considered as the southern part of the Bjarmeland Platform, comprising the positive features known as the Samson Dome located in the southern part of the basin and the Norvarg Dome, situated in the northern parts of the basin (Figure 2.4) (Breivik et al., 1995).

### 2.3.1 Loppa High

Located between the Hammerfest Basin to the north and the Bjørnøya Basin to the southeast (Figure 2.4). The high consists of a crestal western and northwestern margin and an eastern platform. The Asterias Fault Complex bounds the high to the south, and to the west by the fault complex known as Bjørnøyrenna. A monocline marks the limit towards the Hammerfest Basin and Bjarmeland Platform. The Svalis Dome, a large salt structure, along with its associated syncline known as the Maud Basin marks the border to the northeast (Gabrielsen et al., 1990).

The uplift of Loppa High has been reactivated several times due to the tectonics of both the Late Jurassic - Early Cretaceous and the Late Cretaceous - Cenozoic eras. The development of the high took place in Late Permian and Early Triassic. The tectonic regime was diverging, which created the uplift (Gabrielsen et al., 1990). The metamorphic basement of the area lies at relatively shallow depths as a result of the many uplifts, which is characteristic for the western areas (Gabrielsen et al., 1990).

### 2.3.2 Nordkapp Basin

The Nordkapp Basin can be classified as a salt-filled rift basin from the Late Paleozoic with a trend generally in the NE-SW direction with an exception as the central part has an E-W orientation (Figure 2.4) (Gabrielsen et al., 1990). When defined at pre-Permian levels, the southwestern part is a half-graben while the central and northern parts are symmetrical grabens. The southern and northern margins are associated with halokinesis and deep faults underlying the salt pillows. The basin is defined as a gravity low, and its central parts have undergone deformation from several salt structures (Gabrielsen et al., 1990).

### 2.3.3 Hammerfest Basin

A relatively shallow basin that possesses an ENE-WSW oriented axis. Situated south of the Loppa High, separated from it by the Asterias Fault Complex (Figure 2.4). The establishment of the basin likely occurred in the Late Carboniferous (Gabrielsen et al., 1990). The main rift events with subsequent subsidence transpired during the Triassic and Early Cretaceous (Faleide et al., 1984; Gudlaugsson et al., 1998). Mid-Cretaceous marks the culmination of the development of the basin (Faleide et al., 1993). Evaporite deposits stemming from the Late Paleozoic seems to be absent from the basin even though their presence in neighboring basins such as the Nordkapp- and Tromsø Basin have been documented. The internal structure of the basin is characterized by a central dome and a complex pattern of faults that have a dominating W and WNW trend (Gabrielsen et al., 1990).

### 2.3.4 Bjarmeland Platform

The platform signifies a stable area between the Hammerfest and Nordkapp Basins in the south and southeast, and the Loppa High to the west (Figure 2.4). A regional uplift during the Paleogene - Neogene resulted in the sediments dipping toward the south. However, the platform is still regarded as being a stable structural element, which it has been since the Late Paleozoic (Gabrielsen et al., 1990).

Late Carboniferous marked the beginning for the development of the stable platform. The platform is assumed to be underlain by rocks of Paleozoic and Precambrian origin. A fault zone with a N-S orientation resulted in a westerly termination in the Early Triassic (Gabrielsen et al., 1990).

### 2.3.5 Norsel High

A high initiated by tectonism in the Early Carboniferous and remained as a positive structural feature until Mid Triassic. The high is bounded by the Nysleppen Fault Complex to the southeast, and has a NE-SW orientation (Figure 2.4). The development of the high is assumed to be a result of Paleozoic rifting and the subsidence of the Nordkapp Basin (Gabrielsen et al., 1990).

### 2.3.6 Norvarg Dome

Located in the northern parts of the Ottar basin (Figure 2.4). The dome is described as having a circular/elongated geometry, with a diameter of approximately 25km. In the core of the dome there are evaporites stemming from Carboniferous. Covering the evaporites is a carbonate succession stemming from Late Carboniferous – Permian (Gabrielsen et al., 1990).

### 2.3.7 Samson Dome

Located in the southern parts of the Ottar basin, this dome represents a circular to elliptical body of evaporites (Figure 2.4). These evaporites are believed to be of Carboniferous age, and similar to the Norvarg Dome, the evaporites are covered by Late Carboniferous – Permian deposited carbonates. The salt movements that created the dome is believed to have occurred before the Cretaceous (Gabrielsen et al., 1990).

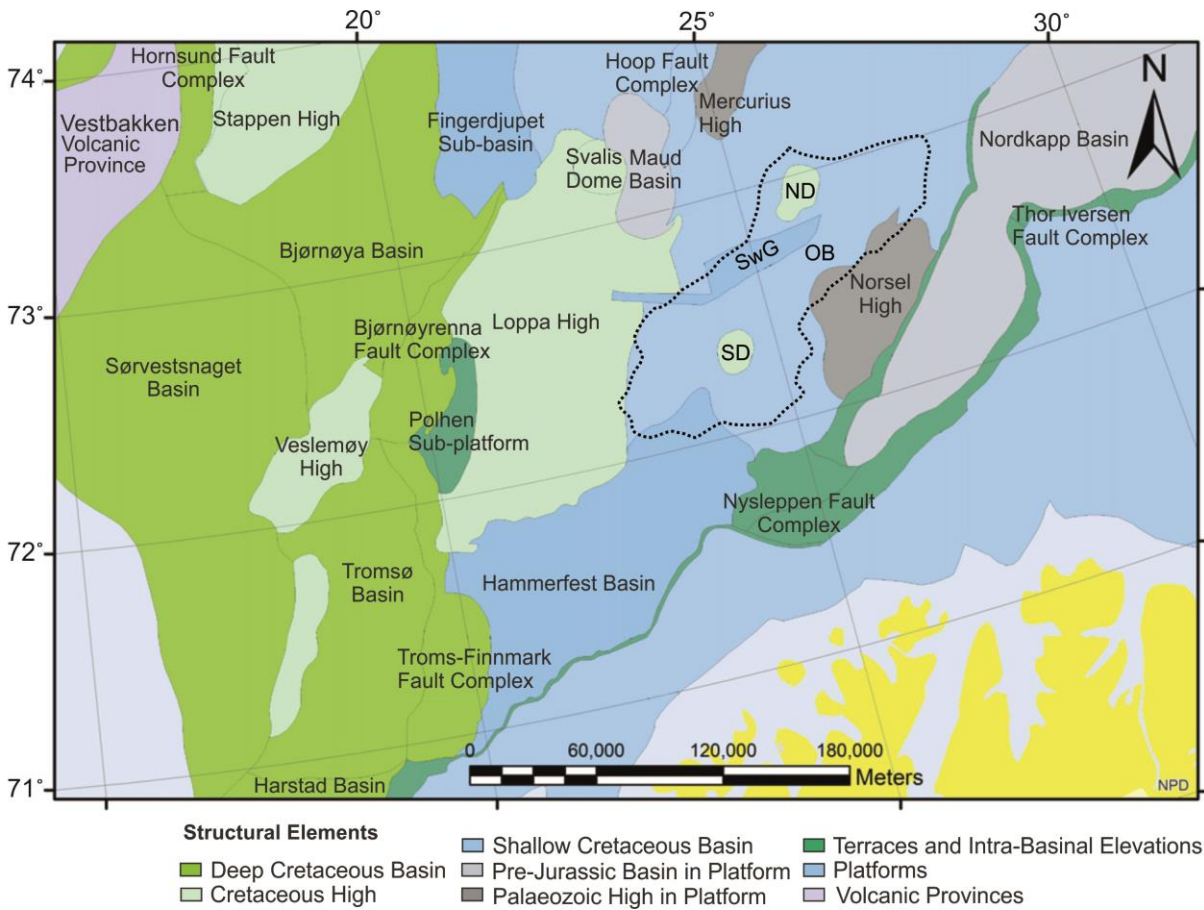


Figure 2.4: Structural elements of the Barents Sea. The dotted black line shows the presumed delineation of the Otta basin. SD = Samson Dome, SwG = Swaen Graben, ND = Norvarg Dome, OB = Otta basin. Figure modified from Mattos et al. (2016)

### 3. Data and Method

#### 3.1 Dataset

This study is based on five 3D seismic surveys (Table 1) covering an extensive area on the SW Barents Shelf ( Figure 3.1).

*Table 1: Overview of the data sets used in the study*

<b>Data Type</b>	<b>Name</b>	<b>Gathered By</b>	<b>Year</b>
<b>3D</b>	BG1002	BG Norge AS	2010
<b>3D</b>	NH0608	Norsk Hydro	2006
<b>3D</b>	ST10M01	Statoil	2010
<b>3D</b>	SG9804	Saga Petroleum ASA	1998
<b>3D</b>	WIN12003	Wintershall Norge ASA	2012



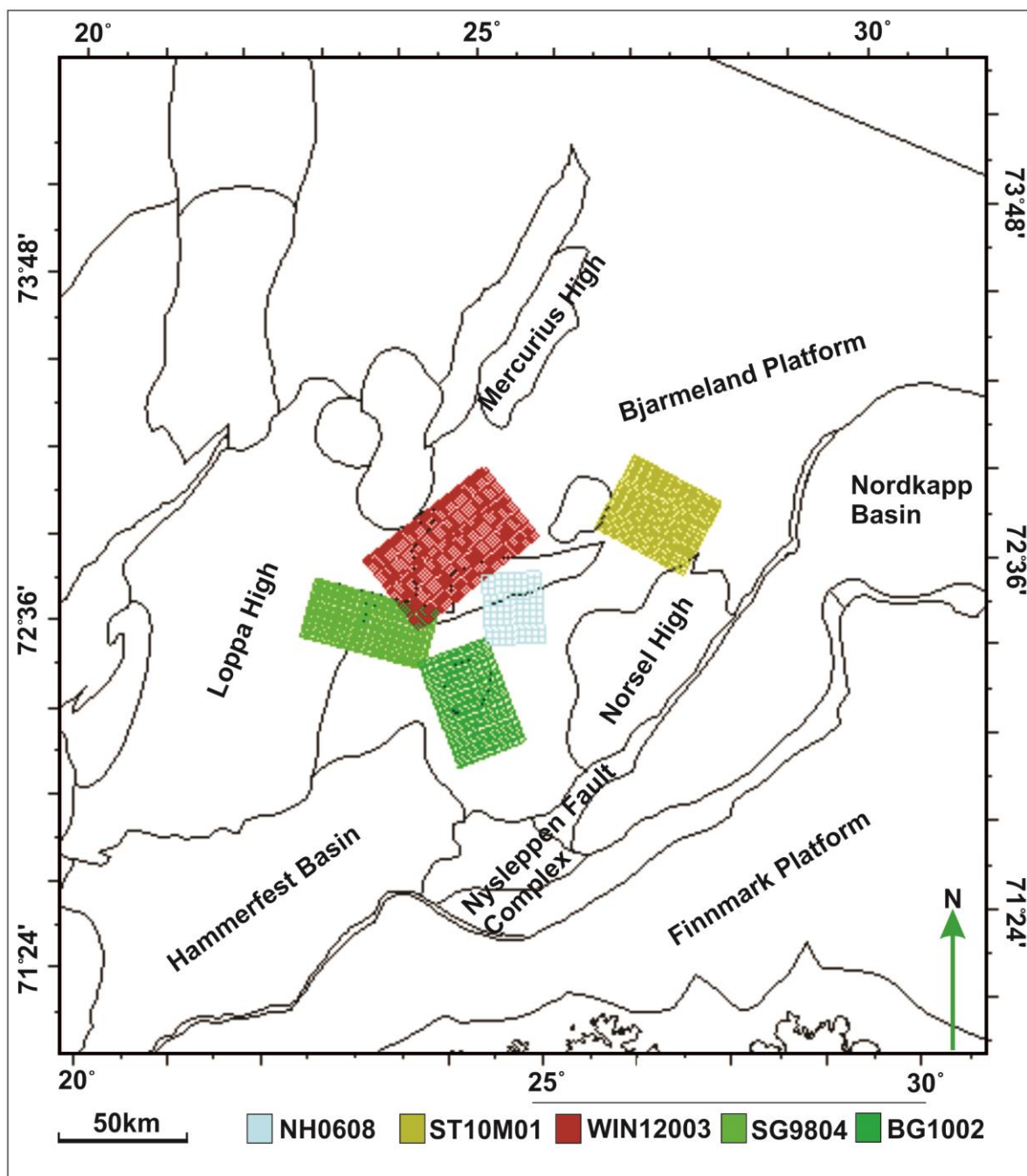


Figure 3.1: Location of the different seismic surveys. Main structural elements surrounding the study area are shown.



### 3.1.1 3D - Seismic Survey

All the data received was processed and ready to use in Petrel. By looking at the seismic response from the seafloor the polarity and phase of the data was established. There are several conventions for phases and polarity in use, such as the conventions of Badley (1985) and the Society of Exploration Geophysicists (SEG) standard of Sheriff (2006).

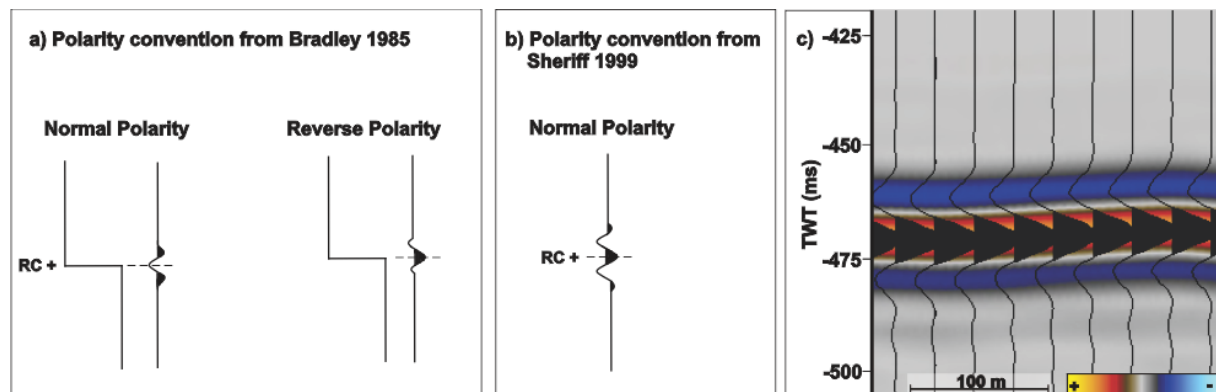


Figure 3.2: The polarity convention for the seismic data used in this study is the zero-phase normal polarity (b) of Sheriff (2006). The phase could also be the reverse polarity convention of Badley (1985) shown in a). The seismic trace shown in (c) is retrieved from the 3D survey ST10M01.

The data follows the reverse polarity convention described by Badley (1985) or normal polarity when using the convention established by Sheriff (2006). This is marked by a black peak signaling the contact of the seabed horizon and the seismic energy (Figure 3.2).

### 3.2 Seismic Reflection Theory

Reflection seismic is a basic technique but still the most crucial tool in order to map subsurface structures and features in detail. Seismic waves travel through the subsurface and when they interact with a boundary (reflector) they are reflected. The seismic waves travel through the subsurface as body or surface waves. When conducting seismic surveys, the waves transmitted as elastic body waves that travel through water and other mediums are the ones of interest. When the waves travel they do so as either shear or pressure waves with only the latter having the ability to travel through water (Badley, 1985; Veeken, 2007a)

When the waves are generated by an energy source, they travel downwards and are reflected by a boundary due to a difference in acoustic impedance (Equation 3.1). This difference is between layers in the subsurface. The amount of energy reflected by the

boundaries is controlled by the reflection coefficient (Equation 3.2). The reflection coefficient is a numerical value for the difference in acoustic impedance between two layers. The seismic lines that reveal features and structures in the subsurface are dependent on this value (Badley, 1985)

### Equation 3.1 – Acoustic Impedance

$$Z = \rho V$$

*Equation 3.1: Z (acoustic impedance) is equal to a layer's  $\rho$  = density (kg/m<sup>3</sup>) multiplied by the velocity of the wave travelling through the layer  $V$  = velocity (m/s).*

### Equation 3.2 – Reflection Coefficient

$$R = \left( \frac{Z_2 - Z_1}{Z_2 + Z_1} \right) = \frac{\rho_2 V_2 - \rho_1 V_1}{\rho_2 V_2 + \rho_1 V_1}$$

*Equation 3.2: The difference in acoustic impedance between two layers determine the strength of the seismic reflection, this is calculated as the reflection coefficient (R). Z,  $\rho$ , V is the value for acoustic impedance, density and velocity of the different layers. The subscript number marks which layer the values belong to, with 1 marking the uppermost sedimentary layer. The equation shows that if  $Z_2 > Z_1$  then the value of R will be positive, subsequently if  $Z_1 > Z_2$  R will be negative. R is zero when  $Z_2 = Z_1$ .*

As shown in equation 3.2 the value for the reflection coefficient (R) could be either positive or negative. The value is dependent on the physical properties of the rocks located in the subsurface. The negative or positive value of R points towards softer rocks overlying harder rocks or vice versa (Badley, 1985).

#### 3.2.1 Wavelet Processing

When processing the seismic gathered it is important to create a wavelet shape that is identical for each trace (Sheriff, 1980). The effective wavelet will often be substituted for a zero-phase wavelet. The SEG-convention establishes an international wavelet standard. This is done by using a positive peak as a positive reflection coefficient (Sheriff, 1980). The zero-phase wavelet is symmetrical with the peak centered at the boundary (Figure 3.2). The shape of the zero-phase wavelet makes it ideal for interpretation. This is because it has the highest peak amplitude compared to other signals such as minimum-phase and mixed-phase. Zero-phase also has a short duration, and this coupled with the

aforementioned highest peak amplitude makes the signal the best equipped for resolution capability (Sheriff, 1980).

### 3.3 Seismic Resolution

As seismic waves travel through the subsurface the acoustic impedance contrast creates seismic reflections. The contrast needs to be great enough to be detected and is dependent on the processing and acquisition. There are both horizontal and vertical aspects when considering the resolution of seismic. Resolution is defined to be the ability to distinguish sedimentary features in the subsurface (Brown, 1999). Equation 3.3. Shows the connection between wavelength, frequency and velocity and is given by Brown (1999).

#### **Equation 3.3 - Relationship between Wavelength, Frequency and Velocity**

$$\lambda = \frac{V}{f}$$

*Equation 3.3:  $\lambda$  = Wavelength (m),  $V$  = velocity (m/s),  $f$  = frequency (Hz).*

Seismic velocity increases downwards through the subsurface as a result of diagenesis. The seismic waves propagate faster in more dense and compacted material. The increase in velocity is observed simultaneously as the frequency decreases. This is a result from the attenuation of higher frequencies, which occurs at a quicker pace than that of lower frequencies. The result of these processes is a sharp increase in wavelength which in turn makes the seismic resolution of the data significantly poorer (Brown, 1999). The effects of depth on the relationship between the different parameters is shown in Figure 3.3.

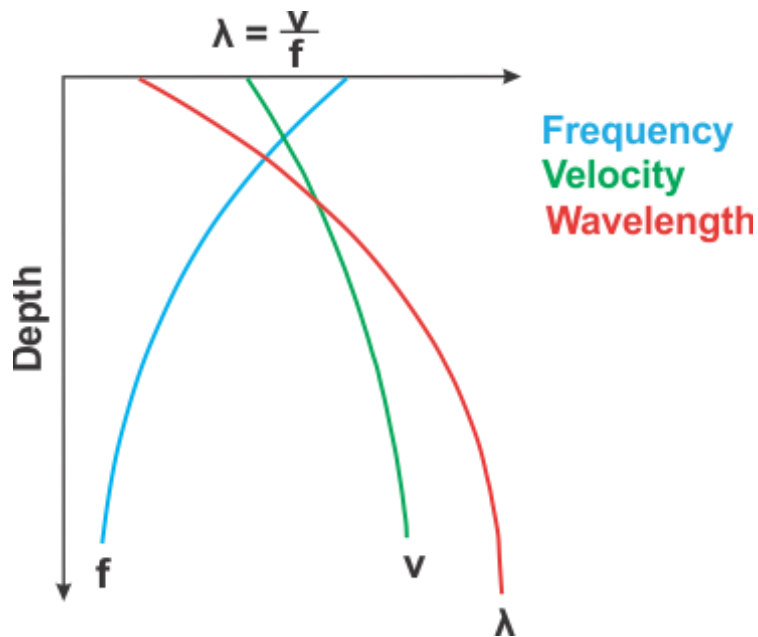


Figure 3.3: The relationship between wavelength, velocity, and frequency and their evolution through depth. The wavelength increases drastically with depth while frequency decreases resulting in a poorer resolution. Figure is modified from Brown (1999).

### 3.3.1 Vertical Resolution

According to Brown (1999) there are two limitations on the vertical resolution, the limit on visibility and the limit of separability. The vertical resolution determines what can be observed on a seismic section by limiting the smallest size a feature can possess in order to be viewed (Sheriff, 1985). The limit on what can be separated is one quarter of a wavelength, which is the same as half the period of the wave. This means that it is possible to identify the top and bottom of a layer as long as the thickness is greater than half the wavelength of the seismic wave. If the layer is thinner than this, the amplitude is continuously attenuated by destructive interference until the limit of visibility is reached. This occurs when the background noise eliminates the reflection signal. Brown (1999) defines the vertical resolution as displayed in equation 3.4.

#### Equation 3.4 - Vertical Resolution

$$Vr = \frac{\lambda}{4}$$

Equation 3.4: Vertical resolution ( $Vr$ ) = Wavelength ( $\lambda$ ) divided by 4.

The amplitude of the reflection decreases when the thickness of the layer decreases from  $\frac{1}{4}\lambda$  to  $\frac{1}{30}\lambda$ , which signifies the lowest thickness possible to observe in a seismic system (Figure 3.4) (Badley, 1985).

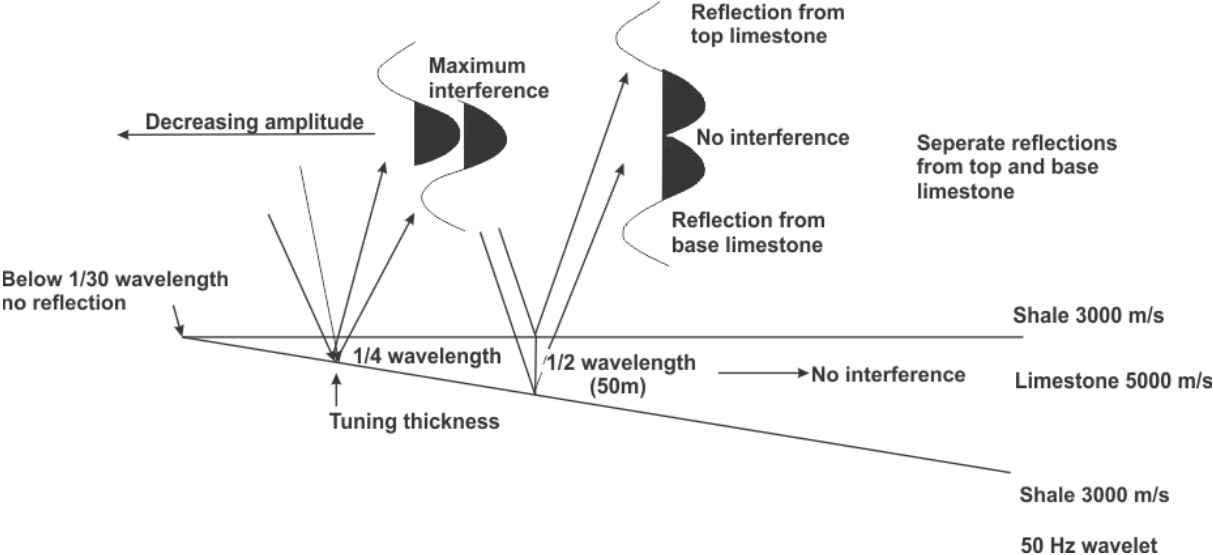


Figure 3.4: The interference effects associated with a large acoustic-impedance wedge interbedded within a lower-acoustic impedance shale. The figure is modified from Badley (1985)

By performing a spectral analysis on the seismic data, the frequency spectrum can be obtained. The sonic logs were utilized in order to get a best possible measurement of the velocity within each horizon. The vertical resolution was calculated on the same horizons in two different data sets, BG1002 and WIN12003 (Table 2).

*Table 2: The vertical resolution of a few selected horizons from two different datasets. The velocity was found from the well-data which crosses a 2D-line.*

<b>Dataset</b>	<b>Horizon</b>	<b>Velocity</b>	<b>Frequency</b>	<b>Wavelength</b>	<b>Vertical Resolution</b>
<b>BG1002</b>	Top Tempelfjord	4377.88 m/s	36.32 Hz	120.54 m	30.13 m
<b>BG1002</b>	Top Bjarmeland	3990.71 m/s	30.98 Hz	128.82 m	32.20 m
<b>WIN12003</b>	Top Tempelfjord	4377.88 m/s	31.25 Hz	140.1 m	35.02 m
<b>WIN12003</b>	Top Bjarmeland	3990.71 m/s	27.15 Hz	146.99 m	36.75 m

### 3.3.2 Horizontal Resolution

Horizontal resolution is the horizontal distance required in order to differentiate between two different subsurface features. The Fresnel zone is often used when describing the horizontal resolution (Figure 3.5). The first Fresnel zone is described as the zone that reflects waves that reaches the detector within half of a cycle. Equation 3.5 gives the radius of the Fresnel zone for an un-migrated seismic section (Sheriff, 1985).

#### Equation 3.5 – Radius of the Fresnel zone

$$rf = \frac{v}{2} \sqrt{\frac{t}{f}}$$

Equation 3.5:  $rf$  = radius of the Fresnel zone (m),  $v$  = average velocity (m/s),  $t$  = Two-way travel time (s),  $f$  = Dominant frequency (Hz).

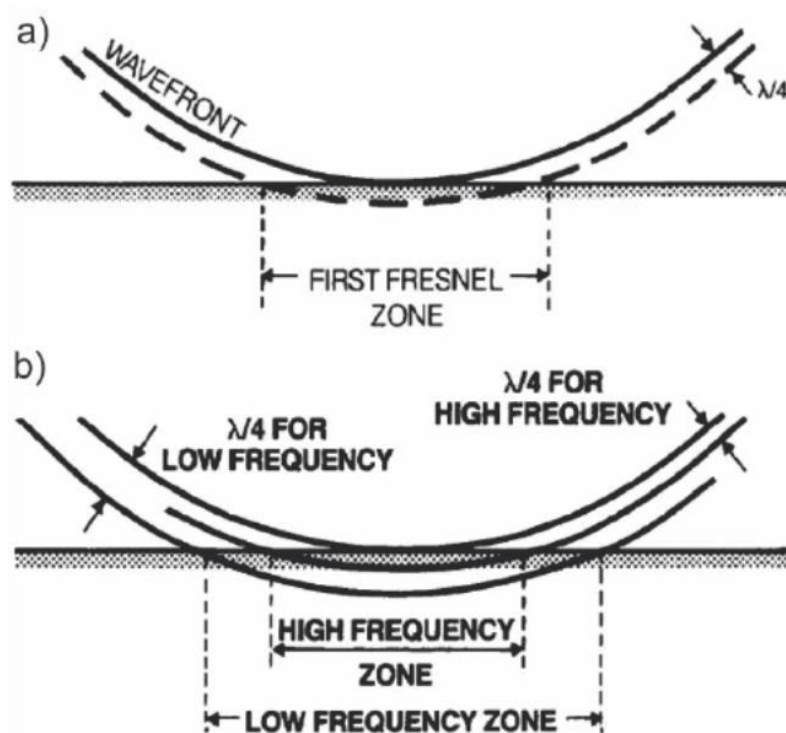


Figure 3.5: a) The first Fresnel zone is dependent on both the frequency and the range of the wave-front. It describes a reflector from where most of the energy is reflected and the arrival times of the different waves are less than half a period from the first encounter. b) Shows how the Fresnel zone is dependent on frequency by illustrating that the zone increases with a decreasing frequency. Figure is modified from Sheriff (1985).



The horizontal resolution of a seismic dataset could be improved by migration, which would decrease the Fresnel Zone and thus decreasing the horizontal distance needed in order for two features to be observed (Figure 3.6). Migration is a technique that improves the resolution by allowing the reposition of reflections that are located out of place because of the effects of a dipping reflector. It involves focusing the energy and collapsing various diffraction patterns (Brown, 1999). There are different results for 2D and 3D seismic. This is because 2D can only be migrated along the seismic line, which in turn will decrease the Fresnel zone to an ellipsoid perpendicular to the line. For 3D data, the migration process can collapse the Fresnel zone to a significantly smaller circle. This is because seismic waves appear in three dimensions, and by just applying migration in a two-dimensional specter one can only expect part of the improvements (Brown, 1999).

#### **Equation 3.6 - Horizontal resolution**

$$Hr = \frac{\lambda}{4}$$

*Equation 3.6: Hr = Horizontal resolution (m),  $\lambda$  = Wavelength (m)*

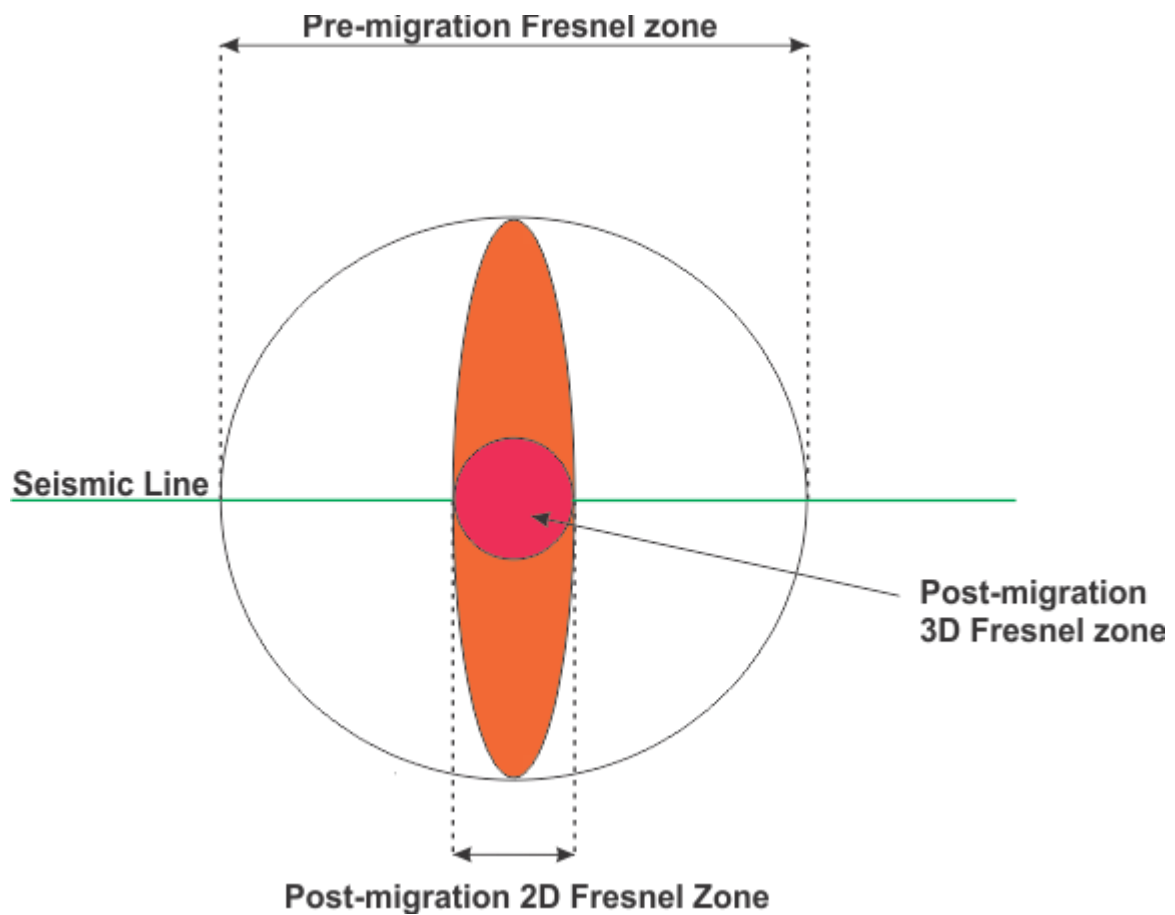


Figure 3.6: Migration of the Fresnel zone. The orange ellipsoid illustrates the collapse of the Fresnel zone in the inline direction of a 2-D seismic line. The zone is perpendicular to the inline. In 3D data the Fresnel zone can be shrunk down to a small circle illustrated by the red circle located firmly within the orange ellipsoid. Figure is modified from Brown (1999).

By using equation 3.5 and 3.6, the radius of the Fresnel zone have been calculated for the selected horizons. The two-way time shown in the table is the estimated depth to the interpreted horizons. Table 3 shows the various calculations done, both for pre-migration resolution and the resolution for a migrated dataset.

Table 3: Results from the calculation of the horizontal resolution on selected horizons in two separate datasets. The table displays the result from both pre-migration and post-migration resolution

Dataset	Horizon	Velocity	Frequency	TWT	Horizontal resolution, pre-migration	Horizontal resolution, post-migration
<b>BG1002</b>	Top Tempelfjord	4377.88 m/s	36.32 Hz	2.469s	570.72 m	30.13 m
<b>BG1002</b>	Top Bjarmeland	3990.71 m/s	30.98 Hz	2.712s	590.37 m	32.20 m
<b>WIN12003</b>	Top Tempelfjord	4377.88 m/s	31.25 Hz	2.492s	618.13 m	35.02 m
<b>WIN12003</b>	Top Bjarmeland	3990.71 m/s	27.15 Hz	2.650s	623.4 m	36.75 m

### 3.4 Artefacts and Noise

There are multiple seismic surveys used in this thesis and all of them seem to contain artefacts that can be found as survey footprints (Figure 3.7). These survey footprints are considered to be systematic noise that correspond with the acquisition geometry, and can easily be discovered in the data as straight lines parallel to the direction the data was sampled (inline direction). These features are important to be wary of as they can obstruct and complicate the interpretation process making it crucial to identify them so they are not mistaken for actual features (Bulat, 2005).

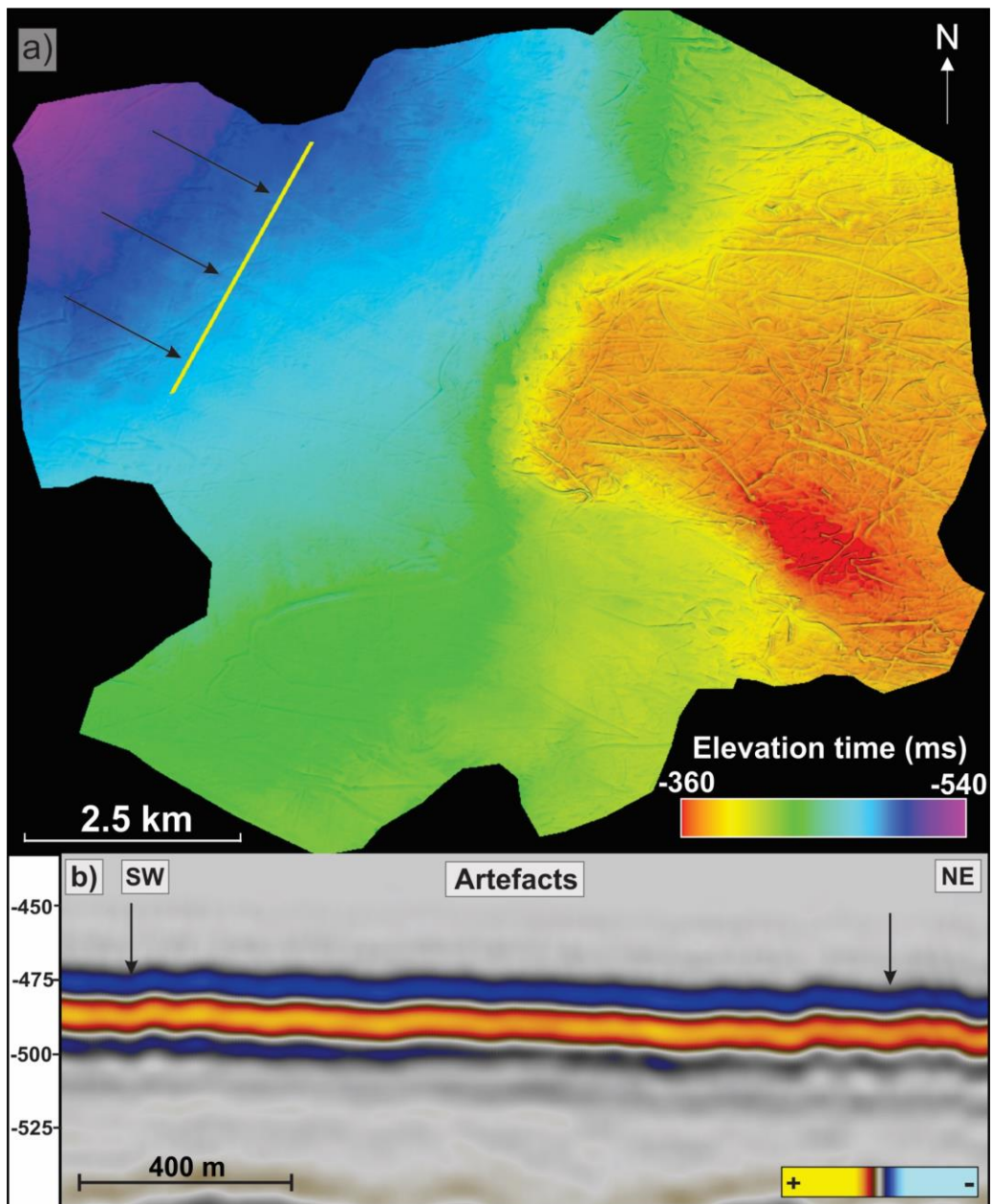


Figure 3.7: Seafloor surface generated from ST10M01. The artefacts are marked by black arrows in a) and b). b) Displays the seismic response of the artefacts. The yellow line in a) shows the location of the seismic section.

### 3.5 Well Data

Two wells were located in close proximity to the study area and have been used to correlate the different stratigraphic units located within the study area (Figure 3.8).

#### 3.3.1 Well 7124/3-1 Nysleppen Fault Complex

The well was drilled by Saga Petroleum ASA in 1987 on the coordinates 71° 45' 36.03" N, 24° 46' 49.99" E at a water depth of 273 m. The wildcat well led to the Bamse discovery, which was a small discovery containing both gas and oil with production being unlikely. The well was permanently abandoned in 1987 (NPDfactpages).

#### 3.3.3 Well 7226/11-1 Norsel High

A wildcat well drilled by Statoil ASA 1988. The well is located on the Norsel High, a structural high that marks the eastern border of the study area. The well penetrated the Early Permian unconformity and works as a reference well for the Paleozoic Formations; Ulv, Polarrev and Ørn (Figure 2.3). The well was a small gas discovery but not viable for commercial exploitation and was permanently abandoned on April 11, 1988 (NPDfactpages).

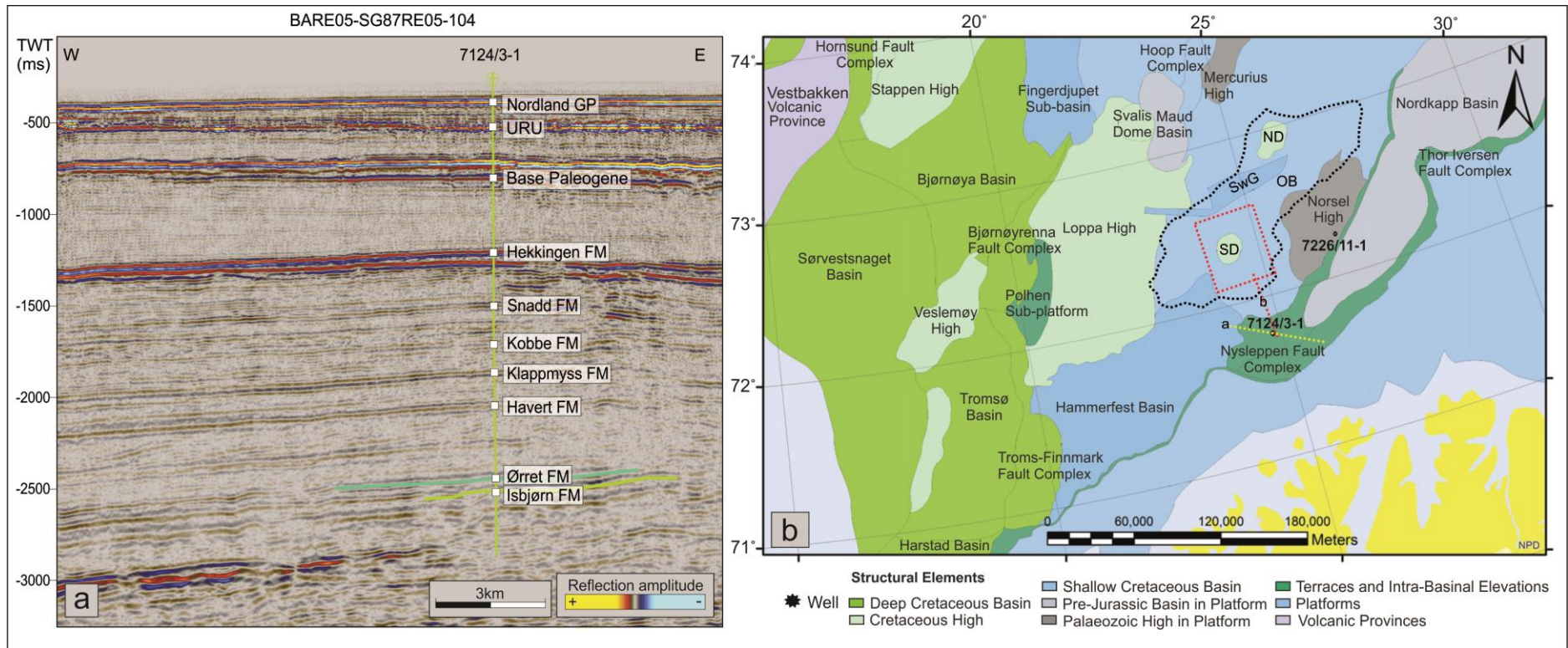


Figure 3.8: a) Well 7124/3-1 on seismic line BARE05-SG87RE05-104. The Ørret Fm. and Isbjørn Fm. signifies the Top Tempelfjord horizon and Top Bjarmeland horizon used in this study. b) Shows the location of the various wells in close proximity to the study area. Dotted black line shows the study area (OB). Dotted line (a) shows the location of the seismic line in figure 3.8 a) while the dotted line (b) a crossing line used to tie the well to the 3D survey (red square). ND = Norvarg Dome, SD = Samson Dome, SwG = Swaen Graben, OB = Ottar basin. Figure 3.8 b) is modified from Mattos et al. (2016)



## 3.6 Software

### 3.6.1 Petrel

Petrel, version 2016.1 (64-bit), produced by Schlumberger is the interpretation software used in this study. The main focus has been 3D seismic. The software contains several different tools that have been proven useful in the interpretation of seismic data, paleo-surfaces and for generating seismic attributes from interpreted surfaces and data volumes.

### 3.6.2 Seismic Attributes

#### *The RMS-Amplitude*

Emphasizes strong amplitudes within a pre-defined volume. The attribute calculates the square root of the sum of the squared amplitudes divided by the number of samples (Schlumberger, 2010). The attribute was used to display different high attribute anomalies within a unit and to interpret different depositional environments and features.

#### *Variance (Edge method)*

Estimates the trace-to-trace variance, over a particular sample interval and is independent of amplitude. The attribute produces lateral differences in acoustic impedance that is possible to interpret. Similar traces will produce low variance coefficients, while discontinuities will produce high variance coefficients (Schlumberger, 2010). It was used to generate time slices and aid in the interpretation of depositional environments and features.

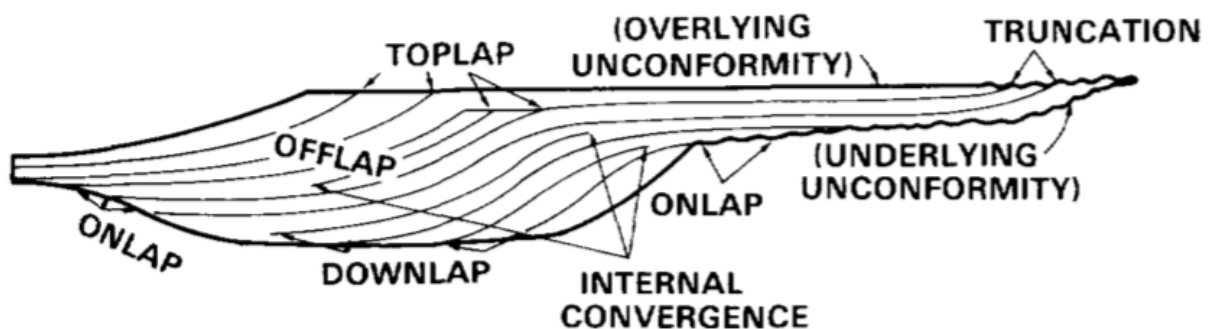
#### *Instantaneous Frequency*

Highlights the frequency differences within a particular sample (Schlumberger, 2010). Was used to interpret lateral changes in lithology, depositional environments and features.

### 3.7 Seismic Interpretation Method

#### 3.7.1 Seismic Sequence Stratigraphy

Essential to the field of sedimentology are the effects of uplift/subsidence, eustatic sea-level changes and the characteristics of the sediments deposited (Nichols, 2009). Depositional sequences are a result of the aforementioned effects, and it is defined as associated units constrained by unconformities and/or their correlative conformities (Mitchum et al., 1977; Vail, 1987; Veeken & van Moerkerken, 2013). The essential principle for identification of these sequences are based on various types of stratal terminations, e.g. erosional truncation, toplap, onlap, and downlap (Figure 3.9).



*Figure 3.9: The various reflection terminations and the different continuities. The names of the discontinuities are underlined. Figure from Mitchum et al. (1977)*

When a reflection terminates against an overlying surface it is called a toplap (Figure 3.9). This is usually interpreted as a result of non-deposition. Truncation describes the phenomenon of a reflection intersected by an unconformity. When a surface is tilted and the reflection is horizontal the termination is named onlap. Downlap describes an occurrence of an incline reflection terminating in a down-dip angle against a horizontal surface. Deformation can make it difficult to distinguish between onlap and downlap (Mitchum et al., 1977). Internal convergence and offlap are terminations that occur within a sequence and not in combination with sequence boundaries. Internal convergence defines the phenomenon when strata is thinning out and reaching below the seismic resolution limit. Offlap occurs in basins by prograding strata.

#### 3.7.2 Seismic Facies

Mitchum et al. (1977) defines seismic facies as mappable, three-dimensional seismic units which consists of groups of reflections with characteristics that differ from the


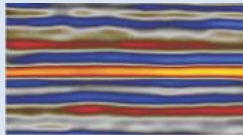

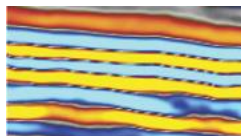

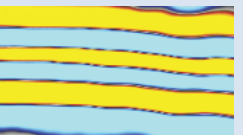
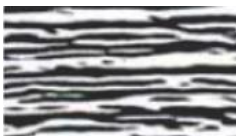
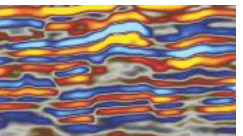

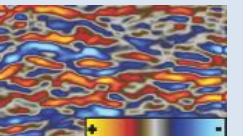
neighboring units. When these facies are grouped together by looking at the reflection characteristics and their external form, several interpretations can be made such as depositional- environment, processes and lithology (Mitchum et al., 1977; Veeken & van Moerkerken, 2013).

The reflection parameters listed in Table 4 give information regarding the subsurface geology. The reflection configuration displays the bedding pattern which in turn can be used to interpreted depositional processes and erosion. The configuration can also give information about fluid contacts that give rise to reflections (e.g. flat spots). Reflection continuity displays the continuity of the deposition. The continuity indicate homogenous depositions with a large lateral extent. The amplitude of a reflection gives information on the velocity – density contrast of various interfaces and the space between them. This is important for predicting the occurrence of hydrocarbons, as well as lateral changes in the bedding. Frequency gives information on the spacing between the reflectors and the lateral variations in interval velocity, which is associated with the occurrence of gas. By categorizing these parameters into different facies units it becomes possible to interpret their depositional environment, sediment source and the geological setting (Mitchum et al., 1977)

Table 4: An overview of the various reflection parameters and the corresponding interpretation that is possible to conduct from each parameter. Modified from Mitchum et al. (1977).

Reflection Parameter	Geological Interpretation
<b>Configuration</b>	<ul style="list-style-type: none"> <li>- Bedding Pattern</li> <li>- Depositional Properties</li> <li>- Erosion and Paleotopography</li> <li>- Fluid Contacts</li> </ul>
<b>Reflection Continuity</b>	<ul style="list-style-type: none"> <li>- Bedding Continuity</li> <li>- Depositional Process</li> </ul>
<b>Reflection Amplitude</b>	<ul style="list-style-type: none"> <li>- Velocity – Density contrast of the various interfaces</li> <li>- Bed Spacing</li> <li>- Fluid Content</li> </ul>
<b>Reflection Frequency</b>	<ul style="list-style-type: none"> <li>- Bed Thickness</li> <li>- Fluid Content</li> </ul>
<b>Interval Velocity</b>	<ul style="list-style-type: none"> <li>- Lithofacies Estimation</li> <li>- Porosity Estimation</li> <li>- Fluid Content</li> </ul>

Table 5: Examples of different seismic facies based on frequency, continuity, reflection amplitude and configuration. a-e) Examples in black-white are extracted from Veeken (2007b) while the facies in red-blue is from WIN12003. Modified from Veeken (2007b).

Seismic Facies	Reflection Geometry	Amplitude Characteristics	Seismic Facies after (Veeken, 2007b)	Examples from Survey WIN12003
a)	Parallel Continuous	Medium amplitude		
b)	Parallel Continuous	High amplitude		
c)	Parallel Continuous	High frequency & high amplitude		
d)	Subparallel discontinues	High amplitude		
e)	Chaotic	Medium amplitude		

The internal reflections are important, however, it is also crucial to have an understanding of the external forms of seismic facies units (Table 6). These need to be interpreted in order to be able to understand the geometric interrelation and depositional setting of the various facies units. There are a number of different shapes and geometries which in turn can be further subdivided based upon the internal reflection configuration (Mitchum et al., 1977).

Table 6: Facies parameters and their geological interpretation. Modified from Mitchum et al. (1977).

Reflection Configurations	External forms of sequences and seismic facies units
<p><b><u>Principal Stratal Configuration</u></b></p> <ul style="list-style-type: none"> <li>• Parallel</li> <li>• Subparallel</li> <li>• Divergent</li> <li>• Prograding Clinoforms               <ul style="list-style-type: none"> <li>- Sigmoid</li> <li>- Oblique</li> <li>- Complex sigmoid-oblique</li> <li>- Shingled</li> <li>- Hummocky clinoform</li> </ul> </li> <li>• Chaotic</li> <li>• Reflection-free</li> </ul> <p><b><u>Modifying terms</u></b></p> <ul style="list-style-type: none"> <li>• Even                      Hummocky</li> <li>• Wavy                      Lenticular</li> <li>• Regular                    Disrupted</li> <li>• Irregular                  Contorted</li> <li>• Uniform Variable</li> </ul>	<ul style="list-style-type: none"> <li>• Sheet</li> <li>• Sheet drape</li> <li>• Wedge</li> <li>• Bank</li> <li>• Lens</li> <li>• Mound</li> <li>• Fill</li> </ul>





## 4. Results

In this chapter, the main findings from the seismic interpretation from the 3D-surveys (Figure 3.1) will be presented. The seismic stratigraphic framework that has been established for the Late Paleozoic – Early Triassic units within the study area, are presented and described stratigraphically (oldest to youngest). In addition to interpreted seismic profiles, surface- and time-thickness maps will be presented.

Larssen et al. (2005) proposed a lithostratigraphic scheme for the Paleozoic succession in the Barents Sea. This has been used throughout this study as its nomenclature is well established and broadly accepted in the appropriate academic community.

It should be noted that the seismic appearance of the horizons vary with datasets and their resolution.

A color code scheme has been assigned to the interpreted seismic units along with the related boundaries (Figure 4.1). The horizons mapped in the study area are presented in Figure 4.2.

The Paleozoic stratigraphy have been annotated after the lithostratigraphic chart from NPD (Figure 2.3), with corresponding formation names. To simplify, “Group/Formation” has been left out in the following description.

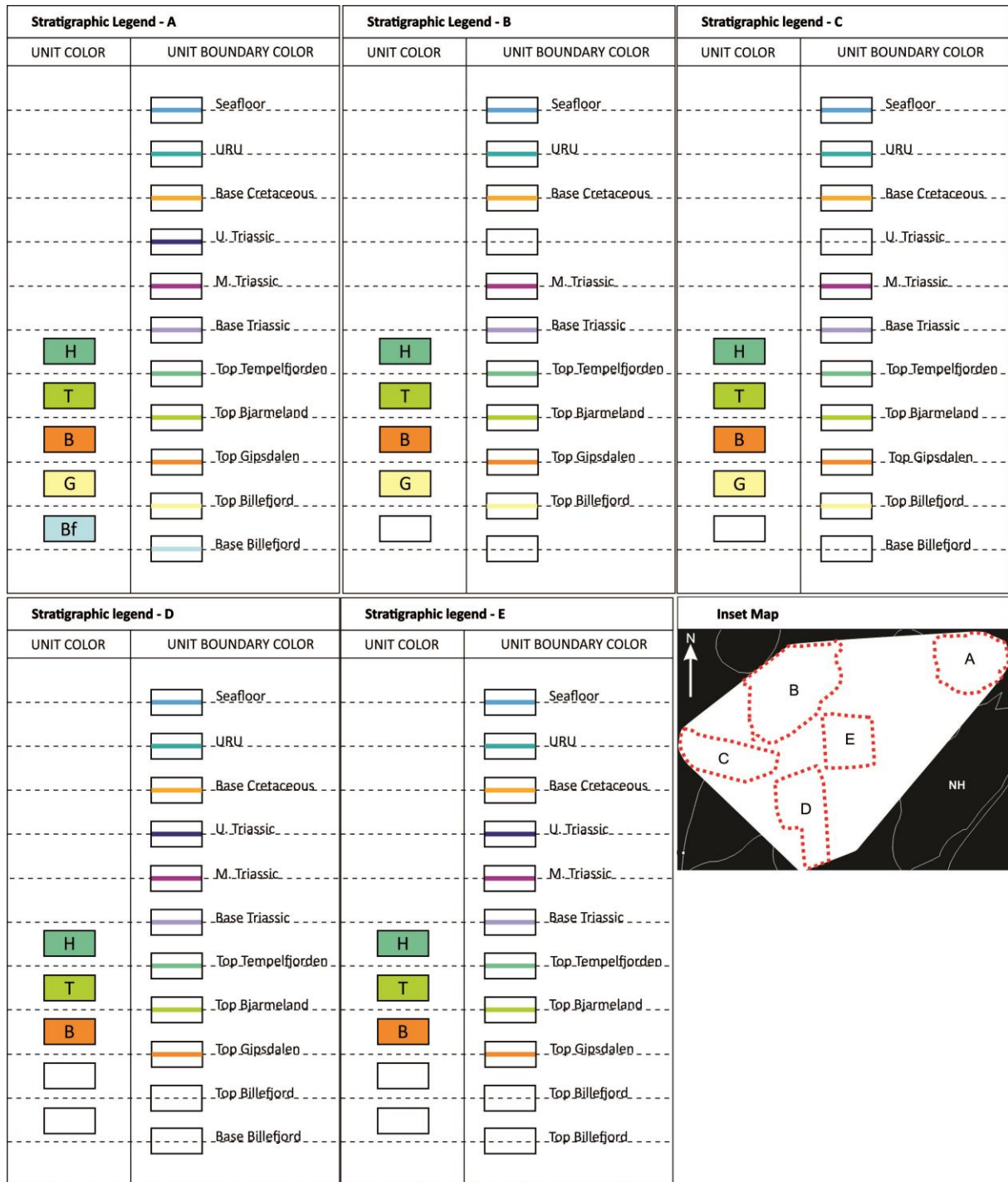


Figure 4.1: Stratigraphic legend displaying the color code and the seismic stratigraphy established in the different datasets. The white boxes symbolizes the absence of the seismic unit and horizon in that particular dataset. H = Havert Formation, T = Tempelfjorden Group, B = Bjarmeland Group, G = Gipsdalen Group, Bf = Billefjorden Group.

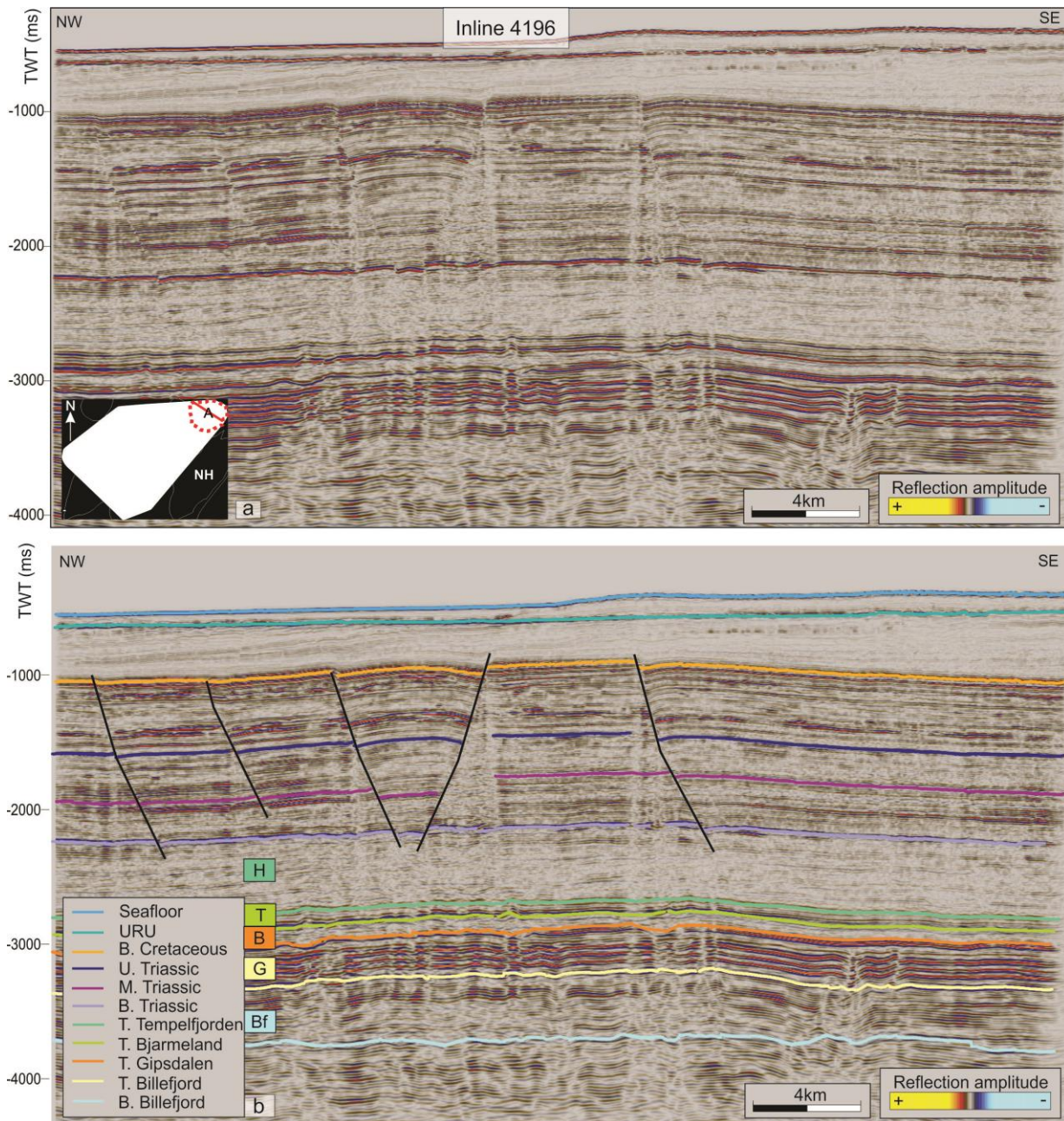


Figure 4.2: a) Inline 4196 from ST10M01. The location of the seismic line is shown in the inset map in the lower left corner. b) Interpreted seismic line showing the main seismic units along with the interpreted horizons. See Figure 4.1 for unit names.

## 4.1 Horizons

### 4.1.1 Base Billefjord

The Base Billefjord horizon represents the lowest stratigraphic level interpreted in this study (Figure 4.2). It is present only in the northern part of the study area (Figure 4.1). The horizon is represented by an overall positive reflection coefficient. It is characterized by low- to medium amplitude and is discontinuous throughout the majority of the interpreted area. However, locally, the horizon appears as continuous before becoming less prominent. The horizon separates the chaotic reflections of the presumed basement from the overlying Billefjorden Group (Figure 4.2).

The horizon resides on a relatively stable depth (twt), only interrupted by two anomalies in the northeast and south, respectively (Figure 4.3). The anomaly in the northeast represents a high, where the horizon is situated at a depth of approximately -3850 ms (twt), while the anomaly in the south represents a low at a depth of -3875 ms (twt).



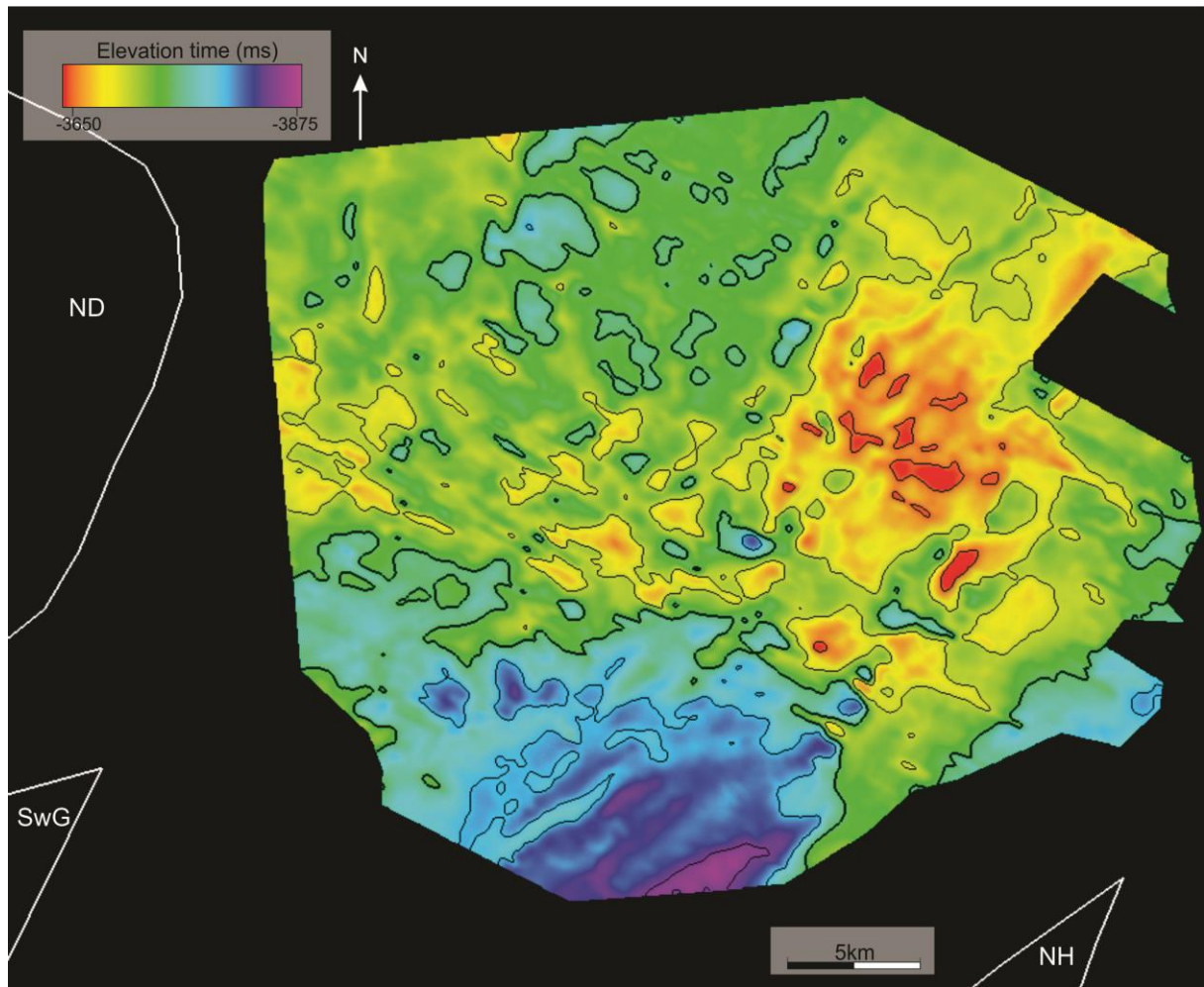


Figure 4.3: Base Billefjord horizon shown in elevation time (ms). ND = Norvarg Dome, SwG = Swaen Graben, NH = Norsel High. Contour intervals set at 50ms (tw).

#### 4.1.2 Top Billefjord

Top Billefjord is interpreted along a semi-continuous to discontinuous reflection. The horizon is interpreted along a positive acoustic impedance. It is interpreted in an area oriented from the northeast to the southwest in the study area, omitting the more central parts (Figure 4.1). It is characterized by an alternating amplitude, changing from low to high throughout the study area, with a semi-continuous to discontinuous character.

The Top Billefjord horizon dips from -2900 ms (twtt) in the west to approximately -3500 ms (twtt) in the northeast (Figure 4.4). The steepest gradients are located in close proximity to the Norvarg Dome.



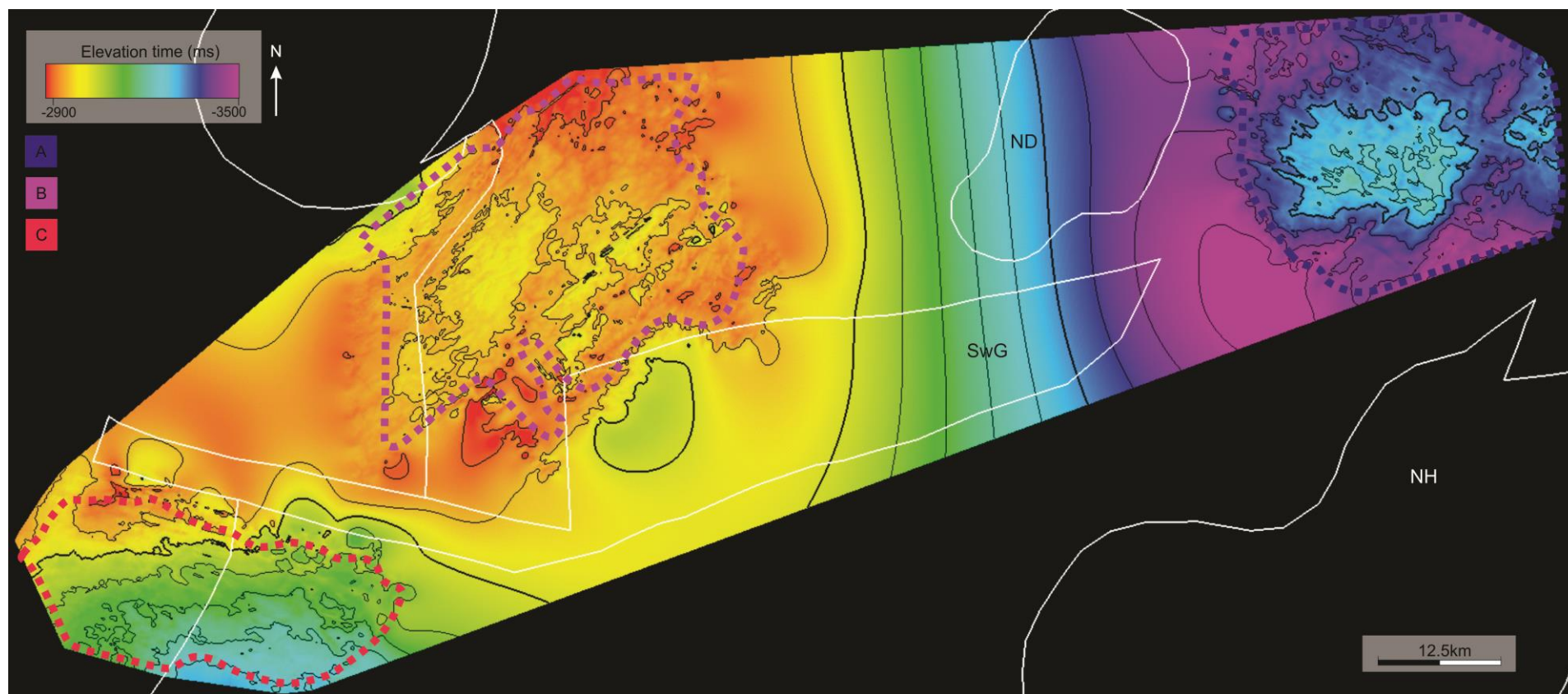


Figure 4.4: Top Billefjord Horizon shown in elevation time (ms). Contour intervals are set at 50ms. The dotted line represent the datasets where the horizon is present. Petrel interpolated the area between them.

#### 4.1.3 Top Gipsdalen

The Top Gipsdalen horizon is interpreted along a semi-continuous to discontinuous reflection for the majority of the study area (Figure 4.5). In the southwestern part of the study area the horizon has been interpreted on a trough, representing a negative reflection coefficient, but in general the seismic pick of the horizon is represented by a positive reflection coefficient, and has been interpreted on a peak. The horizon is characterized by an alternating amplitude, changing from low to high throughout the study area. The continuity and the visibility of the horizon changes throughout the area, becoming discontinuous in the central and southwestern parts of the study area. The polarity difference could be due to uncertainties with the seismic pick.

The horizon has an overall dip towards the south. The shallowest areas (in twt) are observed in the western part of the study area with stable values of approx. 3000 ms (twt) in the eastern parts, shallowing towards the west (Figure 4.5). The Swaen Graben seems to separate the horizon into two distinct areas, where the western side of the horizon is situated at a shallower depth (-2700 ms twt) compared to the eastern side, where the horizon plunges towards the southeast, and reaches a depth of approx. -3500 ms (twt) (Figure 4.5).

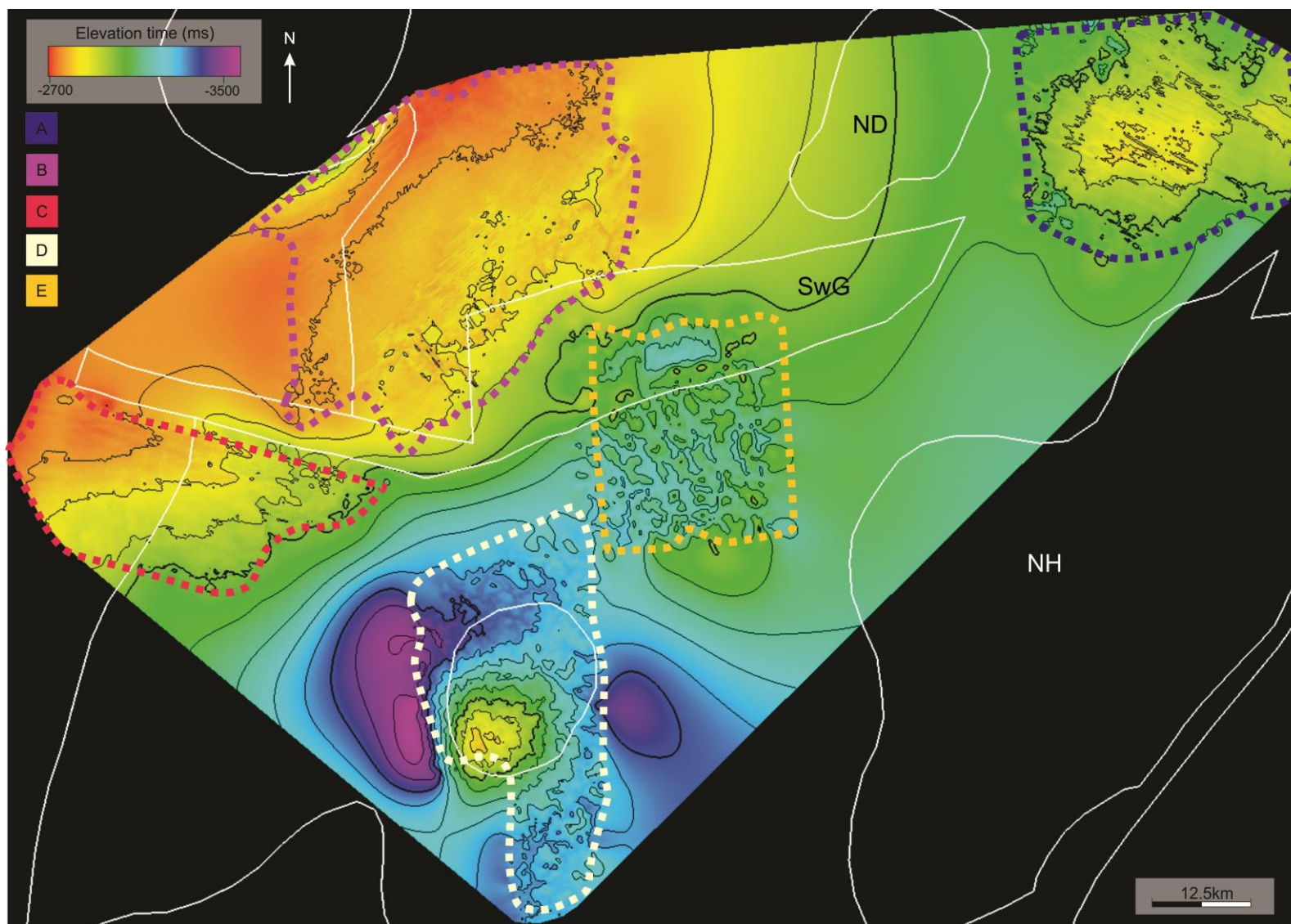


Figure 4.5: Top Gipsdalen horizon. The surfaces that are from the various datasets are marked by the boundaries in different colors. Petrel has interpolated the data between them.

#### 4.1.4 Top Bjarmeland

Top Bjarmeland was tied to well 7124-3/1 located in the Nysleppen Fault Complex (Figure 3.8). It is interpreted along an overall positive reflection coefficient, represented by a peak, and as a semi-continuous to discontinuous reflection with a varying amplitude, changing from low to high. The horizon characteristics change throughout the study area, in the southwestern part, the amplitude is very low making interpretation at times tentative.

Top Bjarmeland displays a similar trend as seen in deeper horizons, with an overall dip towards the east and with the shallower parts located in the western parts of the area (Figure 4.6). In the eastern area, the horizon is situated at depths of approx. -2800 ms (tw). There is a gentle shallowing when moving towards the west, and crossing the Swaen graben, with the western area displaying values of approx. -2600 ms (tw) (Figure 4.6).



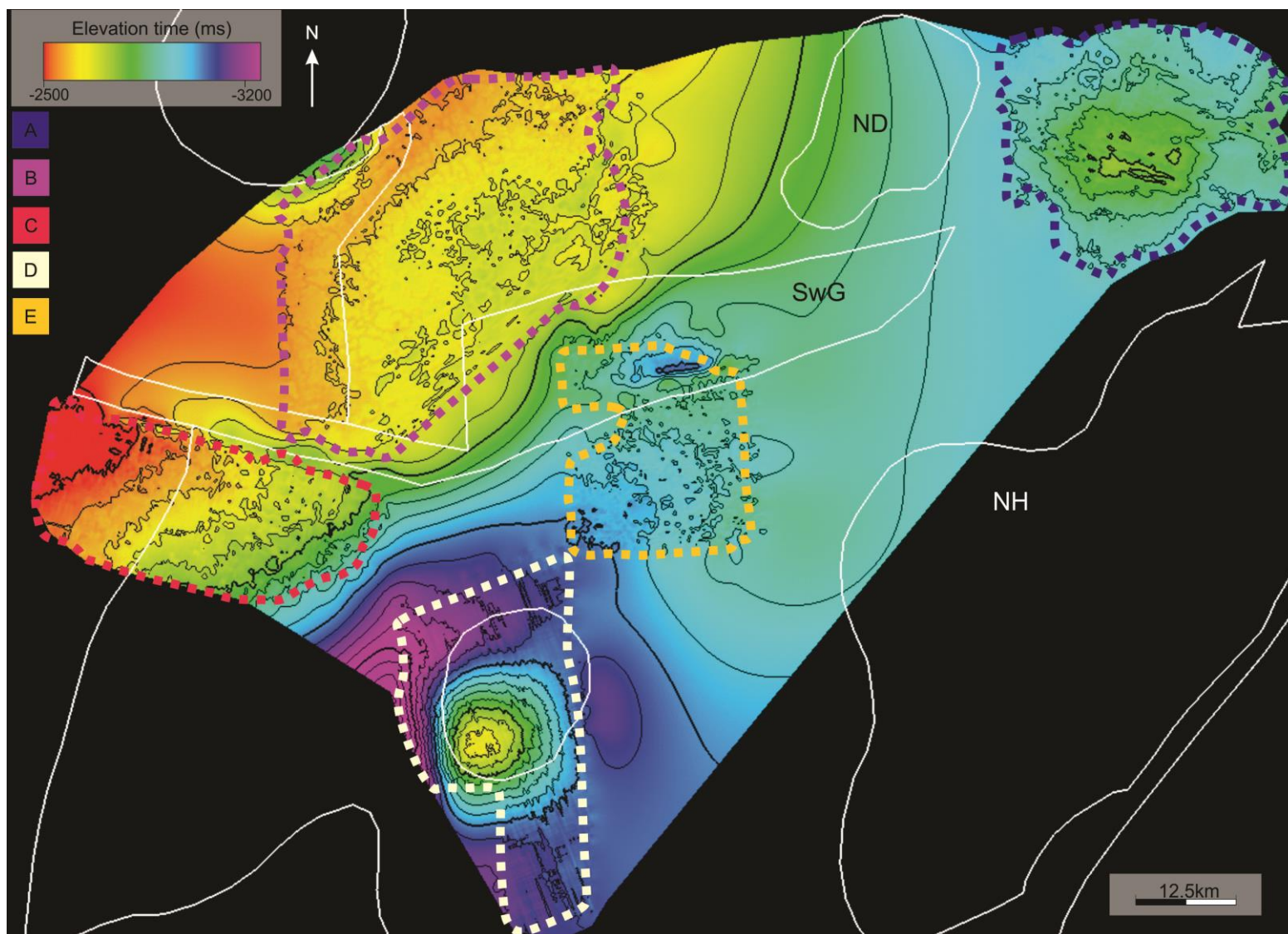


Figure 4.6: Top Bjarmeland horizon displayed in elevation time (ms). The contours are set to 50 ms. Petrel interpolated the area between the different dotted areas.

#### 4.1.5 Top Tempelfjorden

Top Tempelfjorden was tied to well 7124-3/1 located in the Nysleppen Fault Complex (Figure 3.8). The horizon is interpreted along a peak, representing a positive reflection coefficient for the majority of the study area, and along a semi-continuous to discontinuous reflection with a varying amplitude, changing from low to high. In the northern parts of the area, the horizon is interpreted on a trough. This is because of uncertainties with the well-tie. The well is located outside the study area, making the interpretation at times tentative and prone to uncertainties, because of the large distances from well to study area.

The Top Tempelfjorden horizon has a gentle dip towards the east, with a low located in the southeastern part of the study area in close proximity to the Samson Dome (Figure 4.7). In the eastern part of the study area, the horizon is at approx. 2500 ms (twl), only interrupted by the gentle sloping towards the west and the low in the southeast. The Swaen Graben separates the two areas, with the highest area (-2300 ms twl) located on the western side of the graben (Figure 4.7).

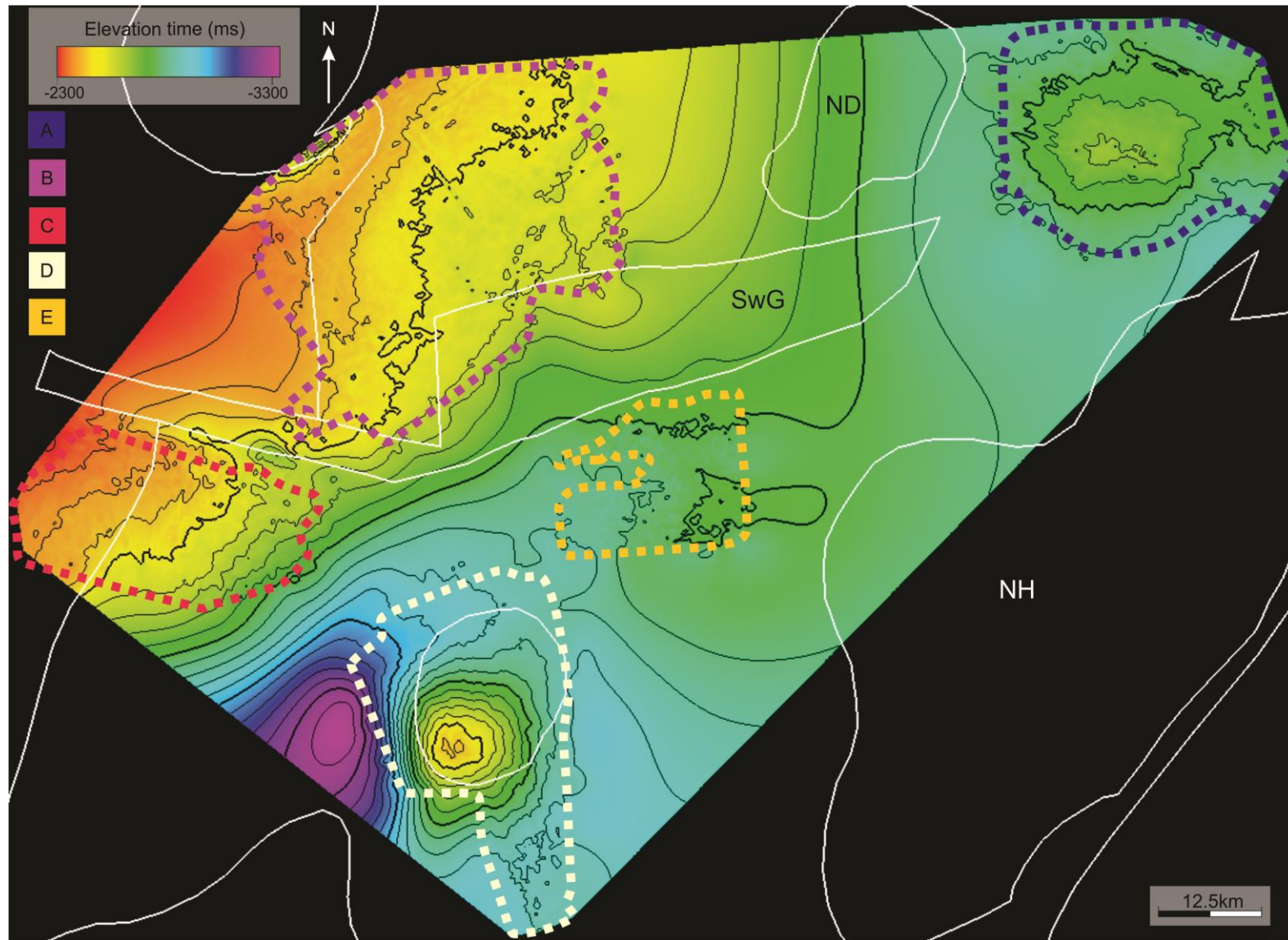


Figure 4.7: Top Tempelfjorden horizon displayed in elevation time (ms). The contours are set to 50 ms. Petrel interpolated the area between the dotted areas.



#### 4.1.6 Base Triassic

The Base Triassic horizon represents the youngest stratigraphic level mapped in this study (Figure 4.1, Figure 4.2 & Figure 4.8). The horizon is characterized by a very low- to medium amplitude and a semi-continuous to discontinuous reflection. It is interpreted along a peak, indicating a positive reflection coefficient for the majority of the study area, but does appear as a trough at certain locations. The change in polarity could be due to uncertainties with the interpretation pick.

The horizon displays the same trend as the deeper horizons in the study area (Figure 4.7, Figure 4.8). The horizon can be defined in two distinct areas, with the western part of the study area being situated at shallower depths (-2050 ms twt) and the eastern area situated deeper (-2450ms twt), with the Swaen Graben separating the two areas (Figure 4.8). The horizon has a low relief but shows a deepening trend towards the south and a sharp shallowing towards the northwest.

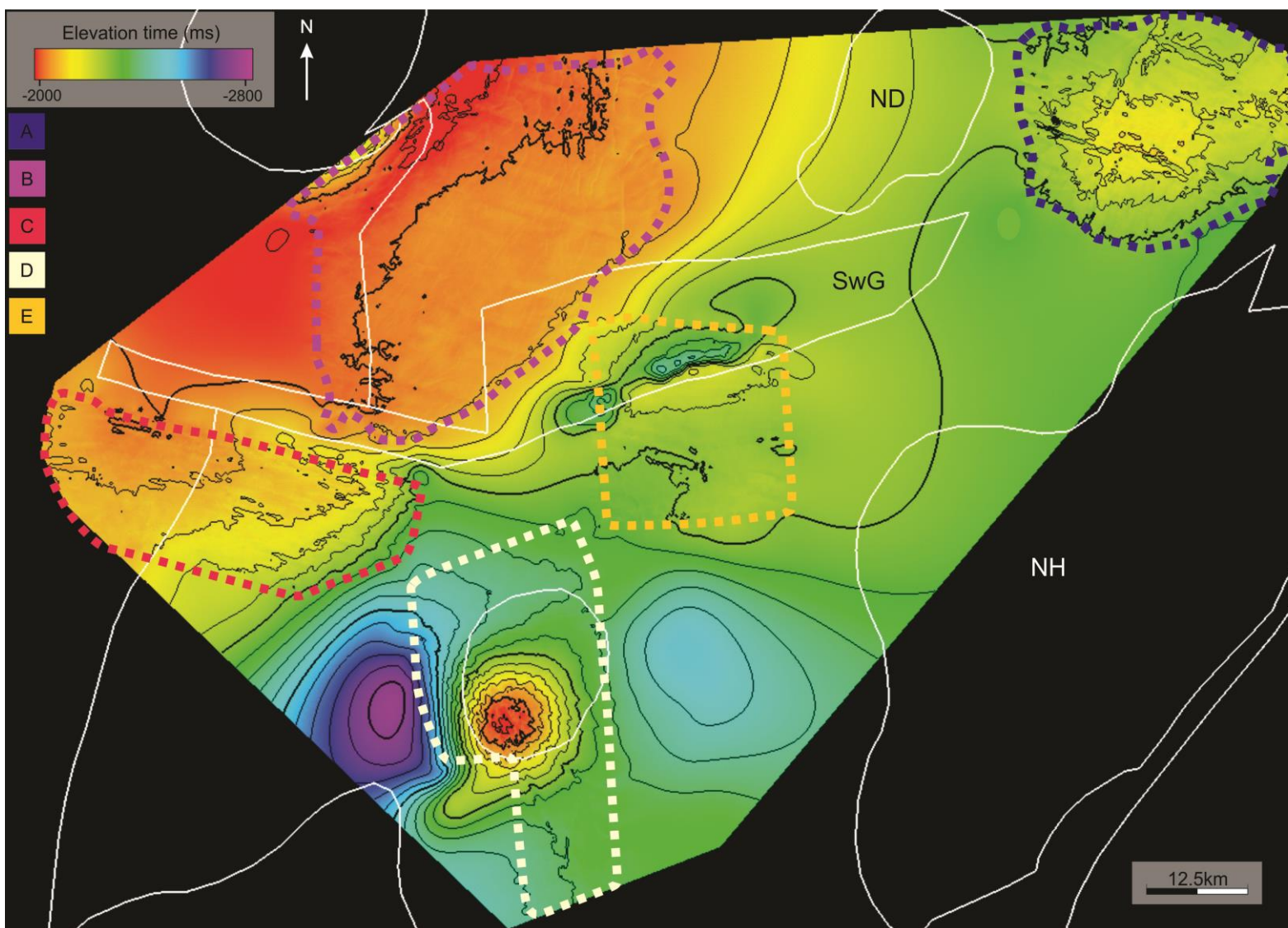


Figure 4.8: Base Triassic horizon displayed in elevation time (ms). The contours are set to 50 ms. The sections between the dotted areas was interpolated by Petrel.

## 4.2 Seismic Units

### 4.2.1 Billefjorden Group

The Billefjorden Group (Figure 4.9) is stratigraphically limited by the Base Billefjord horizon at the base and the Top Billefjord horizon at the top. It is mainly confined to the northern parts of the study area, in close proximity to the Norvarg Dome.

The highest sediment thickness occurs in the central part of the study area, reaching a time-thickness of 550 ms (tw<sub>t</sub>) (Figure 4.10 A). The thickness decreases gradually towards the edges of the area, reaching its thinnest concentration (325 ms tw<sub>t</sub>) in the southeast. An external lens-like geometry characterizes the unit, with the central parts having a thickness of approximately 550 ms (tw<sub>t</sub>).

Sub-parallel, semi-continuous to discontinuous reflections of low- to medium-amplitude characterize the internal seismic signature of the Billefjorden Group. In some areas, the internal reflections are located within a semi-transparent pattern (Figure 4.9). High-amplitude reflections appear locally and seem to follow the thickness trend of the unit (Figure 4.10 B), with the highest amplitudes situated along the margin of the mapped area, where the unit is thinnest. Low-amplitude reflections appear in the central part of the mapped area, where the sediment has the highest thickness (Figure 4.10 A-B). The amplitudes change vertically, with the lowest amplitudes near the base of the unit, while higher amplitudes dominate the upper half (Figure 4.10 C).

Subtle, elongated and positive features can be observed within the unit (Figure 4.11 A). These seem to be concentrated in the center of the unit and can be traced with a dominantly SW-NE and E-W orientation. These features seem to appear less frequently in the southern part of the study area, with a higher concentration and occurrence in the northern parts (Figure 4.11 A-C). The elongated features seem to appear as limited seismic high amplitude reflections within the unit (Figure 4.11). The features range in size from 1-4 km in length, with a width ranging from 40 – 150 meters.



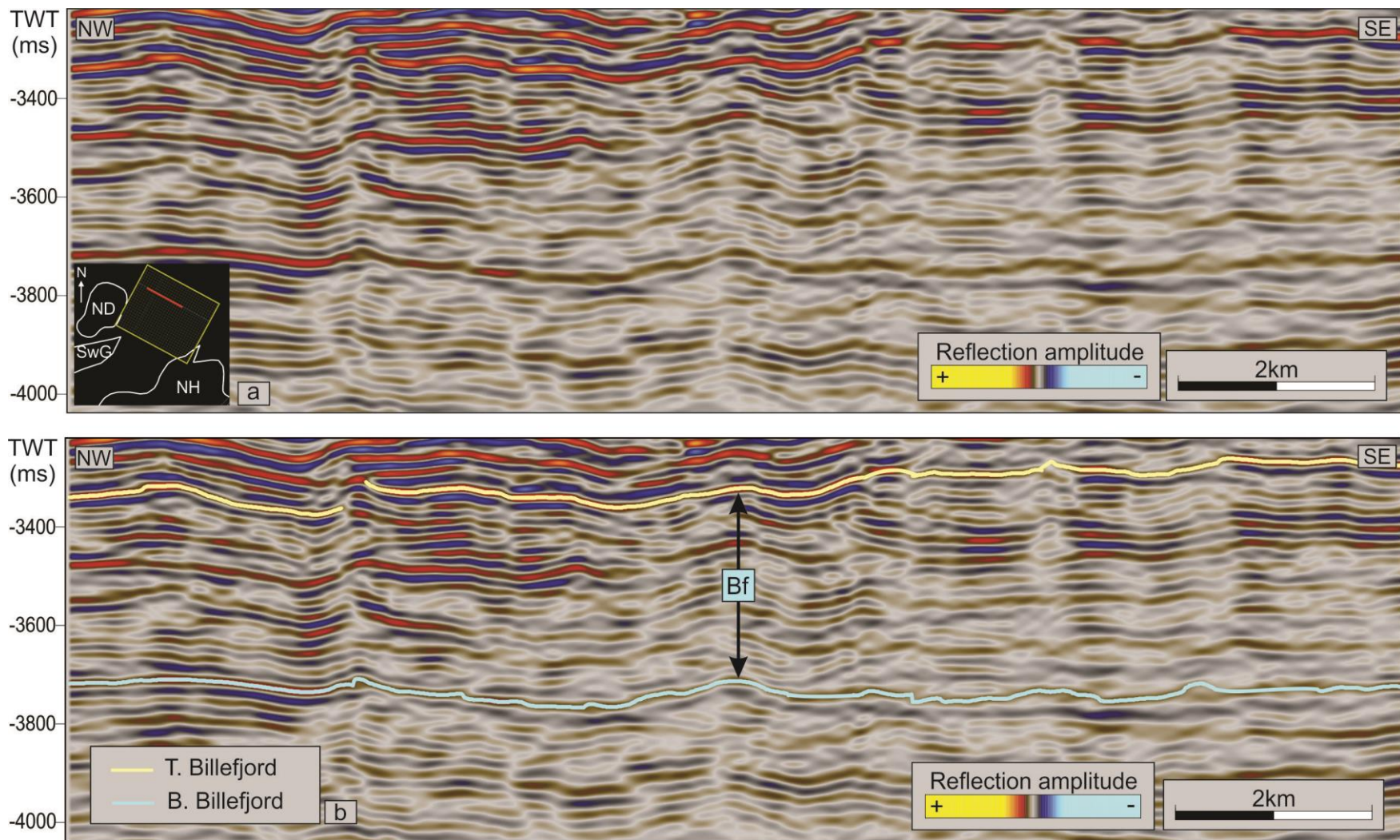


Figure 4.9: Inline 3996 from ST10M01 showing the Billefjorden Group (Bf). The unit is confined by the horizons Base- and Top Billefjord. A) is an uninterpreted section, while B) shows the interpreted section.



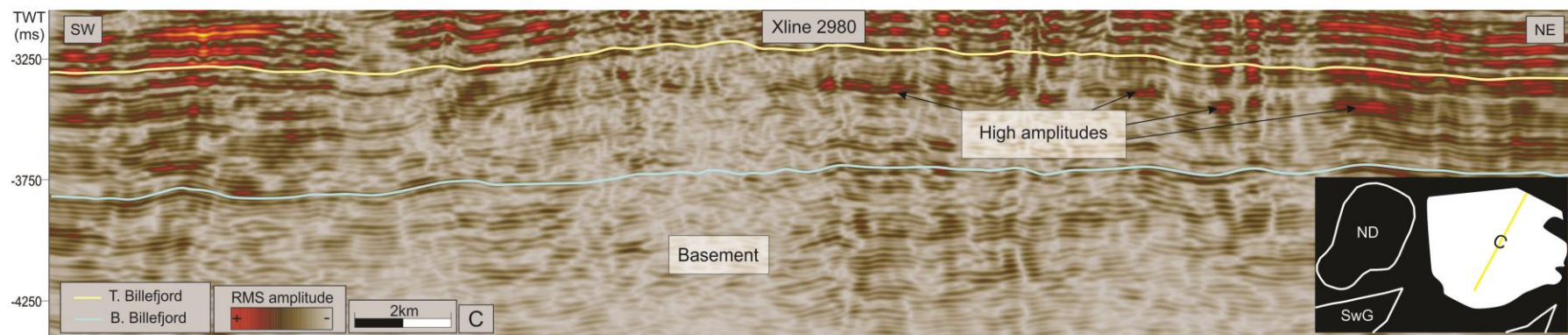
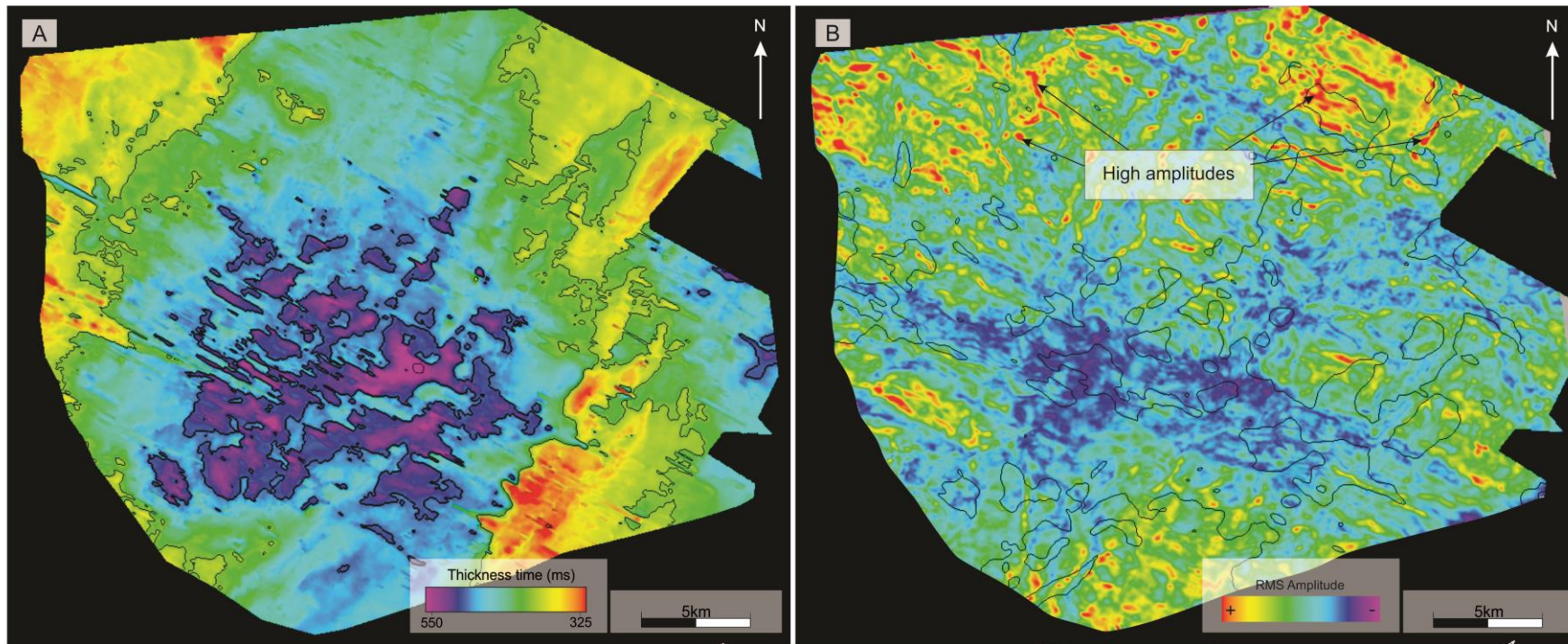


Figure 4.10: a) Time - thickness map of the Billefjorden Group. b) RMS map of the Billefjorden Group, generated from the data volume that comprises the entire Billefjorden Group, c) X-line 2980 displaying the high amplitudes. The location of the X-line is shown on the RMS-surface. The inset map shows the location of A), B) and the seismic line C). ND = Norvarg Dome, SwG = Swaen Graben.

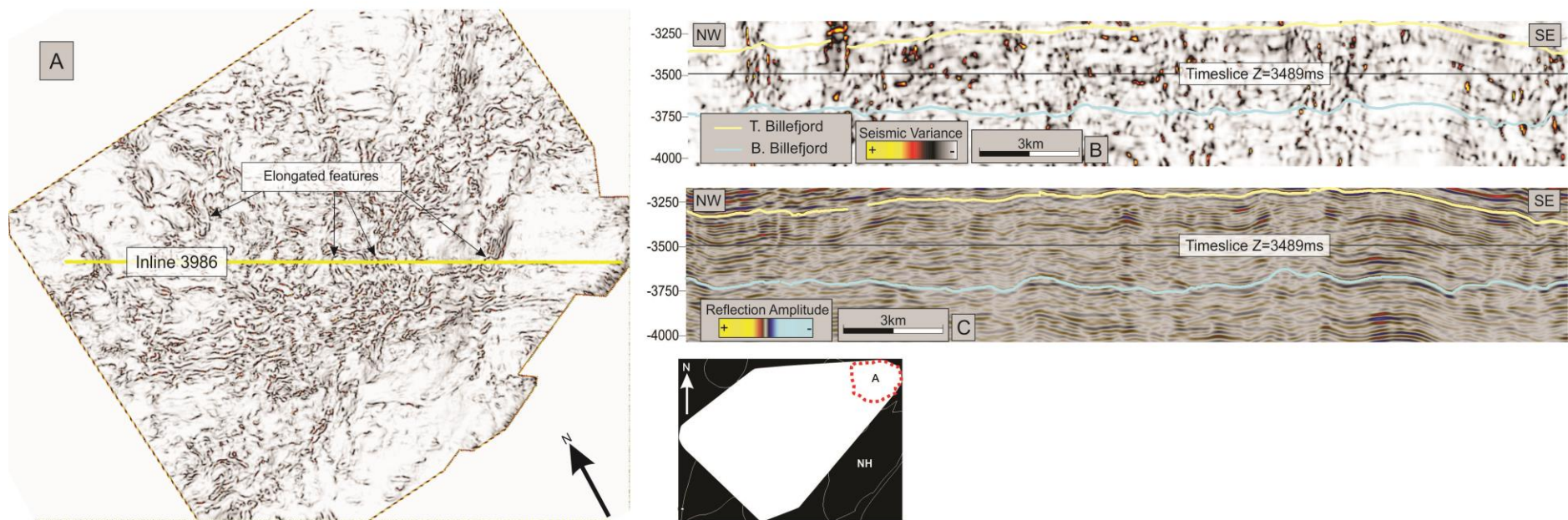


Figure 4.11 A) Variance time slice taken at -3489 ms. B) Variance in line, the location of the inline is displayed by the yellow line in A. C) Seismic section of the same inline (3986).



#### 4.2.2 Gipsdalen Group

The Gipsdalen Group is stratigraphically limited by the Top Billefjord horizon at the base and the Top Gipsdalen horizon at the top (Figure 4.12). The unit is distributed in a W/SW to E/NE orientation in the study area (Figure 4.13).

The largest sediment thickness appears in the NE of the study area, towards the Norvarg Dome, reaching a time-thickness of 375 ms (twt) (Figure 4.13). The thickness decreases towards the SW of the area, reaching the thinnest concentration in the western part with a time-thickness of 50 ms (twt).

Parallel to sub-parallel, continuous to semi-continuous reflections of low- to high amplitudes characterize the internal seismic signature of the Gipsdalen Group. In some areas, the internal reflections display a semi-transparent pattern (Figure 4.12 C). High amplitudes appear locally, with the highest concentration in the west (Figure 4.14 B). Towards the north, a seismic pattern of low-amplitude reflections resulting in a reflection-free zone is observed (Figure 4.14 A). The low-amplitude pattern ranges in length from 13km when stretching from N-S and a length of 13.2km, stretching from W-E. The width of the zone is approx. 0.7km. The central zone of low-amplitudes have a width of 5.7km and a length of 11km.

Circular features occur in the study area along a time slice, but with an uneven distribution (Figure 4.15). The highest concentration seem to appear along the western margin of the study area (Figure 4.15 B). The width of the circular features vary greatly, with the largest located in the western part having a diameter of approx. 4.7km. They appear to be decreasing to the SW, where they seem to have a width of 1km. The features seem to appear in clusters, concentrated at certain areas of the time slices. They do not appear as isolated features (Figure 4.15) The circular features produce elongated highs in the seismic profiles (Figure 4.16 a-c). These elongated highs are generally situated close to the base of the unit.



Elongated features can also be observed within the unit. These features are most prominent in the north and southwest (Figure 4.15). They vary in size (Figure 4.15 A). The most noticeable elongated feature in the northern area produces a series of velocity push-downs in the seismic (Figure 4.15 A). The feature has a width of 0.35km.

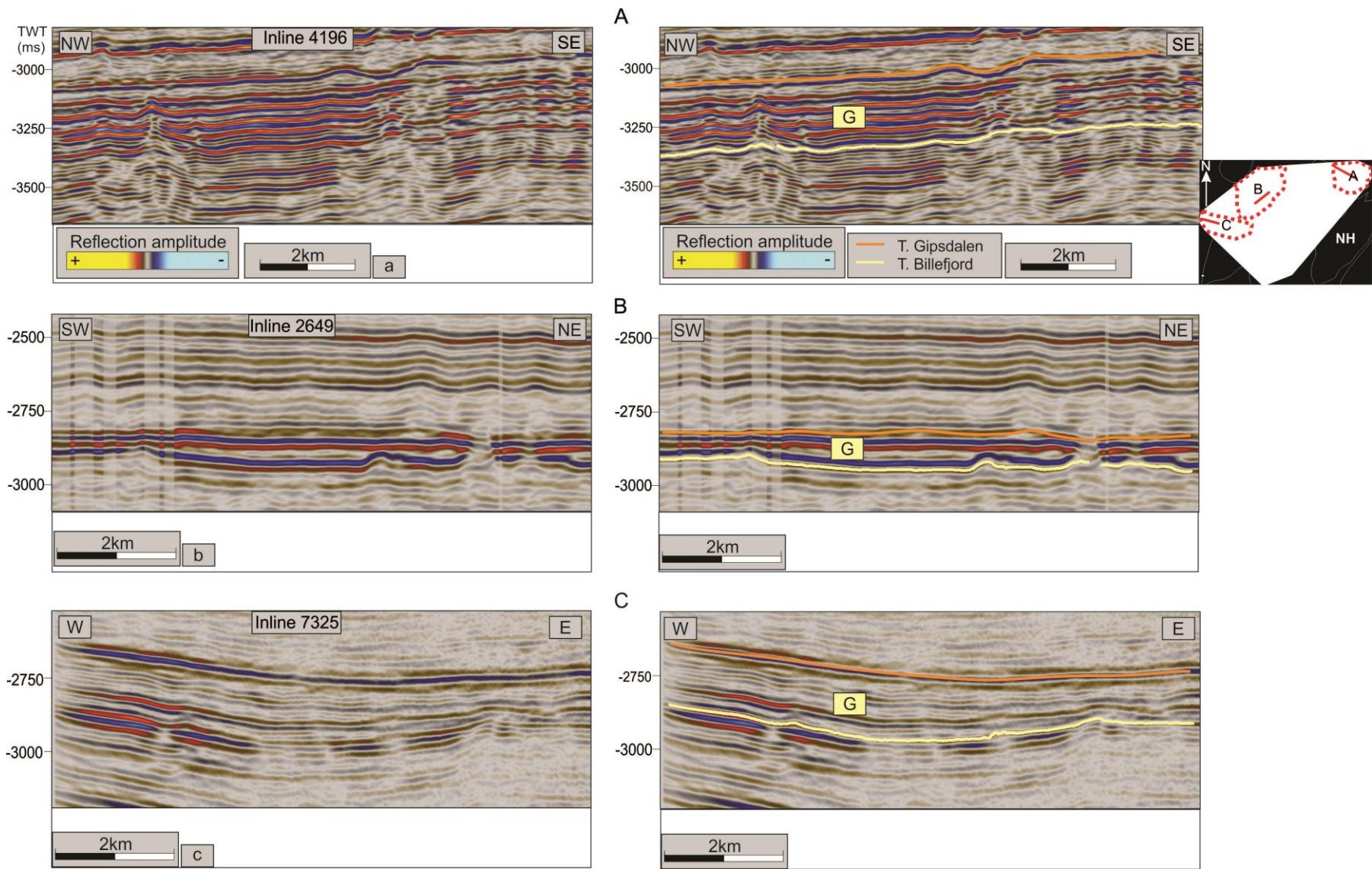


Figure 4.12: Seismic section showing the Gipsdalen Group throughout the study area. The location of the various inlines are shown in the inset map. Uninterpreted sections to the left, while the interpreted sections are displayed on the right.

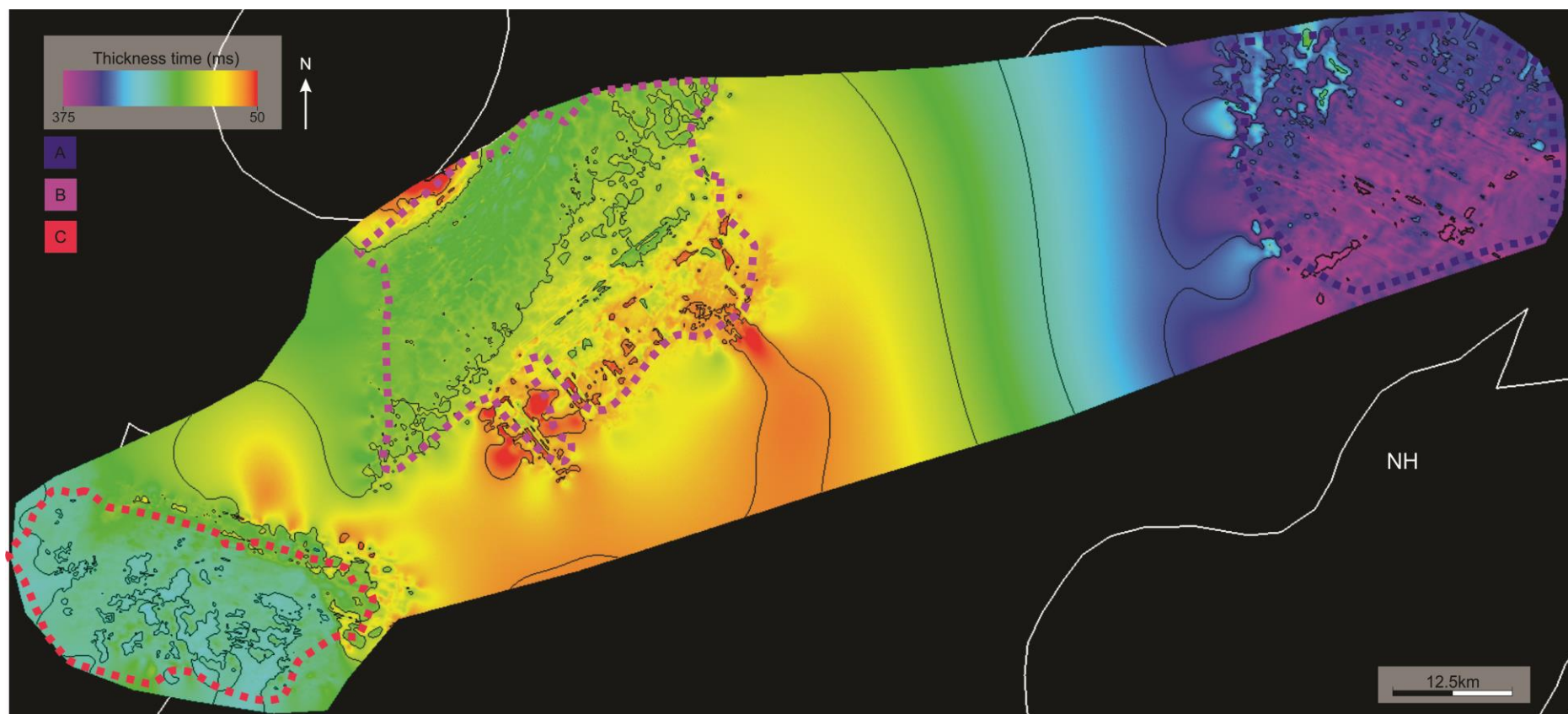


Figure 4.13: Time-thickness map of the Gipsdalen Group. The color legend shows the name of the different areas. The area between them have been interpolated.



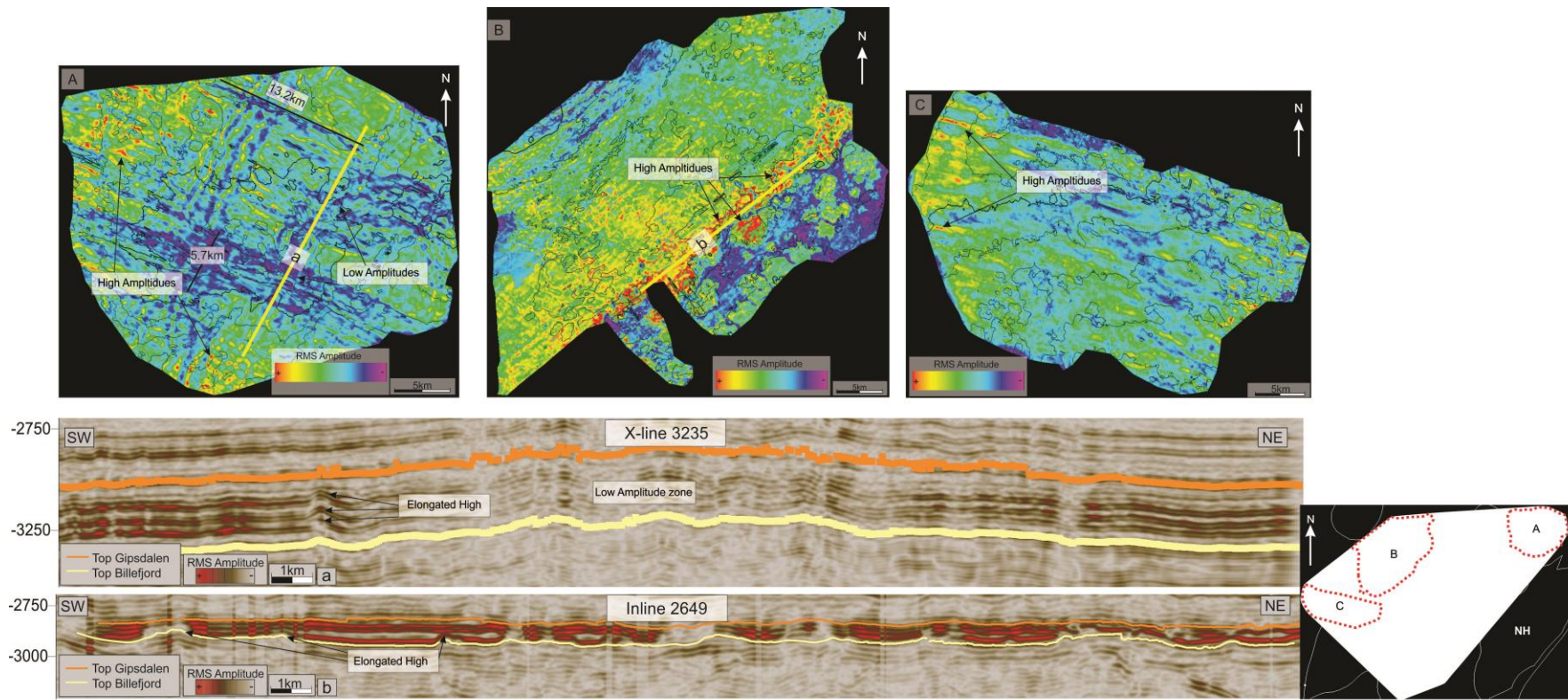


Figure 4.14: RMS-surface attribute generated of the Gipsdalen Group. The inset map displays the location of the different surfaces. The RMS surfaces are generated from the data volume that comprises the entire Gipsdalen Group.

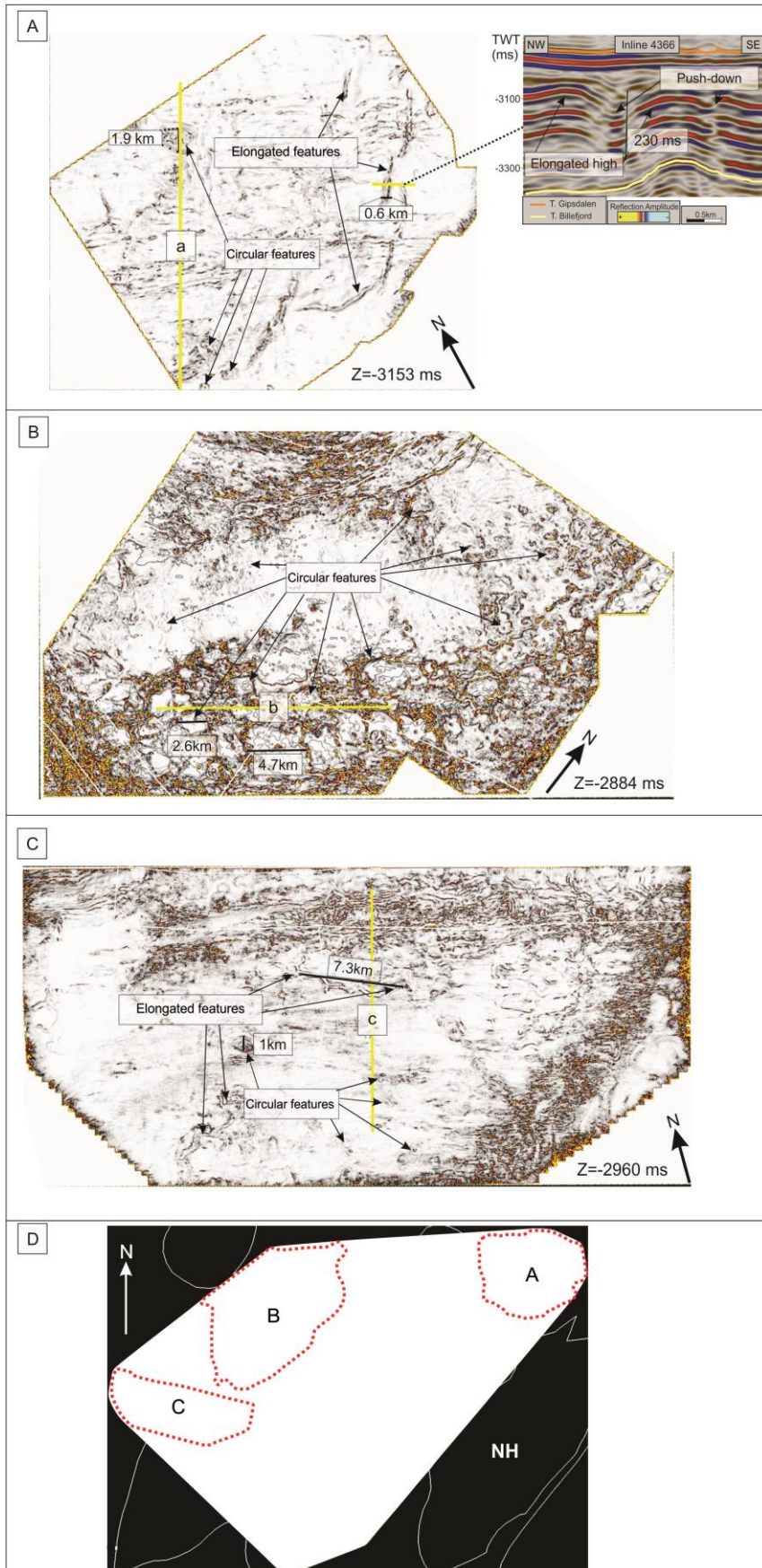


Figure 4.15 A-C: Variance time slice taken at different locations within the study area. D) Inset map displaying the location for each time slice.



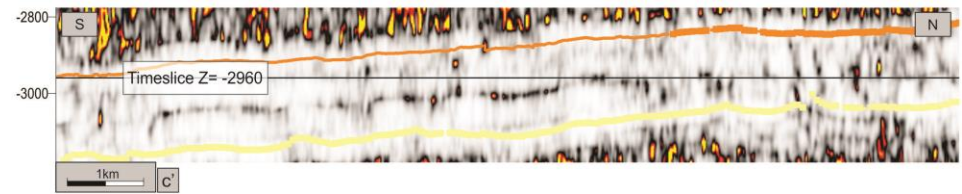
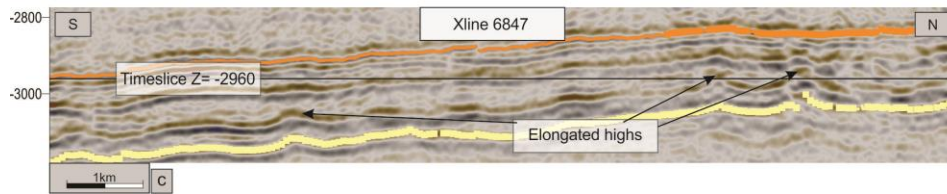
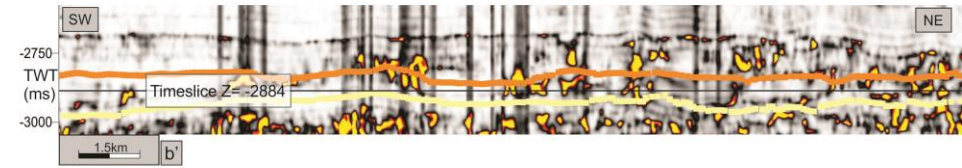
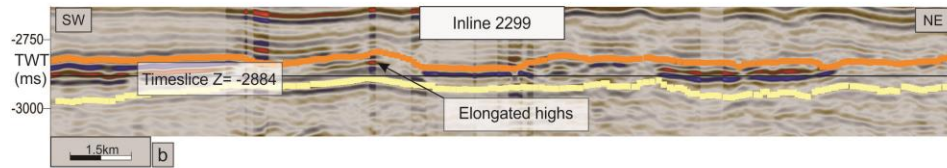
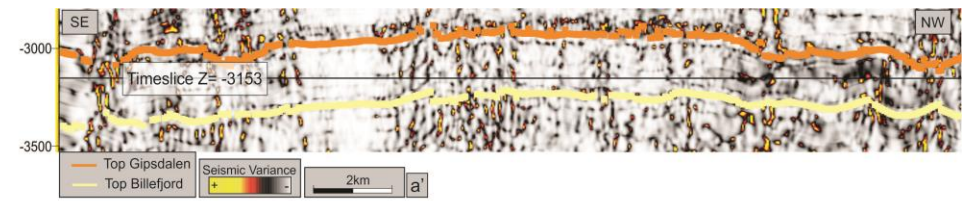
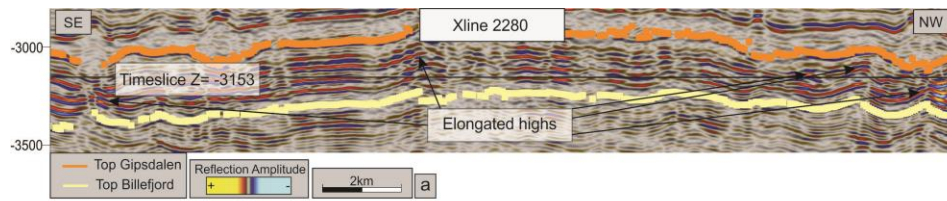


Figure 4.16: Seismic section from the Gipsdalen Group. The color- and attribute legend displayed in a-a' is valid for all seismic sections. The location of the seismic lines are shown in Figure 4.15.

### 4.2.3 Bjarmeland Group

The Bjarmeland Group is stratigraphically limited by the Top Gipsdalen horizon at the base and the younger Top Bjarmeland horizon at the top (Figure 4.17 A-E). It is mapped throughout the study area (Figure 4.18).

The thickest sediment accumulation appears in the southwest of the study area, reaching a time-time thickness of 325 ms (twt). The thickness decreases gradually towards the north, being thinnest in the northeastern part of the area, (approx. 50-75 ms (twt)) (Figure 4.18). The central and southern areas display a network of thickness alternations, where the thickness changes in short intervals, creating a distinct pattern on the surface (Figure 4.18).

Parallel to sub-parallel, semi-continuous to discontinuous reflections of medium- to low-amplitudes characterize the internal seismic signature of the Bjarmeland Group. Locally, the reflections have a wavy configuration. The internal reflections are located within a semi-transparent pattern (Figure 4.17 A-E). High amplitudes appear locally, most noticeable in the central parts of the study area (Figure 4.19 & Figure 4.20). In the northern areas, the low amplitude reflections are more noticeable, forming several elongated features, that stretches throughout the surface (Figure 4.19 A). A concentric shape of low amplitude reflections are situated in the southern part of the study area, overlying the Samson Dome (Figure 4.19 D). A wavy, mounded seismic pattern characterizes the unit (Figure 4.17 & Figure 4.20).

Circular features are observed throughout the unit, with the highest concentration found in the western and central parts of the study area (Figure 4.21 B & E). The circular features range in size from 1-2 km to the largest having a width of 6 km, located in the western area (Figure 4.21). The seismic expression of the circular features are somewhat identical apart for the features appearing in the central parts of the study area (Figure 4.21 E). The circular features produce elongated highs in the seismic profiles (Figure 4.22). The elongated highs range in size from 230 ms (twt) in the northern areas, and 119 ms (twt) in the western areas (Figure 4.22 A & B).



Elongated features can also be observed, with the occurrence most noticeable in the N and southwest (Figure 4.21 A-C). The sizes and length of these features vary greatly, with the largest being observed in the western area with a length of 12km and a width of 250-400 meters (Figure 4.21 B). The feature in the western part of the study area stretches in a NE-SW direction, and measures with a height of 220 ms (twf) and a length of 3km in the seismic. The orientation and the feature's dimensions are not shared by all, as their orientation and dimensions vary with their location (Figure 4.21).

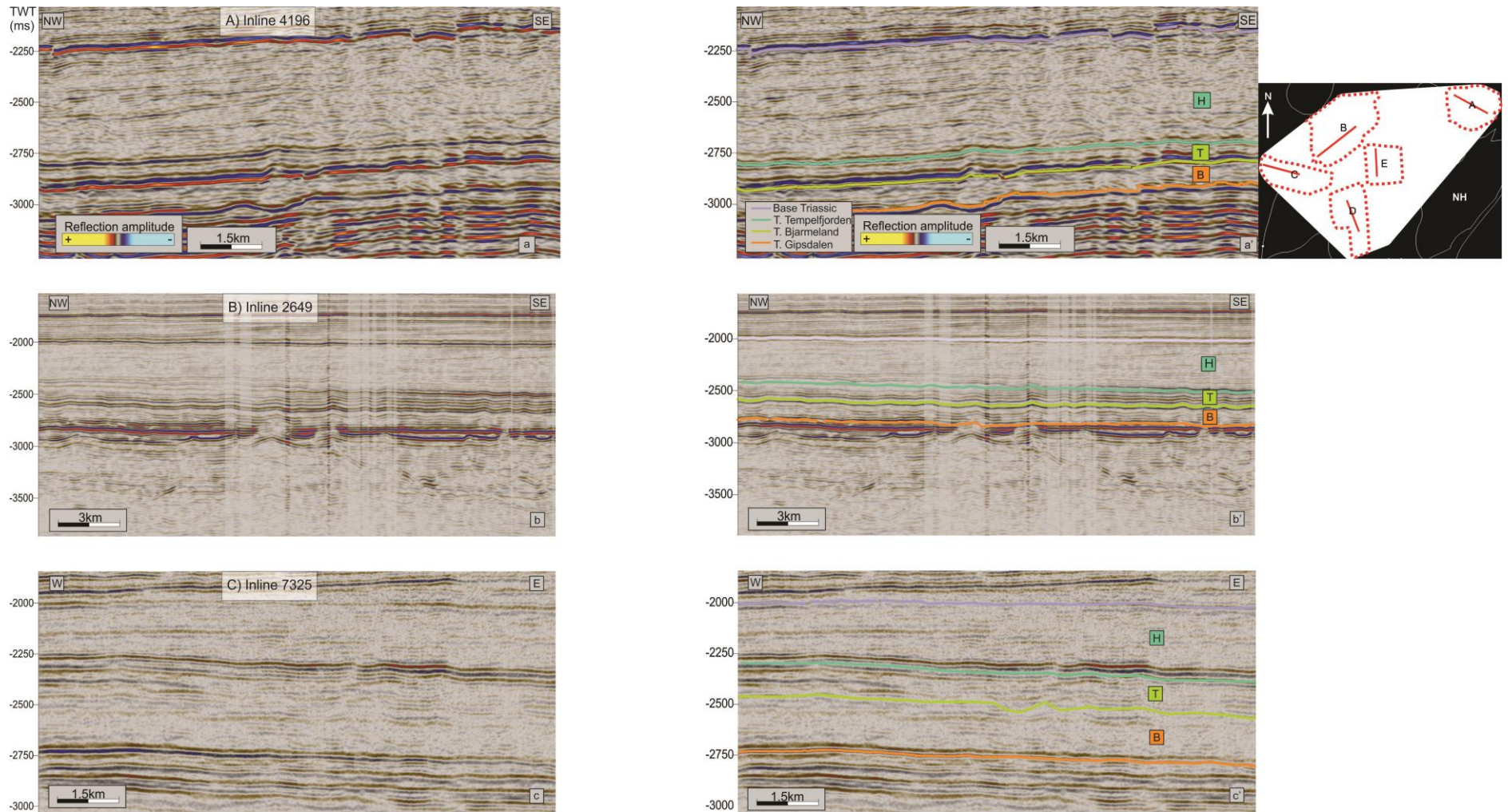


Figure 4.17: Seismic section from the study area displaying the different seismic units. The location for the lines is shown in the inset map. The seismic- and color legend shown in A) is valid for all seismic sections. H = Havert Formation., T = Tempelfjorden Group, B = Bjarmeland Group

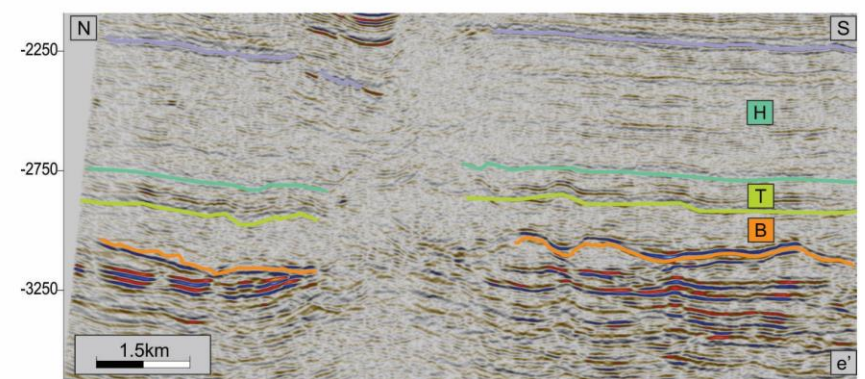
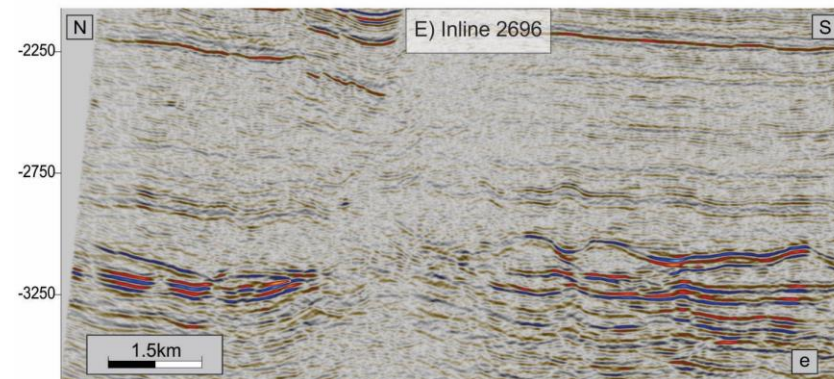
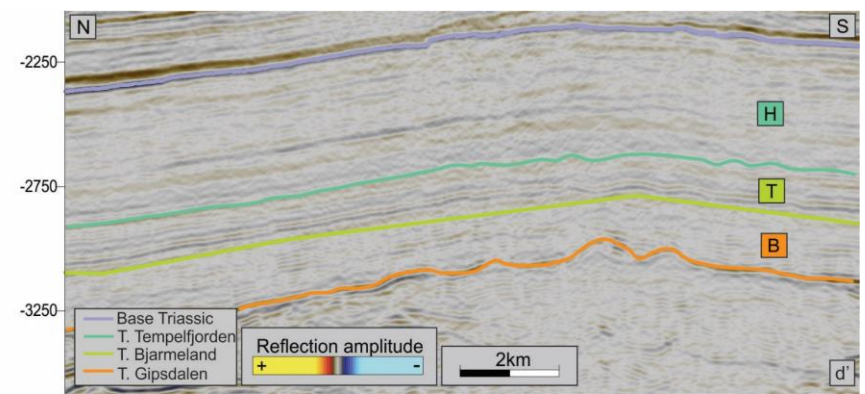
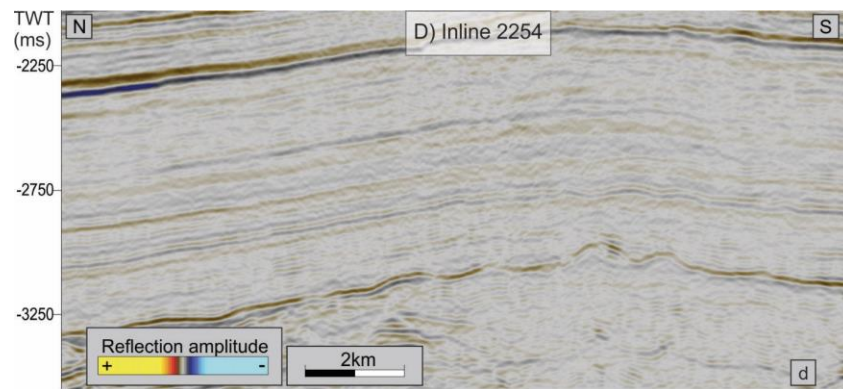


Figure 4.17 continued.



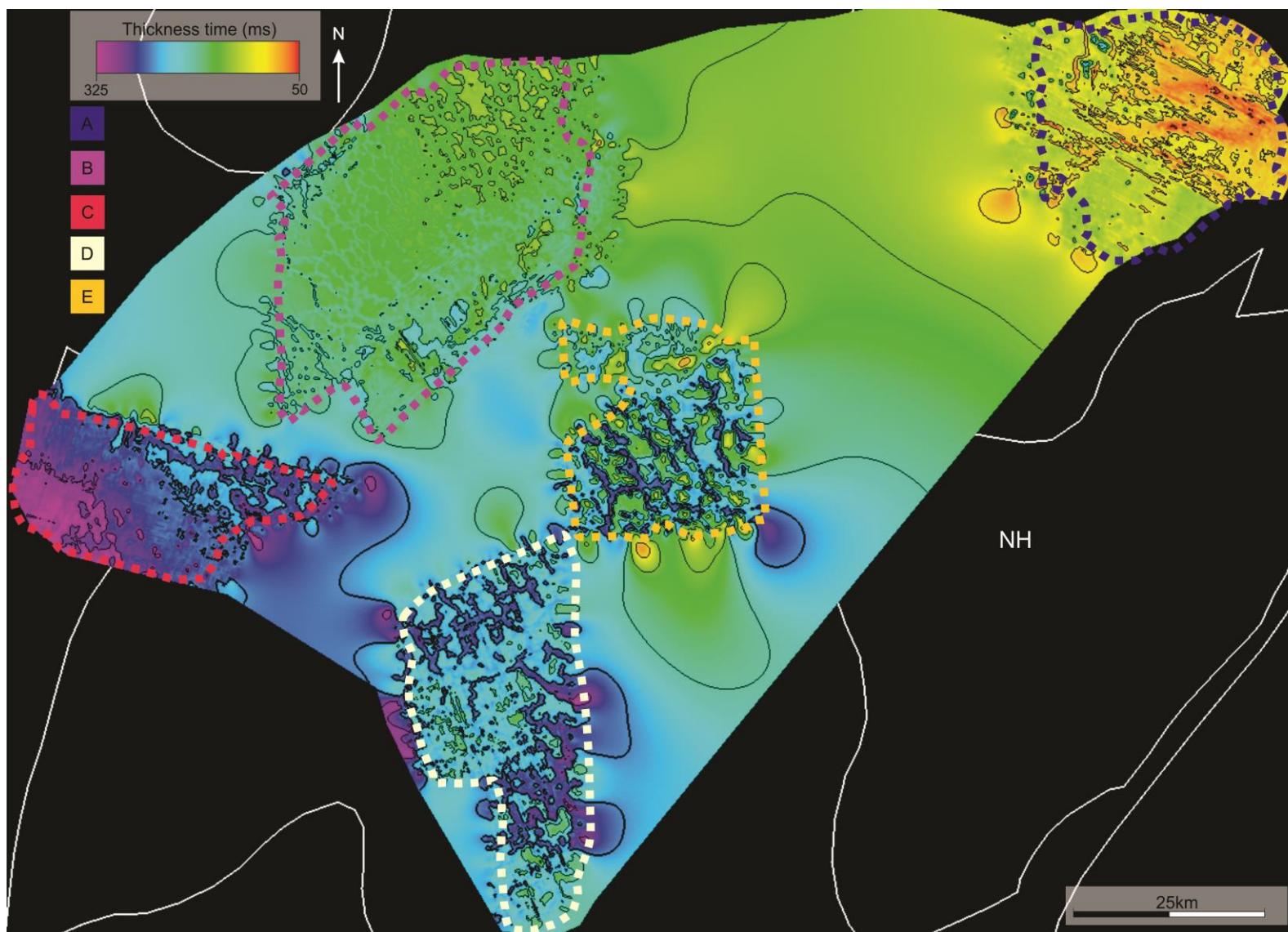


Figure 4.18: Time-thickness map generated of the Bjarmeland Group.

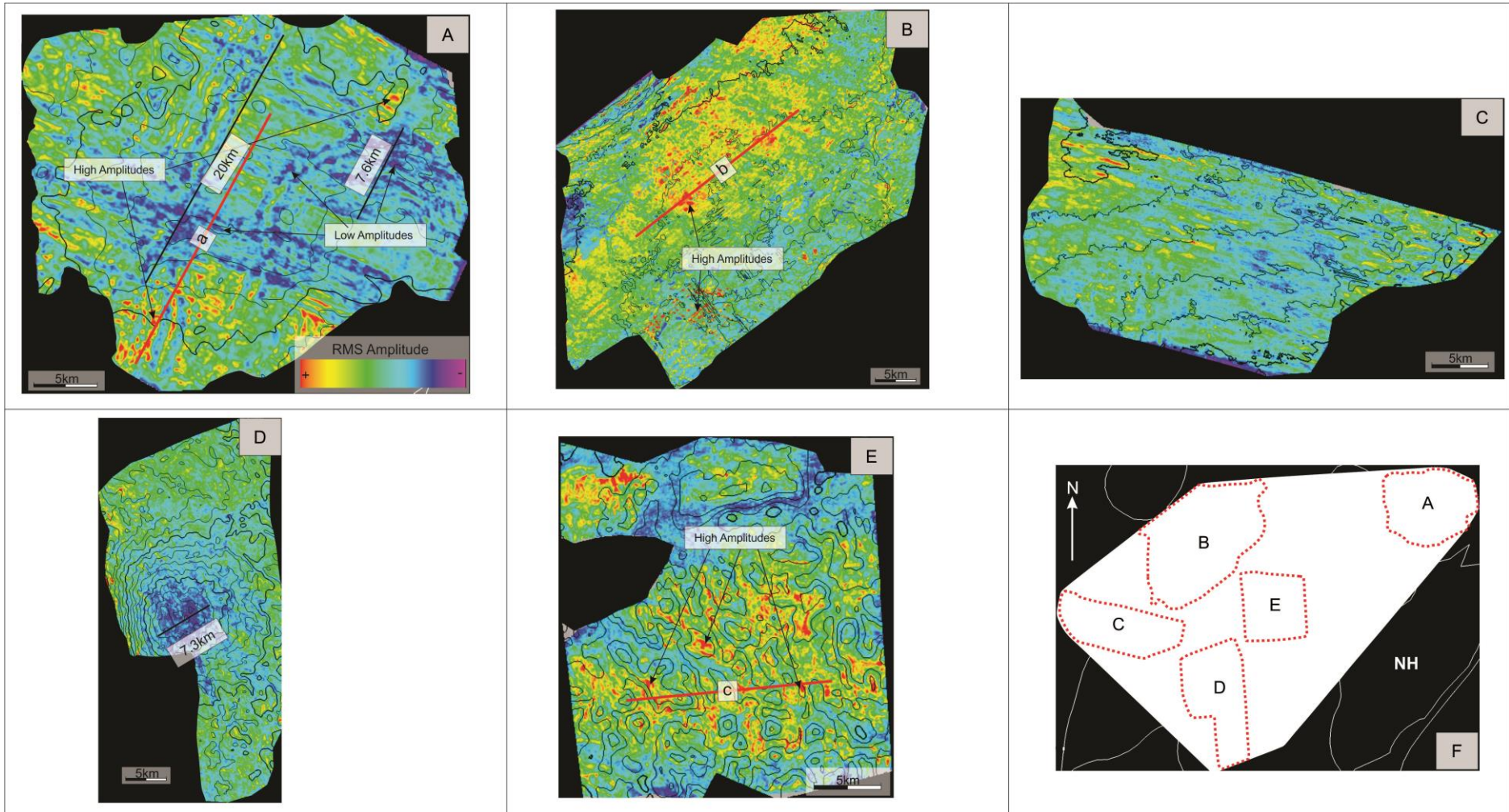


Figure 4.19: RMS surfaces generated for the Bjarmeland Group. Generated from the data volume that comprises the entire unit. The seismic legend displayed in A is valid for all surfaces. The inset map displays the location of the various surfaces.



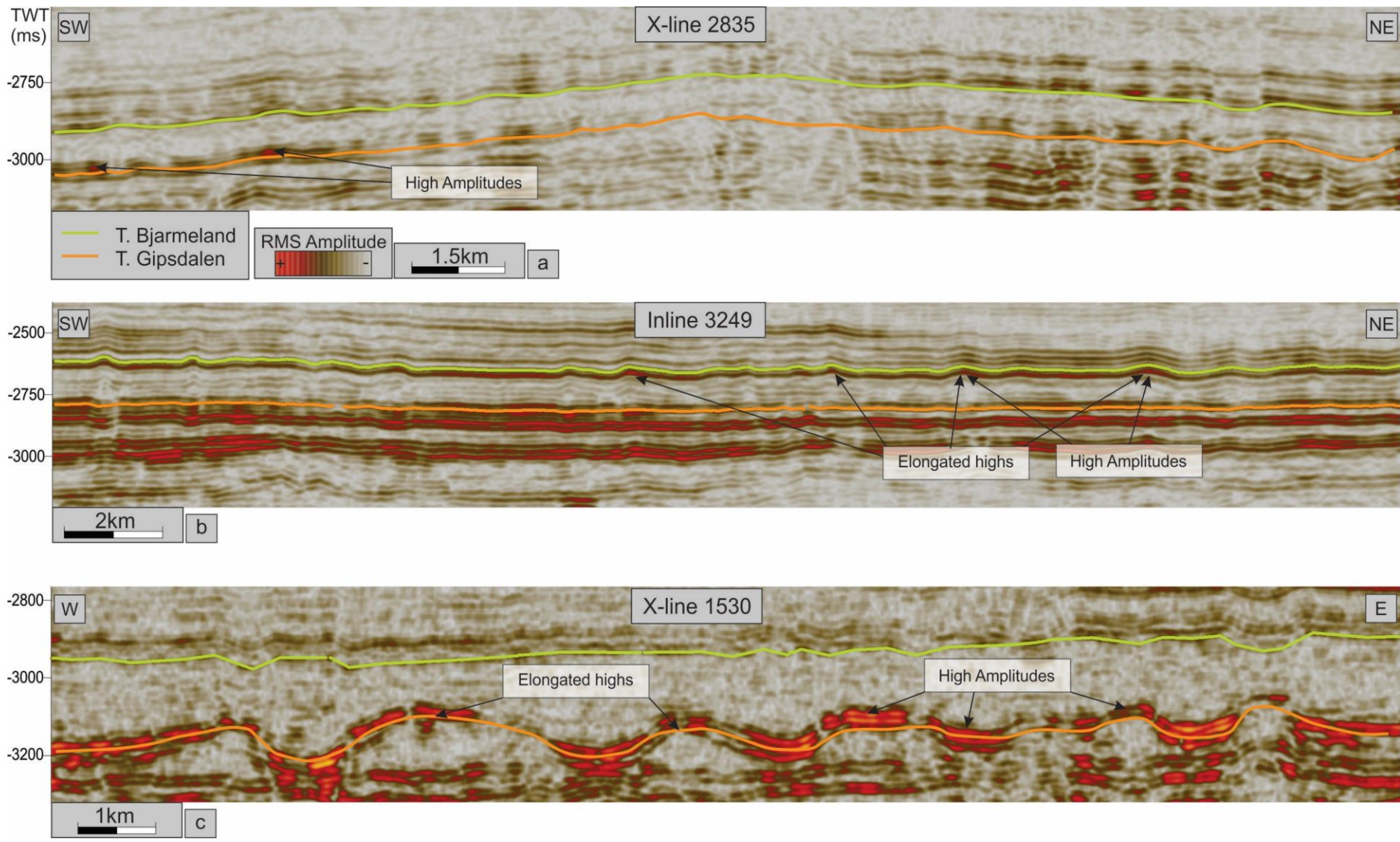


Figure 4.20: RMS-Seismic sections. The location of the various lines are displayed in Figure 4.19. The legend displayed in a) is valid for all sections.



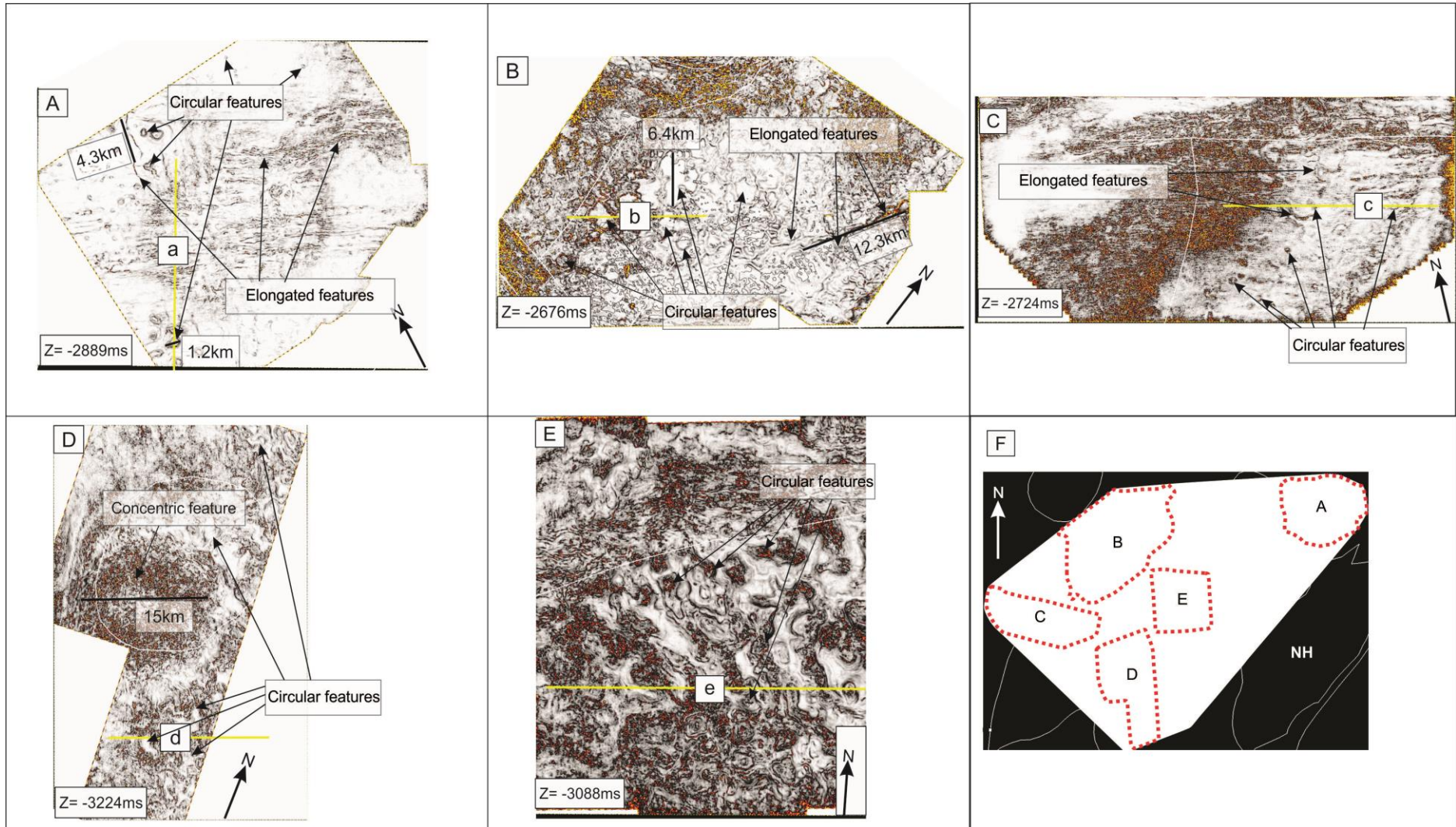


Figure 4.21: Variance time slice of the Bjarmeland Group.



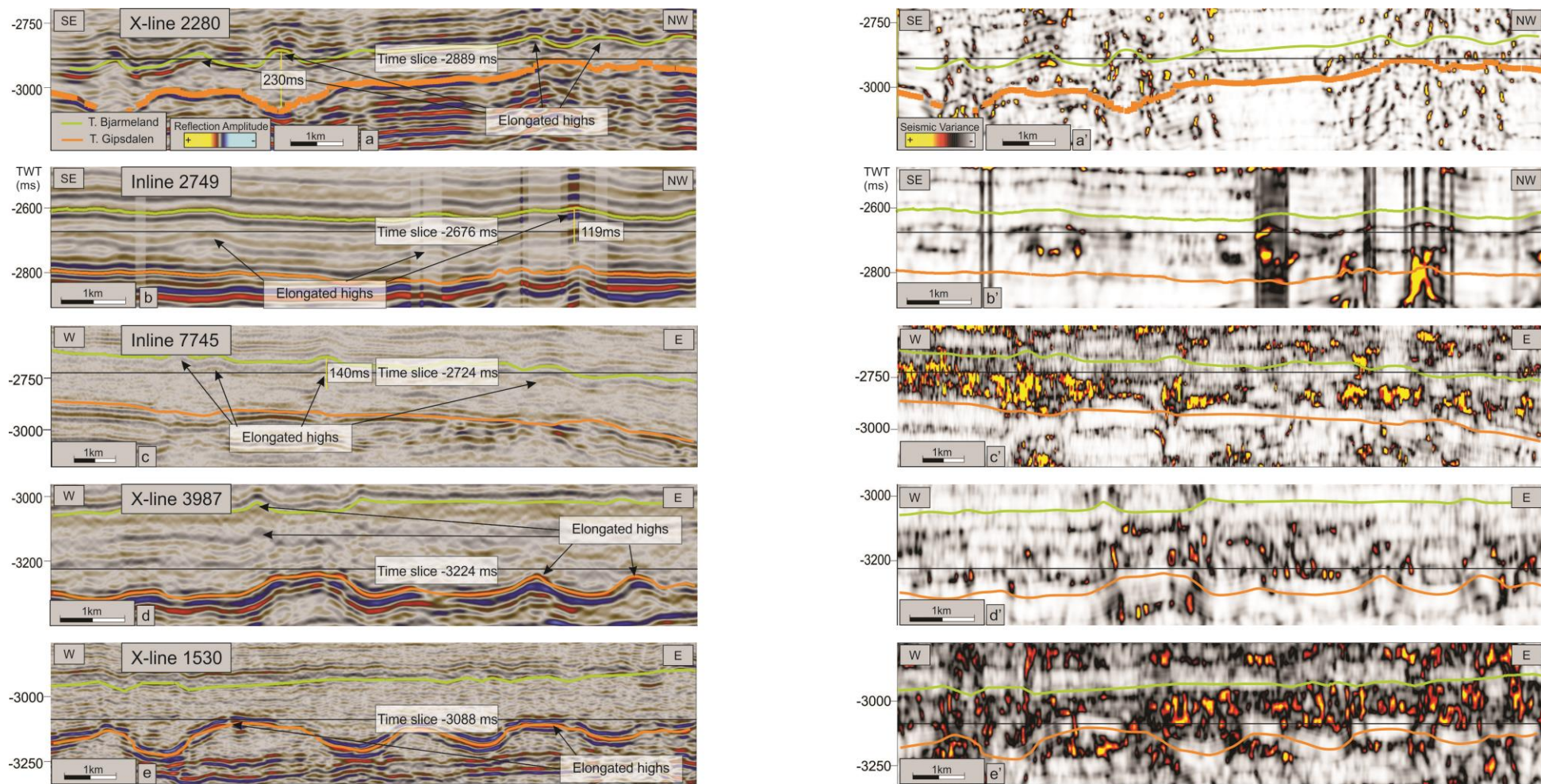


Figure 4.22: Regular and variance seismic section. The location of the different lines are shown in Figure 4.21. The color- and seismic legend shown in A is valid for all sections.

#### 4.2.4 Tempelfjorden Group

The Tempelfjorden Group is stratigraphically bounded at the base by the Top Bjarmeland horizon and at the top by the Top Tempelfjorden horizon. The unit is mapped throughout the study area (Figure 4.17 & Figure 4.23).

The thickest sediments occur in the south and west, reaching a time-thickness of 240 ms (tw) (Figure 4.23). The thickest sediment accumulation occurs in close proximity to the Samson Dome (220 – 240 ms tw). The thickness decreases gradually toward the north and the Norvarg Dome, where it reaches a time thickness of 100-80 ms (tw). The central parts of the study area show a more uniform thickness, with stable values of 180-140 ms (tw).

Parallel to sub-parallel, continuous to semi-continuous reflections of to low- to medium amplitude characterize the internal seismic signature. Locally, the Tempelfjorden Group display occurrences of wavy reflection patterns (Figure 4.17). High amplitudes appear locally, most distinctively in the west (Figure 4.24). There is a concentration of low-amplitudes in the northern and southwestern part of the study area. They appear in an elongated form in both areas, but most noticeably in the northern part (Figure 4.24 A-C).

The circular features occur throughout the study area, with the highest concentration in the west and central parts (Figure 4.26 B & E). The circular features vary in size from 1-4km in width, with the largest situated in the west (Figure 4.26 B). The seismic expression of the circular features are rather similar throughout the study area (Figure 4.26 A-E). The circular features produce elongated highs in the seismic profiles (Figure 4.27). The elongated highs range in size from 85ms (tw) to 130 ms (tw), with the largest being found in the north of the study area (Figure 4.27 A).

Elongated features can also be observed with the highest concentration is found in the northern parts of the study area (Figure 4.26 A). Their orientation varies, some have a north-south direction, while the ones located in the center of the northern part of the study area have a predominantly west-east orientation (Figure 4.26 A). In the southern part of the study area there is a concentrically-shaped feature (Figure 4.27 D). It has a

width of approx. 13km and it is believed to be the top of the evaporite body in the Samson Dome.



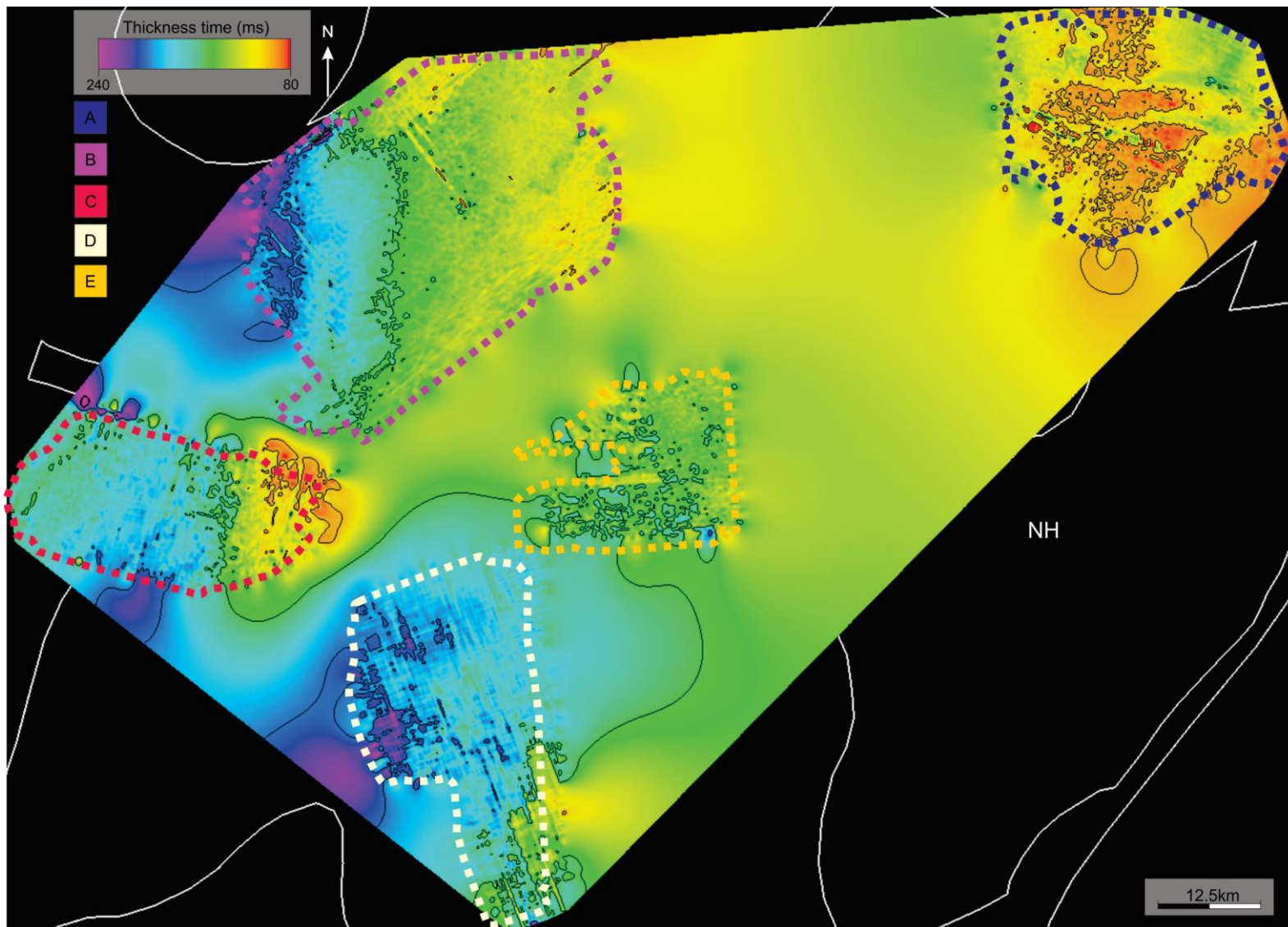


Figure 4.23: Time-thickness map of the Tempelfjorden Group.

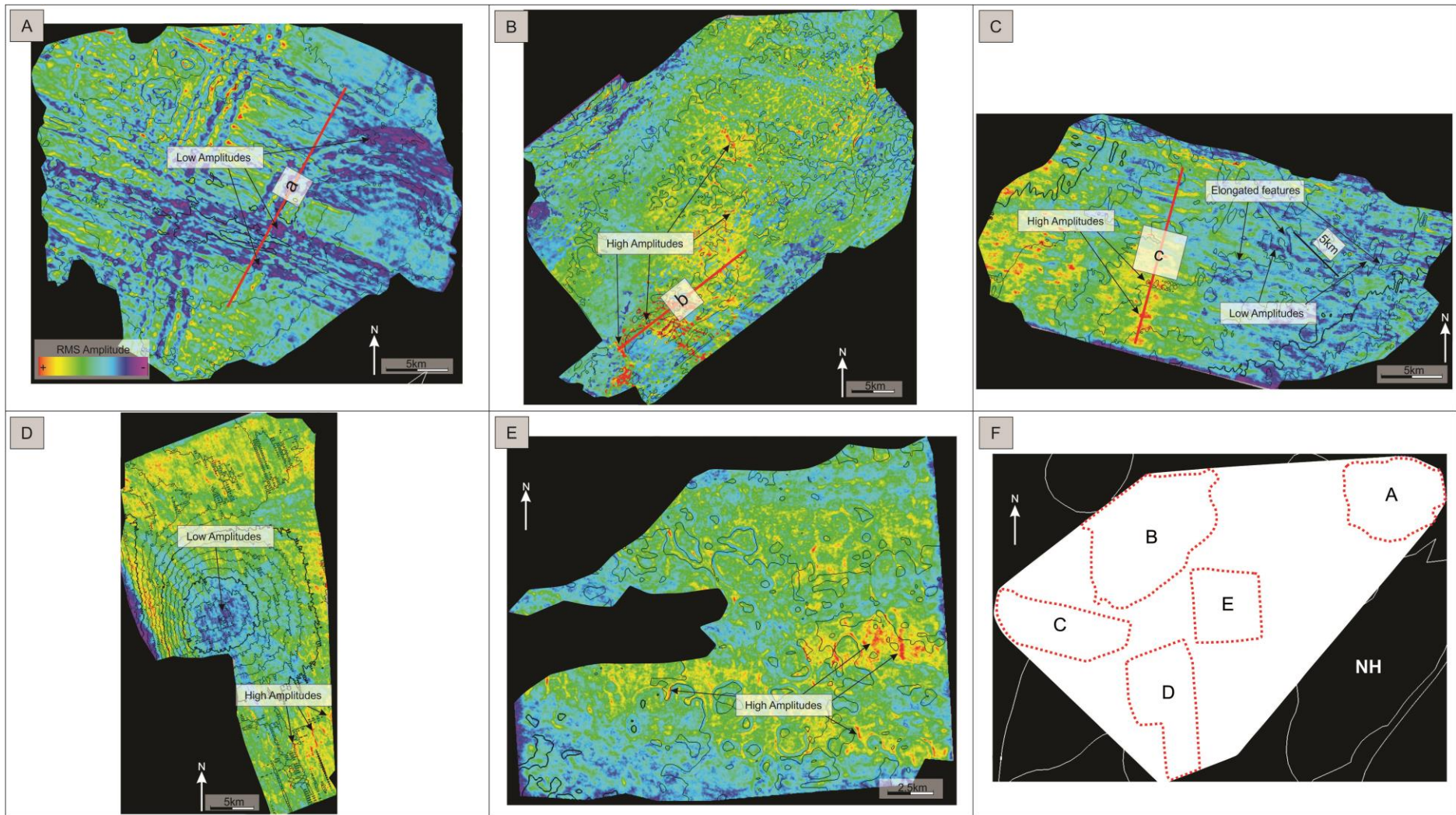


Figure 4.24: RMS surfaces generated for the Tempelfjorden Group. Generated from the data volume that comprises the entire unit. The seismic legend displayed in A is valid for all surfaces.



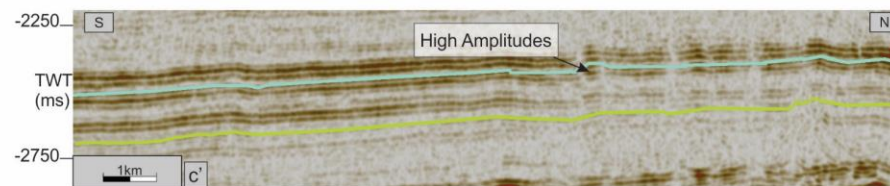
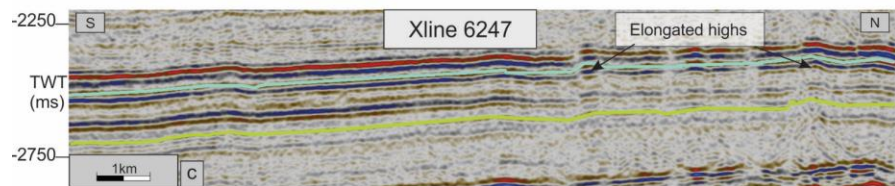
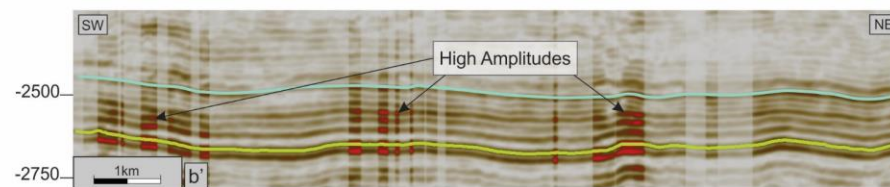
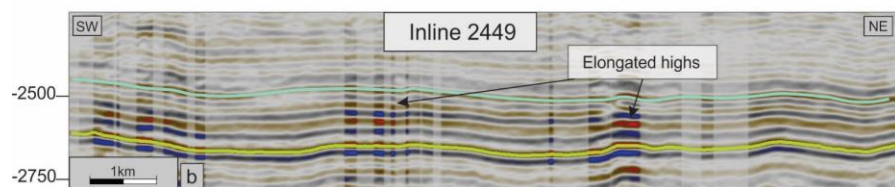
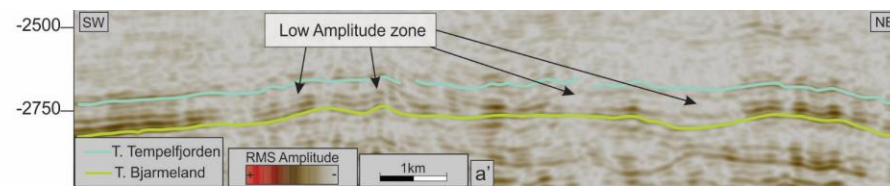
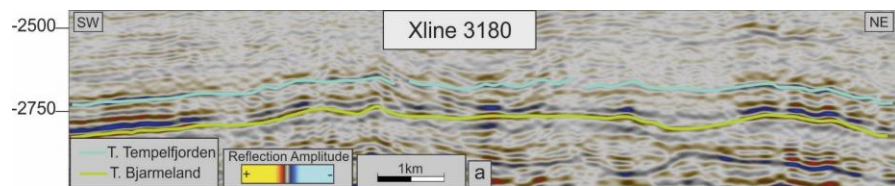


Figure 4.25: Seismic and RMS sections from areas A-C in the study area. Their location is displayed in Figure 4.24



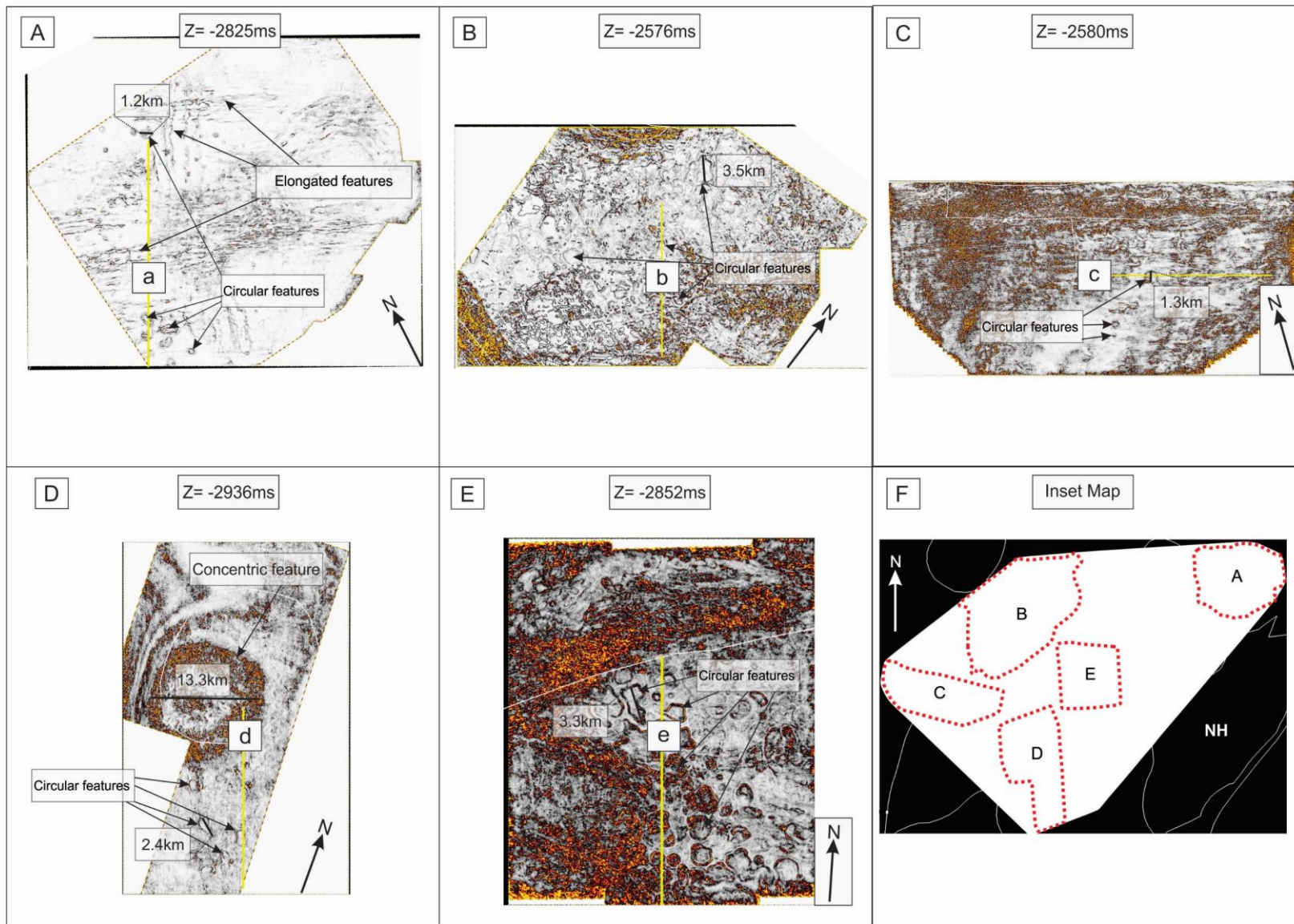


Figure 4.26: Variance time slice from the Tempelfjorden Group. The inset-map shows the location for each time slice.



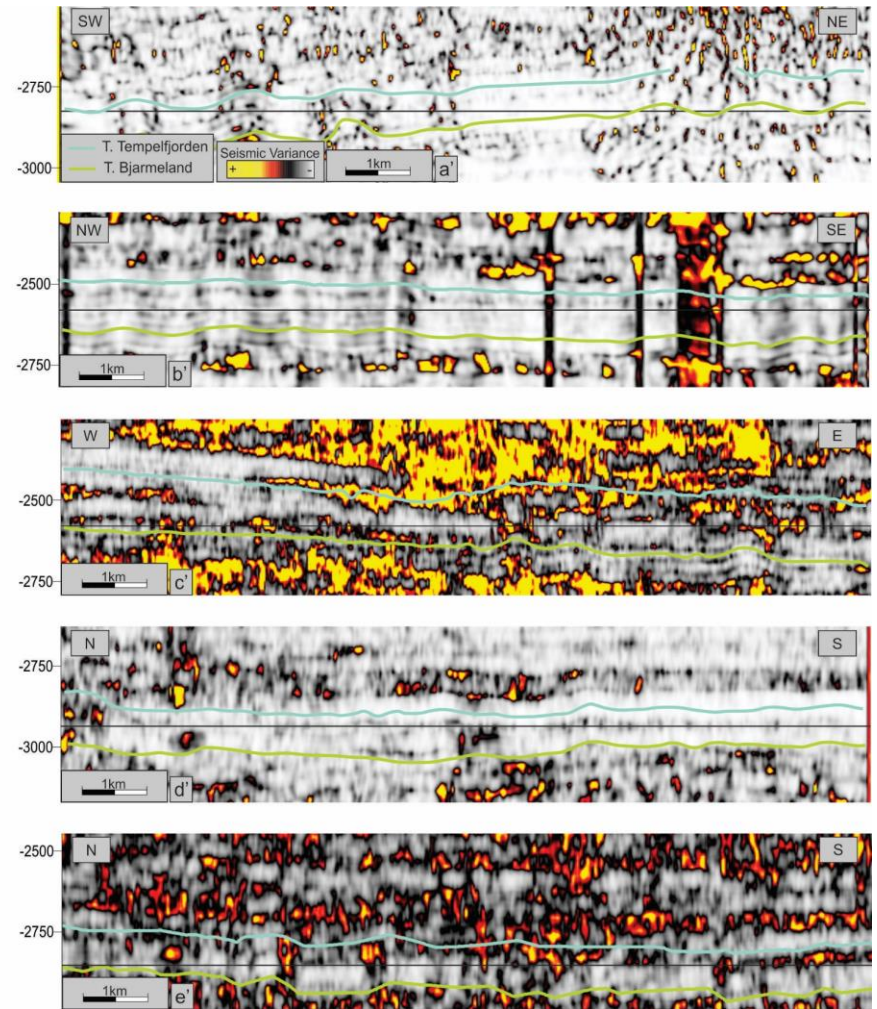
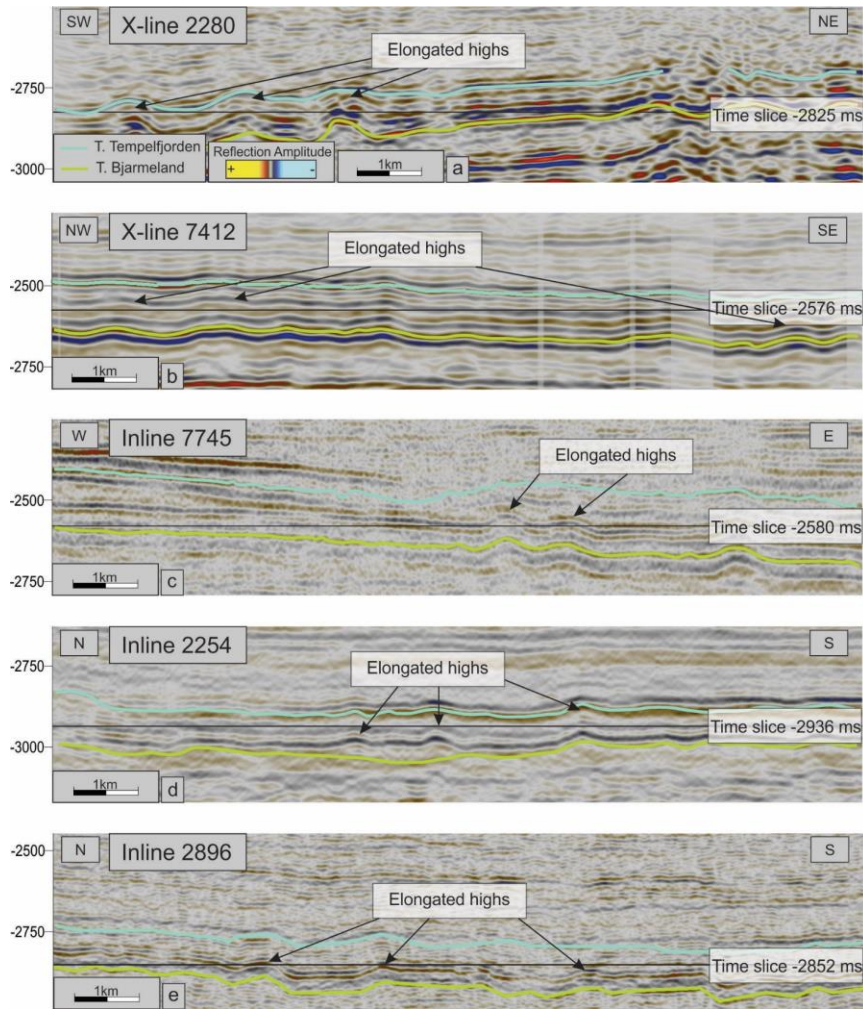


Figure 4.27: Seismic and Variance sections for the Tempelfjorden Group. Their location is displayed in Figure 4.26

#### 4.2.5 Havert Formation

The Havert Formation is stratigraphically limited at the base by the Top Tempelfjorden horizon and at the top by the Base Triassic horizon (Figure 4.17). It is mapped throughout the study area (Figure 4.17 & Figure 4.28).

The largest sediment thickness appears in the central parts and to the north, reaching a time-thickness of 600 ms (twl) (Figure 4.28). There is decrease in thickness towards the southwest and west, reaching a value of 250 ms (twl) in the southwest.

The unit displays segments of a continuous to discontinuous pattern (Figure 4.17 A-C) along with areas where the seismic configuration is parallel to sub-parallel (Figure 4.17 D-E). The internal seismic signature is characterized by reflections of very low- to medium amplitude (Figure 4.17). The very low-amplitude, makes it challenging to distinguish between what should be described as discontinuous and what could be called a continuous seismic pattern (Figure 4.30 & Figure 4.31).

High amplitudes appear locally, most noticeably in the southwest and the central parts (Figure 4.29 C & E). The general amplitude trend of the unit show that high amplitudes are sparsely distributed, with few areas displaying high-amplitude reflections (Figure 4.29 & Figure 4.30). In some areas, the low-amplitudes are more noticeable, as they form an elongated pattern in the north and a lens-shaped pattern along the western margin (Figure 4.29 A & B).

Low internal frequencies characterize the unit. The frequency is stable throughout the study area, with minor interruptions (Figure 4.31 & Figure 4.32). The frequency form a north to southwest oriented stable trend in the study area, where the central parts display a more uneven trend, and a higher concentration of lower frequency signals (Figure 4.31 & Figure 4.32)



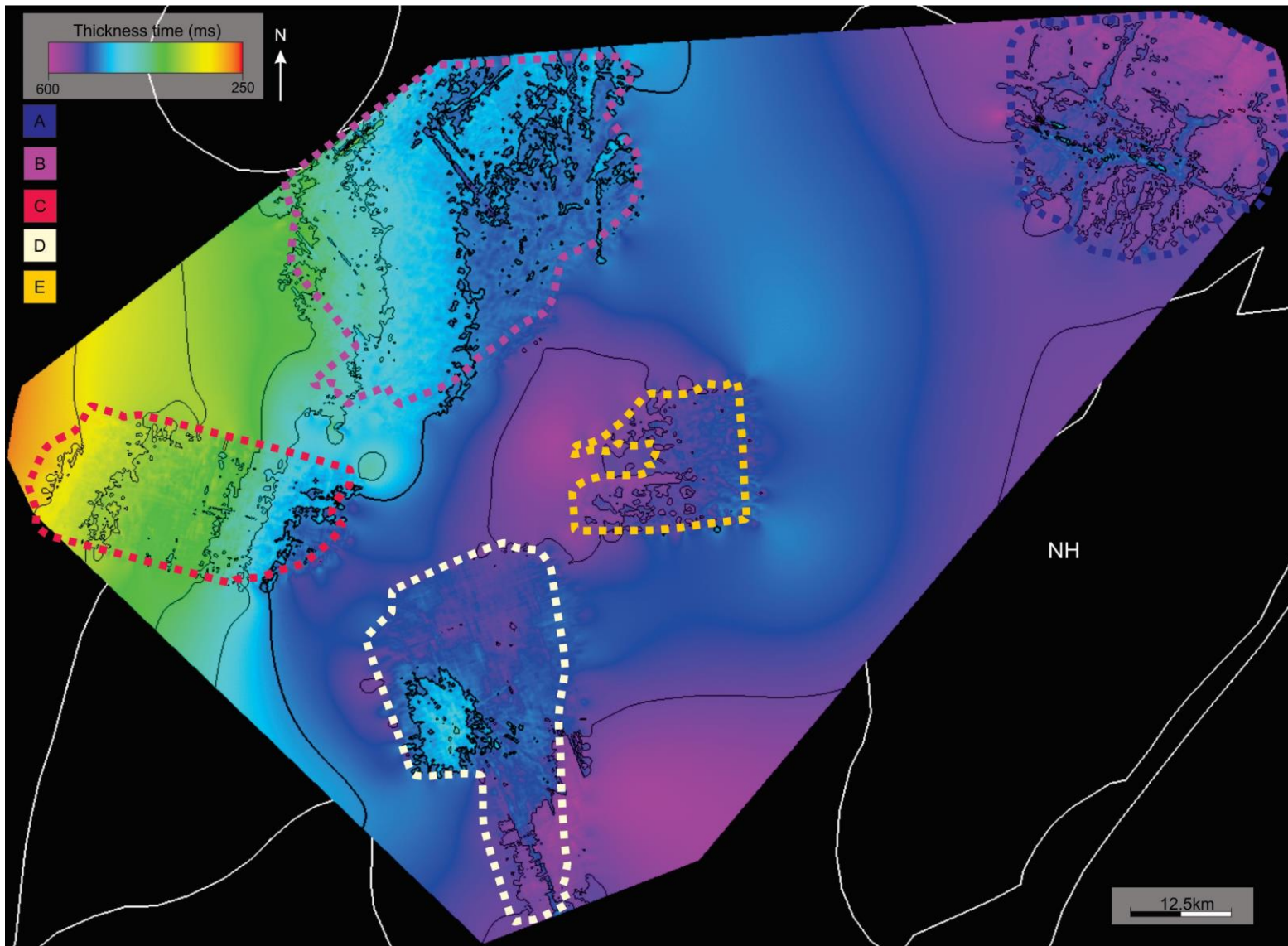


Figure 4.28: Time-thickness map of the Havert Formation.



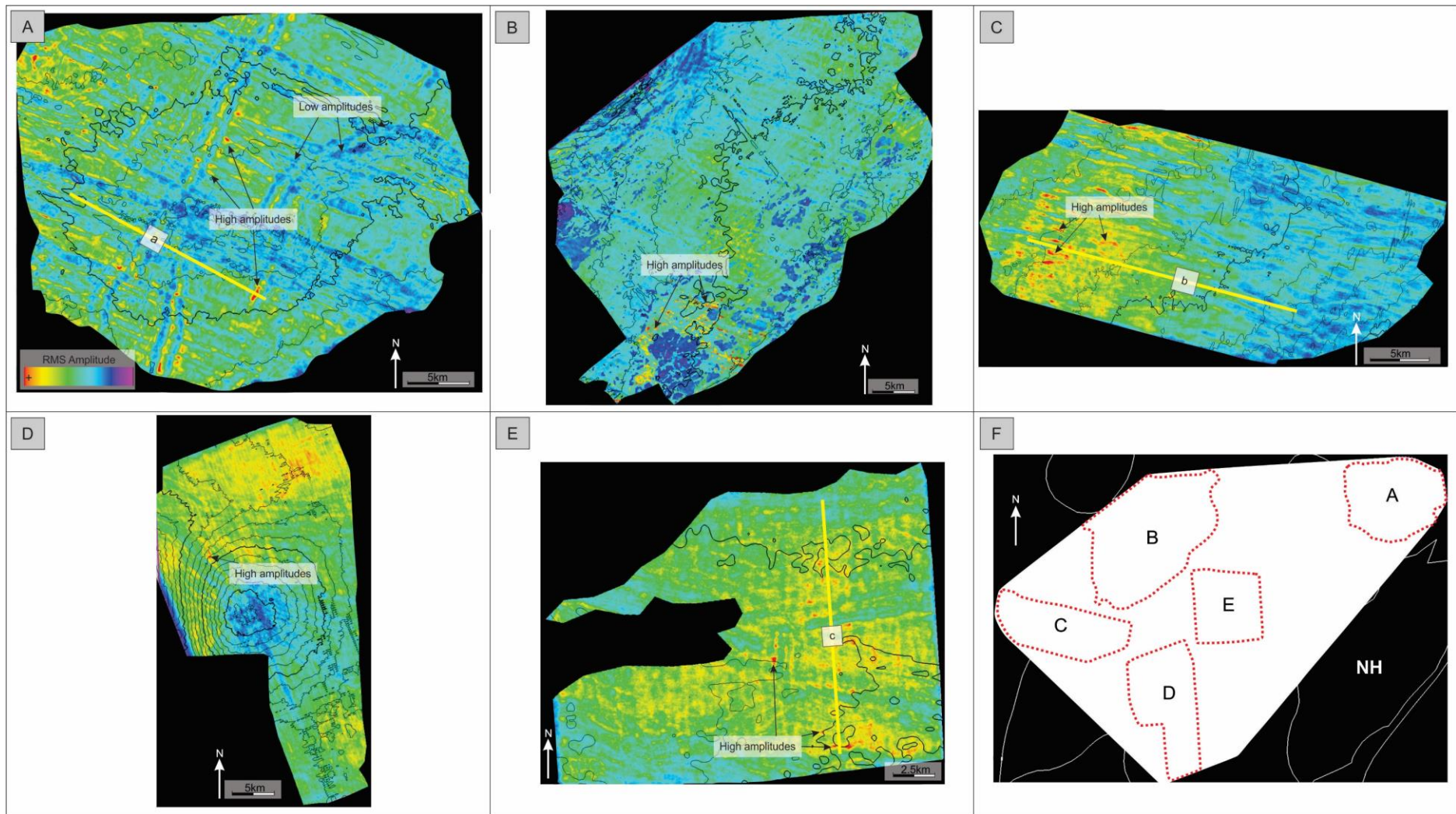


Figure 4.29: RMS-Surfaces generated for the Havert Formation. Generated from the data volume that comprises the entire unit. The seismic legend displayed in A is valid for all surfaces. Their location is displayed in the inset map.

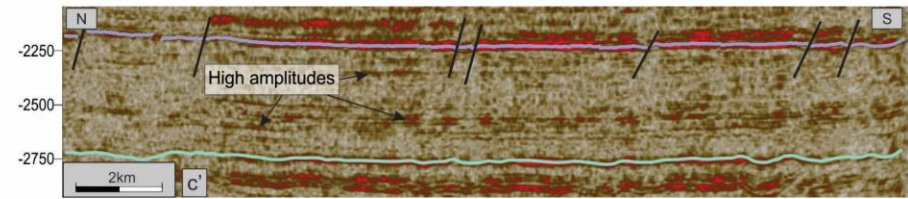
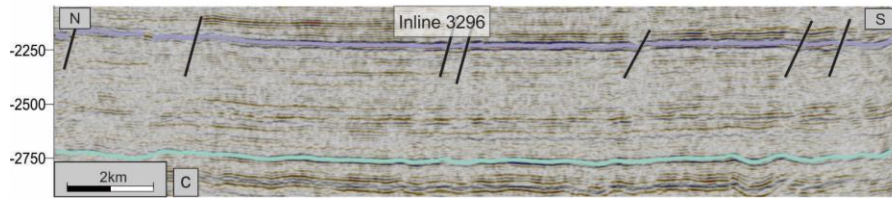
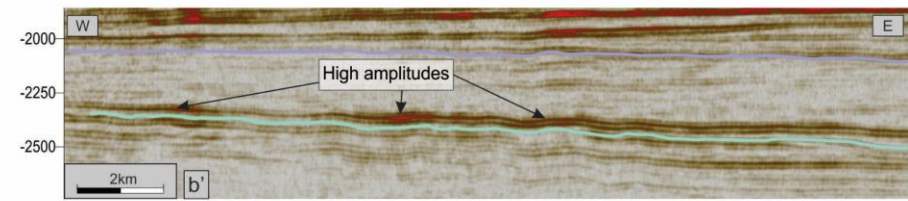
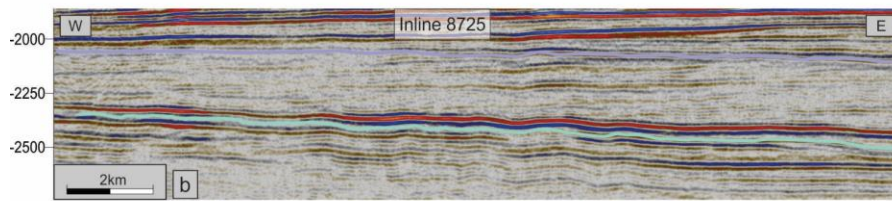
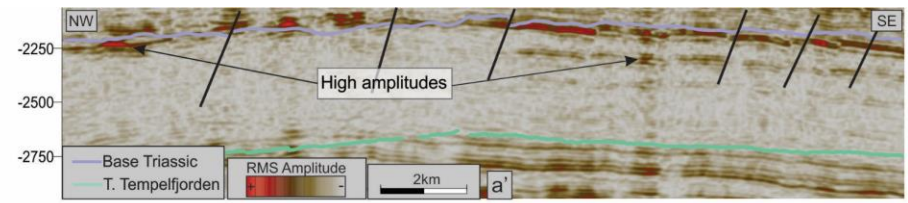
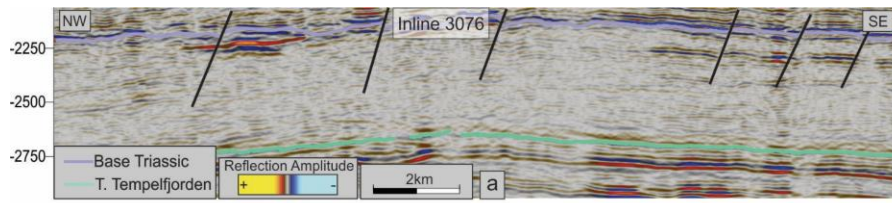


Figure 4.30: Seismic and RMS sections generated for the Havert Formation. Their location is displayed in Figure 4.29.



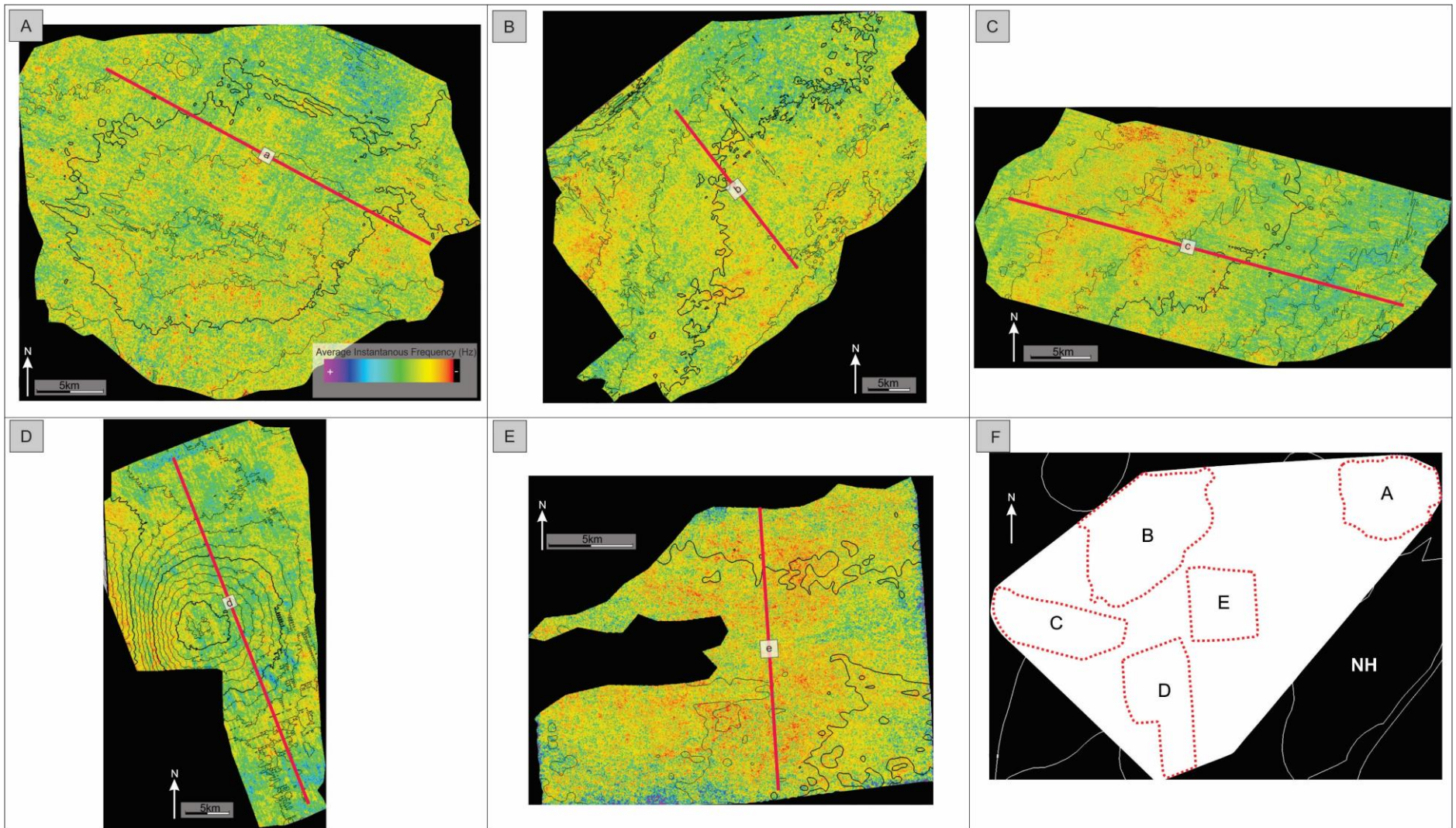


Figure 4.31: Average Iso-Frequency for the Havert Formation. Generated from the data volume that comprises the entire unit. The seismic legend displayed in A is valid for all surfaces. The inset map displays their location.



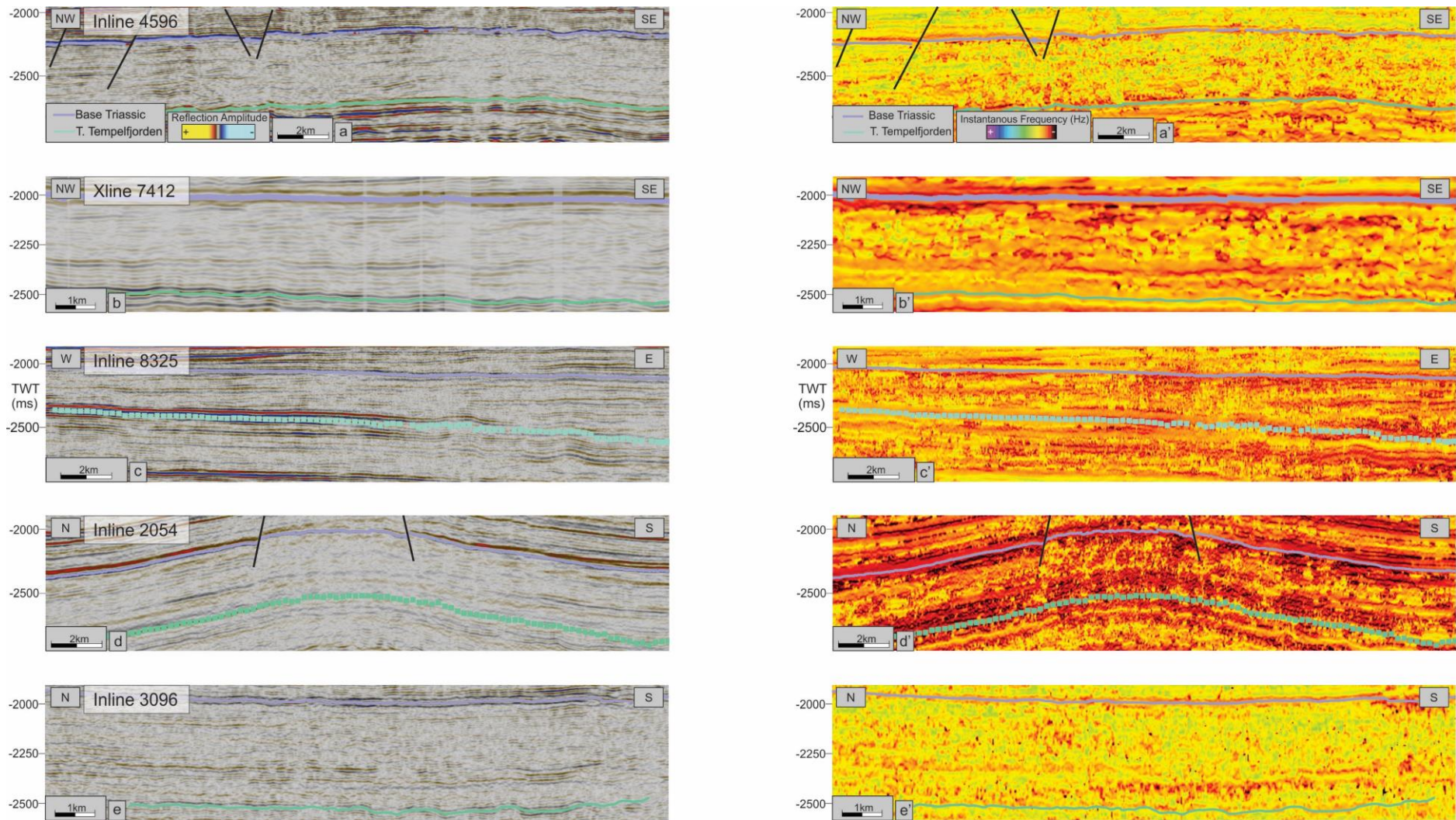


Figure 4.32: Seismic and Iso-Frequency sections displayed for Havert Fm. Color- and seismic legend displayed in (a-a') is valid for all sections. Their location is displayed in Figure 4.31



## 5. Discussion

### 5.1 Depositional Environments of the Ottar basin

The depositional processes and the paleoenvironment for the Late Paleozoic – Early Triassic in the study area is in the following interpreted based on the seismic investigations and regional setting as presented in the previous chapters. The units will be described by starting with the oldest unit.

The evolution of the Samson and Norvarg Domes and their importance for the tectonostratigraphic evolution of the study area will be discussed in a separate section.

#### 5.1.1 The Upper Billefjorden Group

The Billefjorden Group is interpreted to be of Late-Devonian - Mid-Carboniferous age (Famenninan/Viséan – Early Serpukhovian) (see section 2.2.1 Paleozoic). In terms of seismic character, the upper part of the unit – approx. 100 ms (tw) above the base horizon – is represented by sub-parallel, semi-continuous reflections, mainly dominated by low- to medium amplitudes, however, also high amplitudes appear in the upper section (Figure 4.10). The lower part of the unit shows a configuration of semi-continuous reflections with very low-amplitudes (Figure 4.9 & Figure 4.10 B & C). The lower part of the unit share the same reflection characteristics with the section that is presumed to be the basement, making it difficult to separate the sedimentary unit from the basement. The reflection pattern for the entire unit is defined as semi-transparent, which may indicate periods with the deposition of a homogenous lithology (Figure 4.9). Such homogenous zones, normally produce a weak acoustic impedance contrast, creating a reflection free to a reflection transparent pattern (Mitchum et al., 1977; Sangree & Widmier, 1978; Veeken, 2007a).

The unit thickens toward the southwestern part of the mapped area, while thinning towards northwest and southeast (Figure 4.10 A-B). This suggests a higher subsidence rate in the southwestern part. During the deposition of the Billefjorden Group, the tectonic regime was influenced by rifting possibly linked to the breakup between Greenland and Norway (Rønnevik et al., 1982; Dengo & Røssland, 1992; Barrère et al., 2009; Faleide et

al., 2015; Koehl et al., 2018). This event is believed to have created several rift-basins, such as the Ottar basin (Breivik et al., 1995; Faleide et al., 2015). This in turn could explain the difference in thickness, as parts of the Billefjorden Group was deposited in a continuously subsiding basin.

The elongated features observed within the unit (Figure 4.11) ranges in size and orientation, having a length of 1-4 km and a width varying from 40-150 meters. Orientation from W-E in the center, and N-S at the edges can be observed (Figure 4.11 A). The features' shape varies from straight to sinuous throughout the mapped area and are represented by amplitude anomalies (Figure 4.11 B & C). These features appear more frequent in the center of the surface, becoming less distributed toward the edges (Figure 4.11).

During the Viséan, humid and tropical climate conditions prevailed and the subsidence ceased towards the end of the period. This led to the development of a delta plain dominated by fluvial and alluvial processes, which transported material from the highlands (Figure 5.1) (Bugge et al., 1995; Larssen et al., 2005; Worsley, 2008; Smelror et al., 2009; Henriksen et al., 2011). This could indicate that the elongated features within the unit represent channels (Figure 4.11). This however seems unlikely due to their restricted distribution towards the surface edges, which is presumed to be the basin margin. The channels should be originating at the edges, as this is the section with the highest relief and stretch towards the low-relief central parts of the study area. This is not however the case (Figure 4.10 B & Figure 4.11). The Billefjorden Group is deposited in the Early Paleozoic, and in some locations it is deposited directly on basement of pre-Devonian age (Ehrenberg et al., 1998). This could mean that the elongated features are fractures/faults that developed along old Caledonian tectonic features. These however had a predominantly NE-SW orientation, which differs from the W-E and N-S orientation observed for the features in the mapped area (Figure 4.11) (Barrère et al., 2009; Smelror et al., 2009; Clark et al., 2014).

Alternatively, the elongated features may have been initiated at a later time intersecting the Billefjorden Group, as they were created post-deposition. Different tectonic events influenced the study area from Late Devonian and until Triassic times (Torsvik et al.,

2002; Smelror et al., 2009; Glørstad-Clark et al., 2010; Henriksen et al., 2011; Faleide et al., 2015). This could have given rise to the elongated features observed within the unit (Figure 4.11). The elongated features seem to be located in the same areas as larger and more prominent features observed in the overlying Gipsdalen Group, which could create interference by overlying features (Figure 4.15 A). Due to the poor resolution and the depth (twt) of the unit, it is difficult to discriminate between the aforementioned alternatives.

The continuity of the reflections suggest an environment of uniform sedimentation and the low amplitudes indicate a low-energy setting (Sangree & Widmier, 1978; Veeken, 2007b). The high amplitudes within the upper section indicate zones of coal deposition, as Koehl et al. (2018) infers, which is a sedimentary rock found within the Billefjorden Group at different locations (Figure 4.10 B) (Bugge et al., 1995; Larssen et al., 2005; Worsley, 2008).

Based on seismic investigations and earlier conducted studies a depositional model for the group is proposed (Figure 5.1). The entire Group is interpreted to be deposited in a lacustrine setting by fluvial and alluvial processes. As the study area was subsiding, it is likely that alluvial and fluvial systems graded laterally into the subsiding basin and formed a lacustrine environment, where conglomerates and terrigenous sediments were deposited along with the possible development of coal (Figure 4.10 A & Figure 5.1) (Ehrenberg et al., 1998; Worsley, 2008; Smelror et al., 2009; Clark et al., 2014).

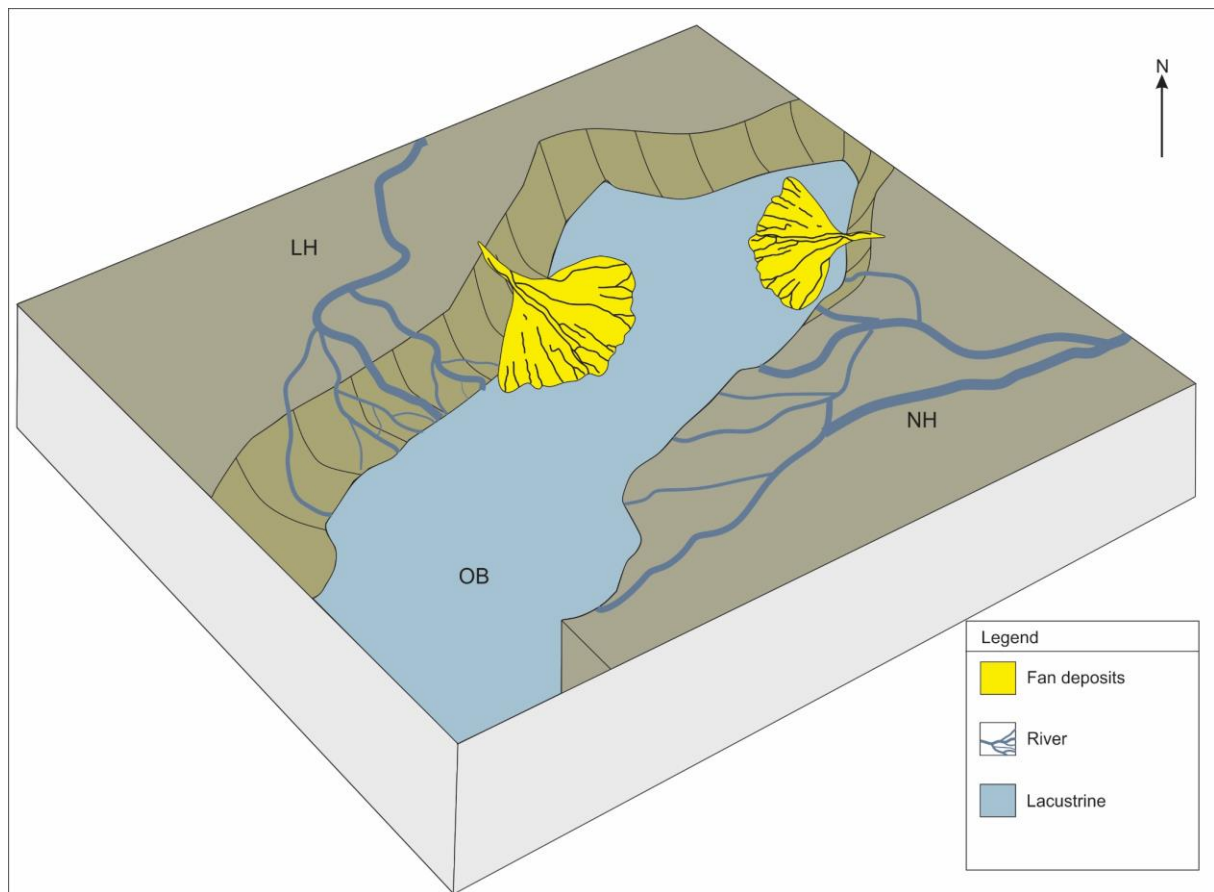


Figure 5.1: Proposed depositional model for the upper Billefjorden Group in the Ottar basin and adjacent areas. LH = Loppa High, NH = Norsel High, OB = Ottar basin.



### 5.1.2 Gipsdalen Group

The Gipsdalen Group is of Mid-Carboniferous to Early-Permian age (see section 2.2.1 Paleozoic). The reflection configuration of the Gipsdalen Group was classified as parallel to sub-parallel, continuous to semi-continuous with amplitudes varying from low- to high. This reflection configuration is intermixed with a semi-transparent pattern, and where locally the reflections have a wavy configuration. (Figure 4.12 & Figure 4.16). In plan-view the wavy configuration produces several circular features (Figure 4.15).

During the time of deposition for the Gipsdalen Group, the regional environment changed from the warm, humid climate of the Viséan period and into a more warm and arid environment, creating a warm water carbonate platform with the simultaneous deposition of evaporites (Figure 5.2) (Cecchi, 1993; Torsvik et al., 2002; Stemmerik & Worsley, 2005; Worsley, 2008; Smelror et al., 2009; Henriksen et al., 2011).

The Gipsdalen Group has been described as consisting of evaporites along with sandstone, carbonates and shale (Worsley, 2008; Rowan & Lindsø, 2017). This varying lithology could give rise to different seismic expressions, as their geophysical properties vary greatly (Bubb & Hatlelid, 1978; Sangree & Widmier, 1978; Badley, 1985; Veeken, 2007b).

The wavy configuration seen within the unit comprises a series of velocity pull-ups, which could be a result of lateral velocity changes (Figure 4.16). Such lateral velocity changes may result from abrupt changes in carbonate facies, as porous carbonate buildups could change laterally into tight buildup flank deposits creating the observed velocity pull-up (Bubb & Hatlelid, 1978; Fontaine et al., 1987; Rafaelsen et al., 2008).

High amplitudes are most prominent in the western margin, but appear throughout the mapped area (Figure 4.14 A, B & C). The highest amplitudes appear more frequent in the apex of the elongated highs (Figure 4.14), and could represent variations or changes in lithology. Carbonates are believed to have a high velocity and density compared to other common sedimentary rocks, and could therefore produce high acoustic impedance contrasts displayed as high amplitude anomalies (Bubb & Hatlelid, 1978; Badley, 1985).

A more disorderly configuration and a thickening and thinning of the reflectors in the north can be observed, along with a general decrease of internal seismic reflections and a general pillow-shape of the reflectors (Figure 4.16 A & Figure 5.3 A). This geometry could be an indication of a mobile evaporite layer: as salt have a smaller density than surrounding layers, creating the possibility for the evaporites to become unstable when overlain by sediments. This could result in the observed disorderly configuration of the reflections, as the density contrast between the layers trigger the evaporites to move (Figure 4.16 A & Figure 5.3 A) (Badley, 1985). The pillow-shaped reflections are also located in the presumed basinal area, whereas the previously described wavy configurations are located on the basin margin and presumed highs. According to Nilsen et al. (1993), this is a common characteristic for this time period as carbonate buildups formed along the margins while evaporites were deposited in the basinal areas (Figure 4.15 A, Figure 4.16 A, Figure 5.2 & Figure 5.3 A).

This characteristic distribution of carbonate buildups could also explain the concentration of circular features along the margins of the study area (Figure 4.15). These circular features are located on the elongated highs, interpreted to be carbonates (Figure 4.16). When seen in plan-view, the carbonate mounds could produce these circular features located along the SW margin of the study area (Figure 4.15 B-C & Figure 4.16 B-C) (Stewart, 1999; Rafaelsen et al., 2008).

According to Rafaelsen et al. (2008), Worsley (2008) and Smelror et al. (2009) a regional subsidence occurred in Mid Bashkirian (323.2 – 315.2 m.y.a.), which led to a transgression and the subsequent deposition of alluvial, shallow marine siliciclastics along with carbonates and evaporites. The period was dominated by frequent sea-level fluctuations, evident by the low-stand deposited evaporites and the presence of high-stand carbonates (Figure 4.15 & Figure 4.16) (Cecchi, 1993; Worsley, 2008; Henriksen et al., 2011). During the sea-level lows the areas of carbonate deposition were subaerially exposed, creating karst-landscapes and paleo-caverns controlling the further distribution of the carbonate buildups, by establishing zones with different subsidence (Figure 4.15) (Elvebakk et al., 2002; Hunt et al., 2003; Henriksen et al., 2011; Ahlborn et al., 2014). Along the margin of the study area several elongated features can be observed (Figure 4.15). The most prominent feature is located to the north, where it produces a series of pull-

down effects adjacent to the elongated highs resulting in the displacement of several reflections within the unit. The pull-down events seem to be confined to the unit as they do not appear to influence the top horizon (Figure 4.16 A).

This could be the result of karstification, as paleo-caverns were created during the sub-aerial exposure or as a result of evaporitic dissolution (Hunt et al., 2003; Rafaelsen et al., 2008; Sayago et al., 2012).

There is also the possibility that the features represent faults, as they seem to interfere with the reflections creating a throw of 25-45 ms (twl) (Figure 4.15 A). The fact that they are confined within the unit points toward an artefact known as fake faulting. This artefact typically occurs within carbonate environments due to the abrupt lateral velocity changes produced by the velocity differences between carbonates and the surrounding sediments (Bailey et al., 2003; Rafaelsen et al., 2008). However, due to the regional paleo-environment and the fluctuations of sea-level, there is also a possibility that the features represent the aforementioned karst environment, established as the margin was sub-aerially exposed (Elvebakk et al., 2002; Rafaelsen et al., 2008; Smelror et al., 2009; Henriksen et al., 2011; Sayago et al., 2012).

The unit thickens toward the northeast, where the proposed deposition of evaporites occurred, while the carbonate buildups are located in the thinner sections along the margin of the study area (Figure 4.13 & Figure 5.2). This could be considered normal for an intracratonic basin, as evaporite precipitation occurs in the central parts, while carbonates are deposited at the margin (Catuneanu et al., 2011). Prior to the precipitation of evaporites, the basin was most likely connected to the world ocean and the sea level was above sill-height. During this time, carbonate production occurred along the margin. When the sea-level dropped, the basin was barred from the ocean and evaporites precipitated at the center (Figure 5.2) (Catuneanu et al., 2011). The large accumulation of evaporites are concentrated in the deepest parts of the basin due to the large amounts of water needed in order for such a large accumulation of evaporites (Nichols, 2009).

Based on the seismic investigations and earlier conducted studies, a depositional model for the Gipsdalen Group is proposed (Figure 5.2). The model displays how the warm-water carbonates of the Gipsdalen Group are deposited along the margins while

evaporites are deposited in the deeper basinal areas. Two major evaporite depocenters were established, which later developed into the Norvarg – and Samson Domes.

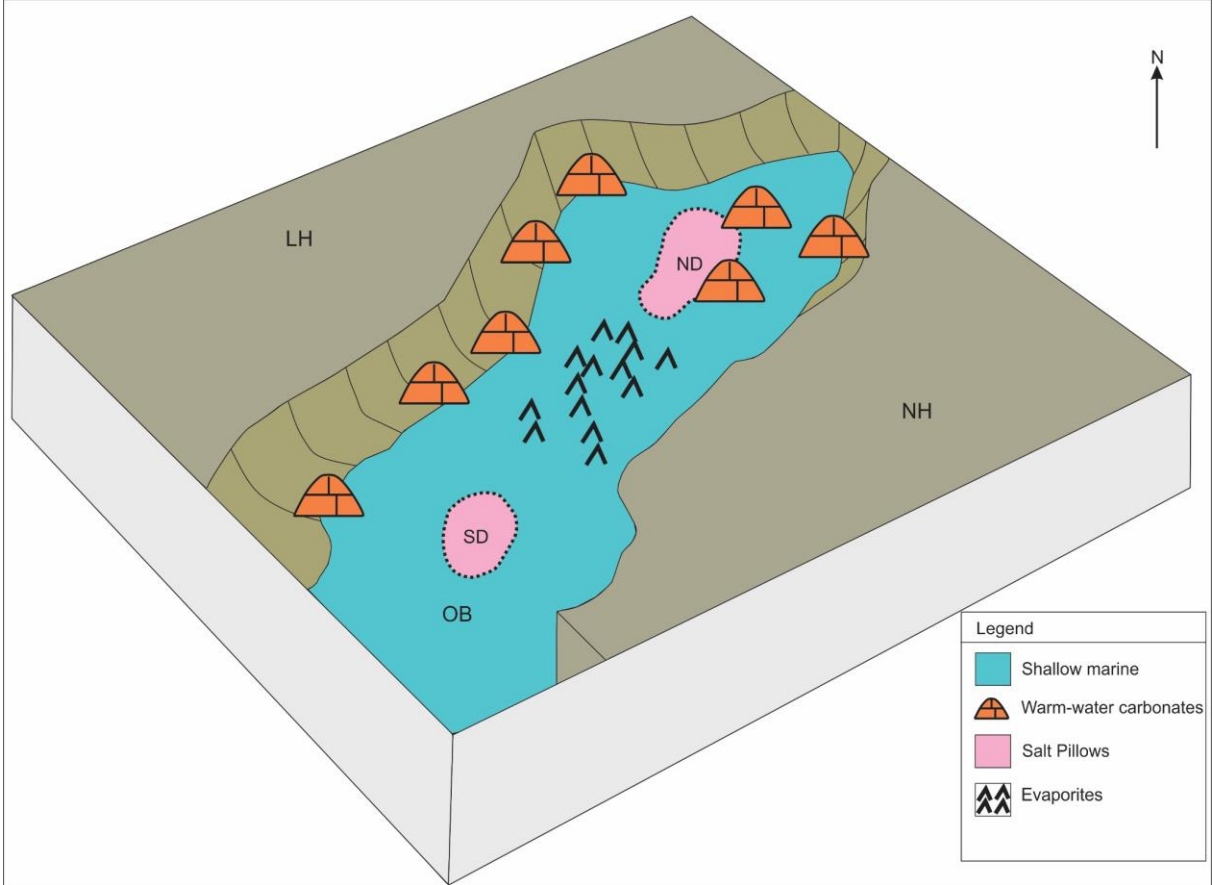


Figure 5.2. Proposed depositional model for the Gipsdalen Group. According to Breivik et al. (1995), there were two large evaporite depocenters, the largest named Norvarg Dome (ND) and a smaller in the south called the Samson Dome (SD), signified by the dotted-lines.



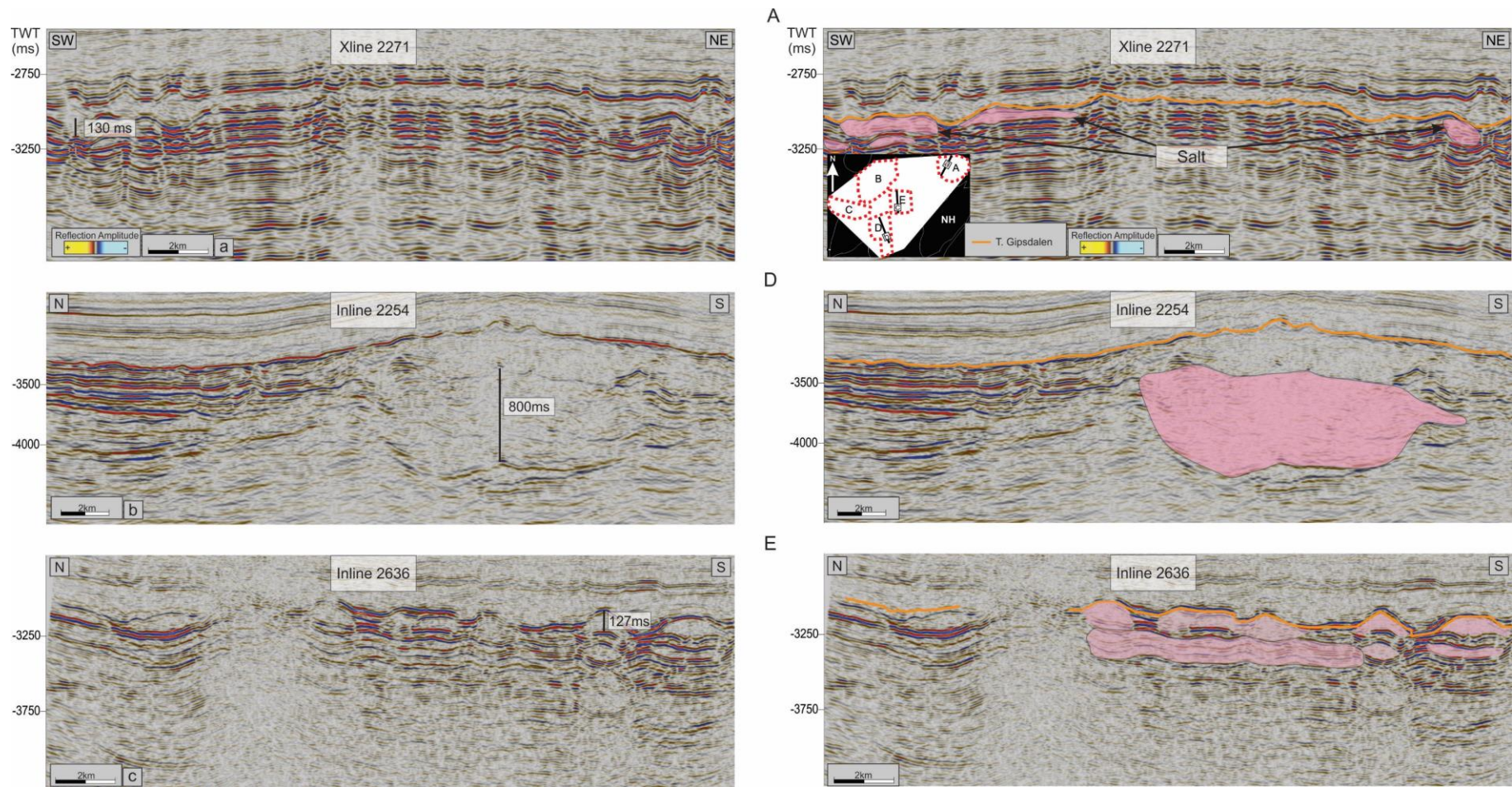


Figure 5.3: The Top Gipsdalen horizon in a north-south trend through the study area. A) Seismic line in close proximity to the Norvarg Dome, displaying an interpreted salt deposition B) seismic line covering the Samson Dome displaying the large evaporite body. C) seismic section from the central parts of the study area. The legend displayed in a) is valid for all seismic sections. A, D & E signifies the location of the seismic sections within the study area.

### 5.1.3 Bjarmeland Group

The Bjarmeland Group is of Early Permian (Sakmarian – Artinskian) age (see section 2.2.1 Paleozoic). The reflection configuration is parallel to sub-parallel, semi-continuous to discontinuous with a low- to medium amplitude. Locally the reflections have a wavy configuration, in an overall semi-transparent pattern (Figure 4.17). The parallel configuration coupled with the low- to medium amplitude points toward uniform sedimentation conditions with the deposition of similar lithologies (Mitchum et al., 1977; Veeken, 2007b).

The thickness of the unit increases toward the southwest, with the thinnest concentration located in the northeast. The thickness distribution has been reversed from previously discussed units (Gipsdalen, Figure 4.13). The smallest amount of the Bjarmeland Group sediments were deposited in the northern part. This could be the result of smaller variations in subsidence. During the Late-Carboniferous a shift to more gentle subsidence took place, as the horst-graben tectonics slowed and gradually ceased (Smelror et al., 2009).

Larssen et al. (2005), Stemmerik and Worsley (2005), Colpaert et al. (2007), Rafaelsen et al. (2008) and Di Lucia et al. (2017) describe the Bjarmeland Group as a unit consisting of cool-water carbonates, which distinguishes them from the underlying warm-water carbonates of the Gipsdalen Group. The separation of the two groups are according to Rafaelsen et al. (2008), signified by an unconformity, which is not easily mapped in the surveys used in this thesis. The Bjarmeland and Gipsdalen Groups in the study area are largely unaffected by tectonics and other factors controlling the depositional geometry, and the Groups are observed to be conformable to one another. This could be due to their presence in a basinal setting, making it a possibility that the sediments were not influenced by the unconformity seen elsewhere in the greater Barents Sea (e.g. Rafaelsen et al. (2008)).

The Bjarmeland Group is interpreted as a unit containing a large homogenous deposition of cold water carbonates (Figure 5.4) (Stemmerik & Worsley, 2005; Rafaelsen et al., 2008; Worsley, 2008; Henriksen et al., 2011). Locally, the carbonates seem to be deposited on top of the underlying salt deposits and older buildups from the Gipsdalen Group (Figure

4.21, Figure 4.22 & Figure 5.4) (Rafaelsen et al., 2008; Mattos et al., 2016; Di Lucia et al., 2017).

High amplitudes are most prominent in the central parts of the study area, where they follow the pillow-shaped geometry of the base horizon in this area (Figure 4.19 E & Figure 4.20). The distinct pattern formed by the reflections could be a result of the density differences between the evaporites from the underlying Gipsdalen Group and the carbonates of the overlying Bjarmeland Group. This could result in the mobilization of the evaporites due to differential loading, which in turn could give rise to the pillow-shaped pattern of the reflections (Figure 4.20 D-E & Figure 5.3 C) (Badley, 1985; Ge et al., 1997; Luo et al., 2012). This thickening and thinning of the reflections below the base horizon and immediately above it along with the high amplitude could indicate an evaporite deposition located beneath the unit (Figure 5.3).

The high amplitudes appear in the apex of the elongated highs, indicating variations or changes in the deposited lithology (Figure 4.20). The amplitudes could be a result of the high velocity and density of the interpreted carbonates (Bubb & Hatlelid, 1978; Badley, 1985). The unit is also internally dominated by circular/polygonal features, with the highest concentration found in the western and central parts of the study area (Figure 4.21 B & E). These features are located on the elongated highs, which in plan-view could produce these circular features (Figure 4.21 B & E & Figure 4.22) (Stewart, 1999; Rafaelsen et al., 2008). The features are believed to indicate the presence of carbonate mounds.

The elongated features found in the north and southwest in the study area might represent paleo-caverns (Figure 4.21 A & C). They occur along the highs where sub-aerial exposure of the carbonates could have occurred, which could result in karst topography (Colpaert et al., 2007; Rafaelsen et al., 2008; Smelror et al., 2009; Henriksen et al., 2011; Ahlborn et al., 2014).

Another interpretation of the elongated features could be that they represent faults (Figure 4.21 A, C & Figure 4.22). The carbonate buildups of the Late Paleozoic seem to be controlled by the underlying tectonic elements (Hunt et al., 2003; Rafaelsen et al., 2008). This could describe why the features seem to limit the extent of the buildups. The faults

could have created zones with different subsidence resulting in areas where the water-level was too high for carbonate production to be sustained, thus haltering its distribution (Elvebakk et al., 2002). The elongated features could be a combination of the two alternatives as they are not similar in appearance and dimensions, thus creating the possibility for the features to represent both faults and paleo-caverns (Figure 4.21 & Figure 4.22).

Based on seismic investigations along with earlier conducted studies a depositional model is suggested (Figure 5.4). During the deposition of the Bjarmeland Group the area was transgressed, creating a favorable environment for the deposition of carbonates (Figure 5.4). The carbonates formed along the margins and on top of the previously deposited evaporites (Figure 5.4). In contrast to the previously deposited unit, carbonate deposition seemed to occur in the deeper parts of the basin as well as along the margins. This could be the result of the aforementioned transgression as well as the transition towards a colder climate, preventing evaporite precipitation (Figure 5.4).

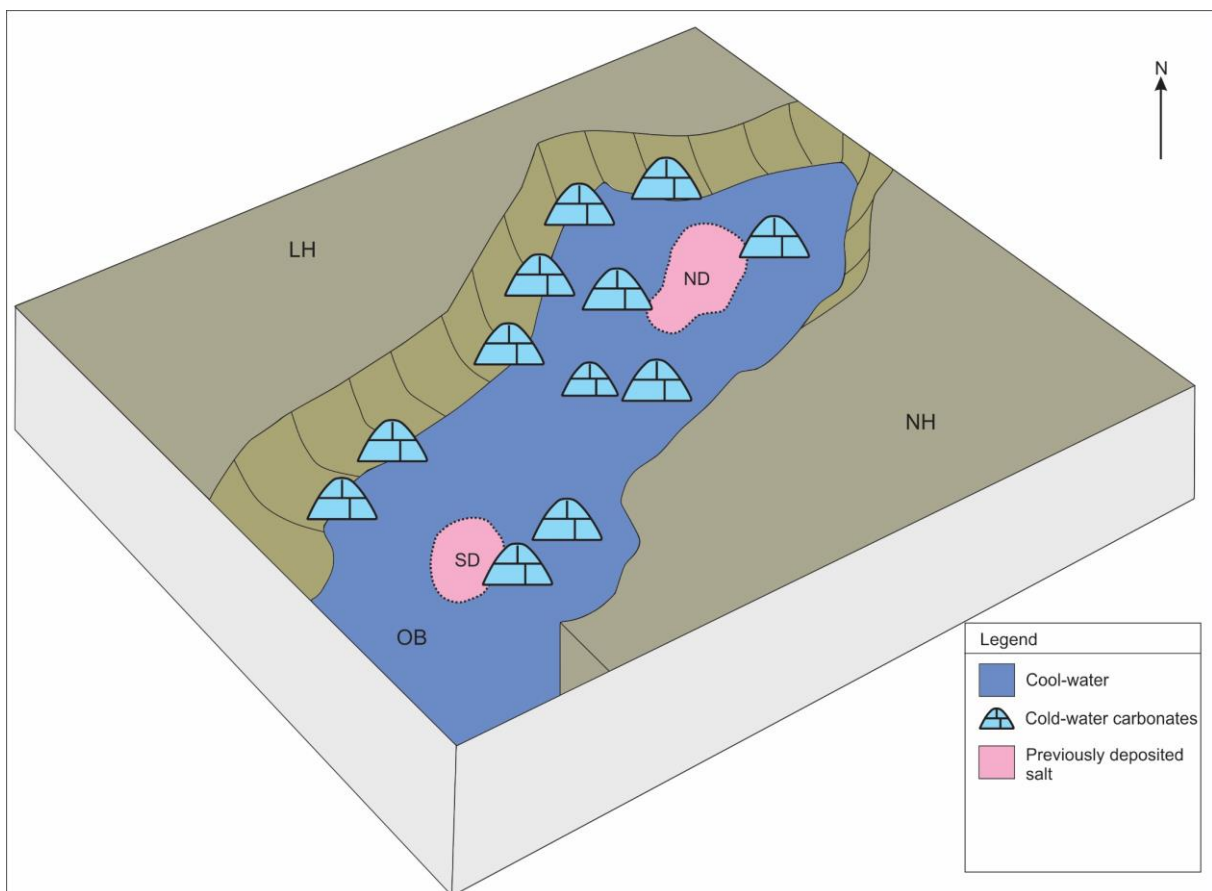


Figure 5.4: Proposed depositional model for the Bjarmeland Group in the Ottar basin. The dotted Samson – and Norvarg Dome marks their eventual position within the study area.



#### 5.1.4 Tempelfjorden Group

The Group is of Mid- to Late Permian age (see section 2.2.1 Paleozoic). This period marked the closing of the Uralian Sea. This led to an increase in subsidence in the SW Barents Sea during the deposition of the Group, which resulted in a flooding event separating the Tempelfjorden Group from the underlying Bjarmeland Group (Ehrenberg et al., 1998; Ehrenberg & Svånå, 2001; Larssen et al., 2005; Stemmerik & Worsley, 2005; Worsley, 2008; Smelror et al., 2009; Alves, 2016; Gernigon et al., 2018). This could be the reason for the abrupt facies change separating the two groups (Figure 4.17, Figure 4.25 & Figure 4.27). As the upwelling of cold nutrient-rich and silica-rich waters transpired on the shelf favoring a spiculite deposition, a difference in facies occurred. This marked a transition into a deeper marine environment, subsequently drowning the carbonates of the underlying Bjarmeland Group (Figure 5.5) (Mazzullo et al., 2009; Smelror et al., 2009).

The reflection configuration of the Group was classified as parallel to sub-parallel, continuous to semi-continuous with a low- to medium amplitude. Locally, it displays a wavy- to semi-transparent reflection configuration. The wavy configuration seems to follow the wavy pattern established by the previously deposited Bjarmeland Group (Figure 4.17). The parallel configuration coupled with the medium- to low-amplitude could indicate uniform sedimentation conditions, with the deposition of similar to homogenous lithologies (Mitchum et al., 1977; Veeken, 2007b).

The unit seems to have a rather uniform thickness, with a small increase in thickness towards the southwest (Figure 4.23). This could indicate a transition towards more stable depositional conditions.

High amplitudes observed in the western part of the study area seem to follow the wavy pattern in the seismic section, where they are located in the apex of the elongated highs, while the synforms are dominated by lower amplitudes (Figure 4.25 B & C).

Several circular features are observed in the unit but they are most noticeable in the western and central parts of the study area (Figure 4.26 B & E). These circular features are believed to be the elongated highs seen in plan-view (Figure 4.27). The elongated highs of the Tempelfjorden Group are located directly on top of the elongated highs of the underlying Bjarmeland Group. The Tempelfjorden Group is believed to consist of a

homogenous package of sediments deposited in a low-energy environment, hence the continuity of the reflectors. The sediments seem to be draped on top of the underlying Bjarmeland Group as they closely follow the underlying topography (Figure 5.5).

In the southwest, close to the Samson Dome, there seems to be some isolated elongated highs that are not located on top of the elongated highs of the underlying group (Figure 4.26 D & Figure 4.27 D). This could be isolated carbonate mounds as suggested by Alves (2016). The background for this interpretation is that the large salt pillow could create an environment where the water level was shallower than the surrounding areas on the SW Barents Shelf, making it possible for carbonate production to be sustained. This however contradicts the regional setting, as the continued northward movement of Pangea altered the depositional environment. The depositional environment transitioned from a carbonate platform towards an open marine favoring siliciclastic deposition (Figure 5.5) (Torsvik et al., 2002; Stemmerik & Worsley, 2005; Rafaelsen et al., 2008). Deep water spiculites were deposited in basins that were deepening due to the major plate re-organization and subsidence (Figure 4.23 & Figure 5.5) (Ehrenberg et al., 1998; Stemmerik, 2000; Ehrenberg & Svånå, 2001; Samuelsen et al., 2003; Colpaert et al., 2007; Smelror et al., 2009; Matysik et al., 2018). Spiculites could also produce elongated highs, which supports the model suggested here that the isolated elongated highs most likely represent the deposition of spiculites (Figure 4.27 & Figure 5.5) (Colpaert et al., 2007; Henriksen et al., 2011).

The suggested depositional model is based on seismic investigations along with earlier conducted studies (Figure 5.5). The model displays how carbonate production ceased as a transgression occurred and subsequently drowned the carbonates of the Bjarmeland Group. Nutrient rich cold water flooded the shelf favoring spiculite deposition. The Tempelfjorden, consisting of fine-grained material and spiculites, was draped on top the underlying Bjarmeland Group (Figure 5.5).

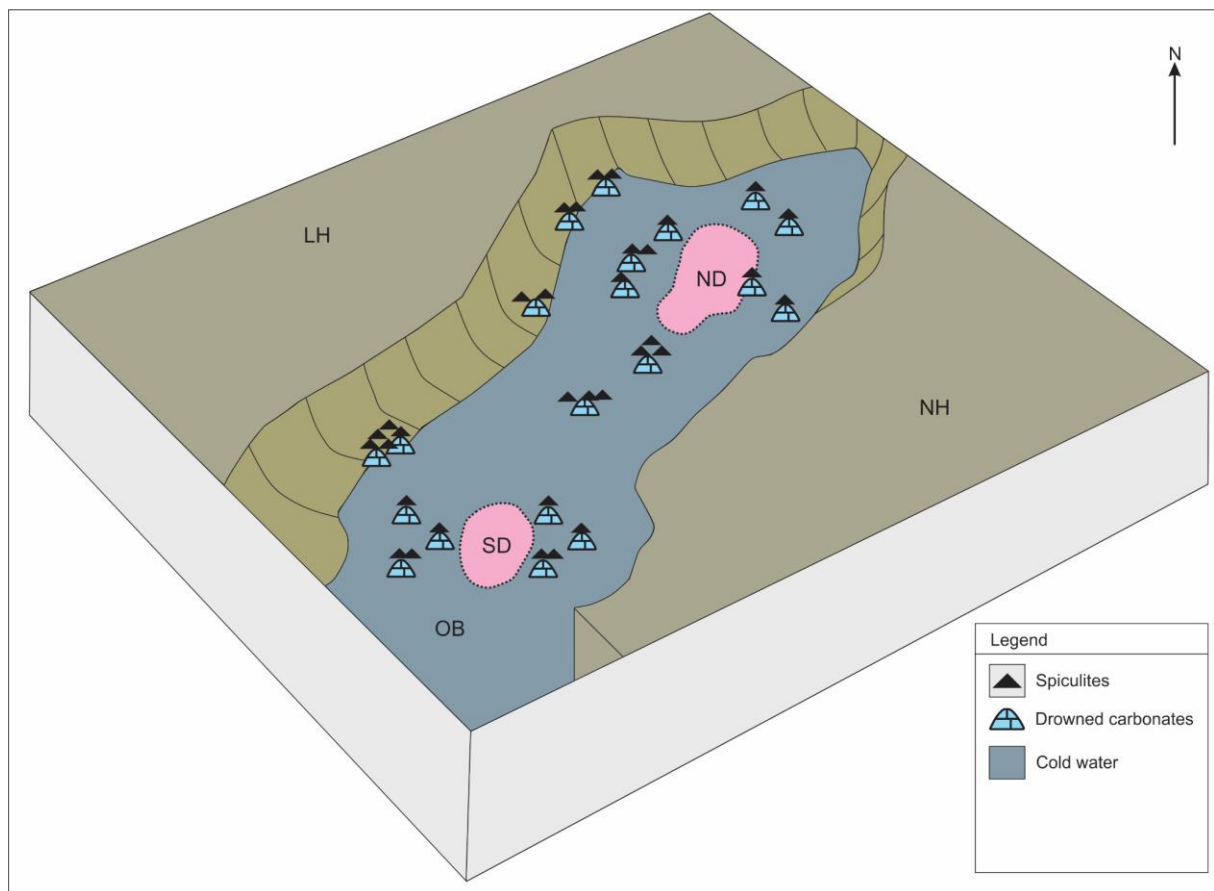


Figure 5.5: Proposed depositional model for the Tempelfjorden Group in the Ottar basin. SD = Samson Dome, ND = Norvarg Dome, the dotted lines signifies their eventual location.

### 5.1.5 Havert Formation

The Havert Formation is believed to be of Early Triassic age (Induan - Olenekian) (see section 2.2.2 Mesozoic). According to Dalland et al. (1988), Worsley (2008) and Riis et al. (2008), the Havert Formation consists mainly of shales, with minor interbedded siltstones and sandstone. The lithology changes and/or porosity changes may give rise to the limited areas of high-amplitudes (Figure 4.29 & Figure 4.30) (Colpaert et al., 2007). The unit also has a uniform distribution of frequency-intervals, which could indicate a homogenous lithology (Figure 4.31 & Figure 4.32). The aforementioned reflection configuration and the absence of a high-amplitude trend, indicate the deposition of a largely homogenous unit, supported by the uniform distribution of frequency-intervals (Figure 4.31 & Figure 4.32).

Continuous to semi-continuous, parallel to sub-parallel reflections of very low- to medium-amplitude characterize the Formation. Locally, the unit is influenced by normal faulting (Figure 4.17, Figure 4.30 & Figure 4.32). The Havert Formation shows an overall uniform sediment distribution across the study area, with a slightly thinning westward trend (Figure 4.28). At the Late Permian – Early Triassic transition, the study area was established as a stable platform area. This could explain the overall uniform thickness of the Havert Formation (Figure 4.28) (Breivik et al., 1995; Mattos et al., 2016)

The Early Triassic (Induan) was a tectonically quiet period for the greater part of the Barents Sea. However, some activity seemed to have occurred in the Loppa High and the western Bjarmeland Platform areas (Wood et al., 1989; Skjold et al., 1998; Smelror et al., 2009; Henriksen et al., 2011; Vadakkepuliambatta et al., 2013). The Loppa High seemed to have been uplifted and eroded during this period, creating a tectonic active region (Figure 4.32 & Figure 5.6) (Smelror et al., 2009; Henriksen et al., 2011). These movements could in the study area be represented by the faulting observed in the Havert Formation (Figure 4.30 & Figure 4.32).

The newly developed Uralian Mountains in the southeast is believed to be an important source area for the clastics deposited (Figure 4.28 & Figure 5.6) (Worsley, 2008; Glørstad-Clark et al., 2010; Clark et al., 2014; Faleide et al., 2015). The Induan also marked the



period of a maximum transgression creating an open-marine environment in the study area, with the potential for source rock accumulation (Figure 5.6) (Henriksen et al., 2011).

The suggested depositional model is based on seismic investigations along with earlier conducted studies (Figure 5.6). The Early Triassic signified the development of the stable Bjarmeland Platform. This resulted in the deposition of the Havert Formation with a rather uniform thickness, consisting of shales and sediments deposited from suspension (Figure 4.28). The environment transitioned towards open-marine with an increased water-level, due to the onset of a transgression (Figure 5.6).

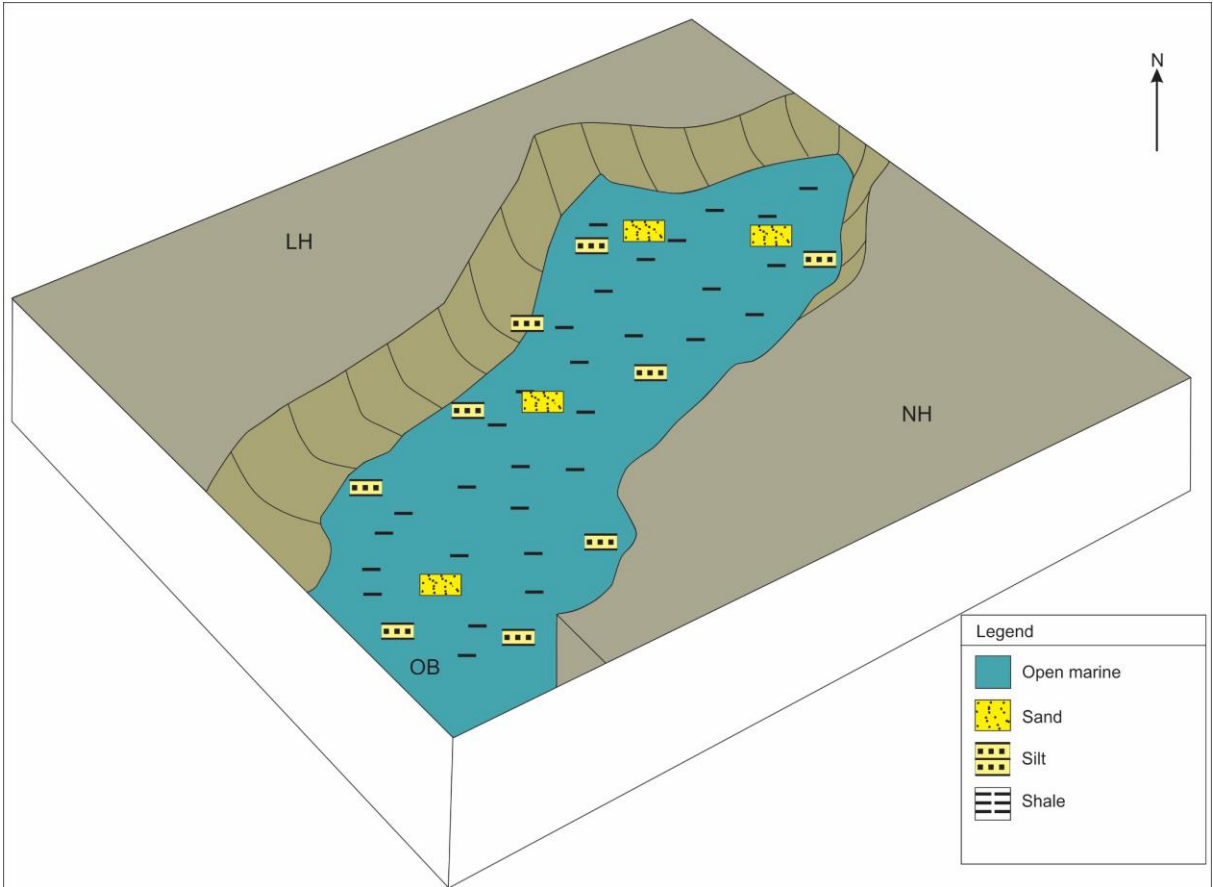


Figure 5.6: Proposed depositional model for the Havert Formation in the Otta basin.

## 5.2 The Samson & Norvarg Domes – Implications for tectonic movements

The study area comprises two different salt features. The Samson Dome located in the south, and the Norvarg Dome in the north.

Deposition of salt in the study area is suggested to have taken place in two periods: one in the Billefjorden Group of Late-Devonian age and during the Gipsdalen Group of Carboniferous – Early Permian age. The latter being the most likely to be represented as mobile salt observed today (Gabrielsen et al., 1990; Rowan & Lindsø, 2017).

Deposition of evaporites, are assumed to have taken place in rift basins such as the Nordkapp-, Ottar- and Maud Basins, while carbonate distribution occurred along the margins and the highs (Figure 5.2) (Gudlaugsson et al., 1998). The deposition of salt in these basins marked a transition from a rifting period and into a regime of thermal subsidence (Dengo & Røssland, 1992). By Late Permian, the evaporites were buried by a thick succession of the carbonate and siliciclastic deposition of the Bjarmeland and Tempelfjorden Group, and followed by the clastic Early Triassic deposits of the Havert Formation (Figure 4.18, Figure 4.23 & Figure 4.28) (Nilsen et al., 1995).

The amount of salt in the study area is substantial, calculated to have an average thickness of 2.4 km by Breivik et al. (1995), which makes it a major evaporite depositional center along with the Nordkapp Basin. The primary salt depocenter in the study area is the Norvarg Dome with the Samson Dome established as a smaller, yet a significant secondary depocenter (Breivik et al., 1995). These two features are discussed to be failed diapirs, and tend to be classified as salt pillows (Figure 5.3 B) (Gabrielsen et al., 1990; Rowan & Lindsø, 2017; Gernigon et al., 2018).

However, there is a distinct difference between the salt evolution in the study area and other large evaporite basins. The Nordkapp and Maud Basins (with the Svalis Dome) located to the east and west of the study area respectively, show large salt diapirs penetrating the overburden. In the study area, the interpreted evaporite succession is generally observed as flat, with the exception of the salt pillows of the Norvarg- and

Samson Domes (Figure 5.3 A & C) (Jensen & Sørensen, 1992; Breivik et al., 1995; Koyi et al., 1995; Nilsen et al., 1995; Rowan & Lindsø, 2017).

Different triggering mechanisms for the salt diapirs, have been proposed. Extension has been suggested as a triggering mechanism, both for the diapirs in the Nordkapp Basin, and for the Svalis Dome located in the Maud Basin. The Svalis Dome have most likely also been influenced by the uplift of Loppa High (Gabrielsen et al., 1990). However, according to Rowan and Lindsø (2017), there appears to be less evidence of extension after salt deposition in the Nordkapp Basin. They propose that progradational loading triggered subsidence which then allowed for the thinning of overlying strata by erosion, creating a possibility for the salt to break through the overburden. This is also consistent with the findings of Ge et al. (1997), who showed through a series of experiments that diapiric evolution could be a result of progradation without the influence of large-scale tectonics.

The Norvarg – and Samson Dome have many shared characteristics, both being lenticular in plan-view and have a conformable overburden of Permian deposits folded along with the top of the salt deposits (Figure 5.3 B) (Gabrielsen et al., 1990; Rowan & Lindsø, 2017; Gernigon et al., 2018). In addition, they also appear to share the same evolution, with movements in the Mid Triassic, which halted in the Late Triassic (Gabrielsen et al., 1990; Breivik et al., 1995; Mattos et al., 2016).

The regional tectonics seem to play an important role in the evolution of salt structures, which could indicate that the study area remained a more stable section while the areas located to the east and west underwent more tectonic activity. There seems to be less Mesozoic tectonic activity in the study area than in the surrounding basins. This can be seen from the deposition of the Havert Formation with a rather uniform thickness and the limited tectonic activity influence on the Paleozoic sediments (Figure 4.12, Figure 4.17 & Figure 4.28). The little Mesozoic tectonic activity could also be an explanation for the horizontal Paleozoic strata, overlying the two domes and their limited development (Figure 4.9, Figure 4.12, Figure 4.17 & Figure 5.3) (Breivik et al., 1995; Gernigon et al., 2014; Gernigon et al., 2018).

The sediment accumulation in the Ottar basin could, due to a more stable platform evolution, become thicker and more rigidly compacted than in the surrounding basins. This thick overburden created a rigid seal making it difficult for the salt to penetrate the formation thus halting diapir-evolution (Figure 5.3 & Figure 5.7) (Breivik et al., 1995). This could explain why the Permian strata overlying the Samson Dome follows the geometry of the underlying evaporite body (Figure 4.17 D, Figure 5.3 B & Figure 5.7). However, the difference in evolution could also be the result of a smaller accumulation of evaporites compared to the surrounding basins (e.g. Nordkapp Basin) (Gernigon et al., 2018).

The evolution of the Norvarg- and Samson Dome are probably a result of all the above-mentioned factors, and a different tectonic evolution compared to the Nordkapp Basin. Mattos et al. (2016) also proposed salt dissolution as an additional factor, leading to the Samson Dome collapsing under its own weight, causing the configuration seen today (Figure 5.3 B & Figure 5.7).



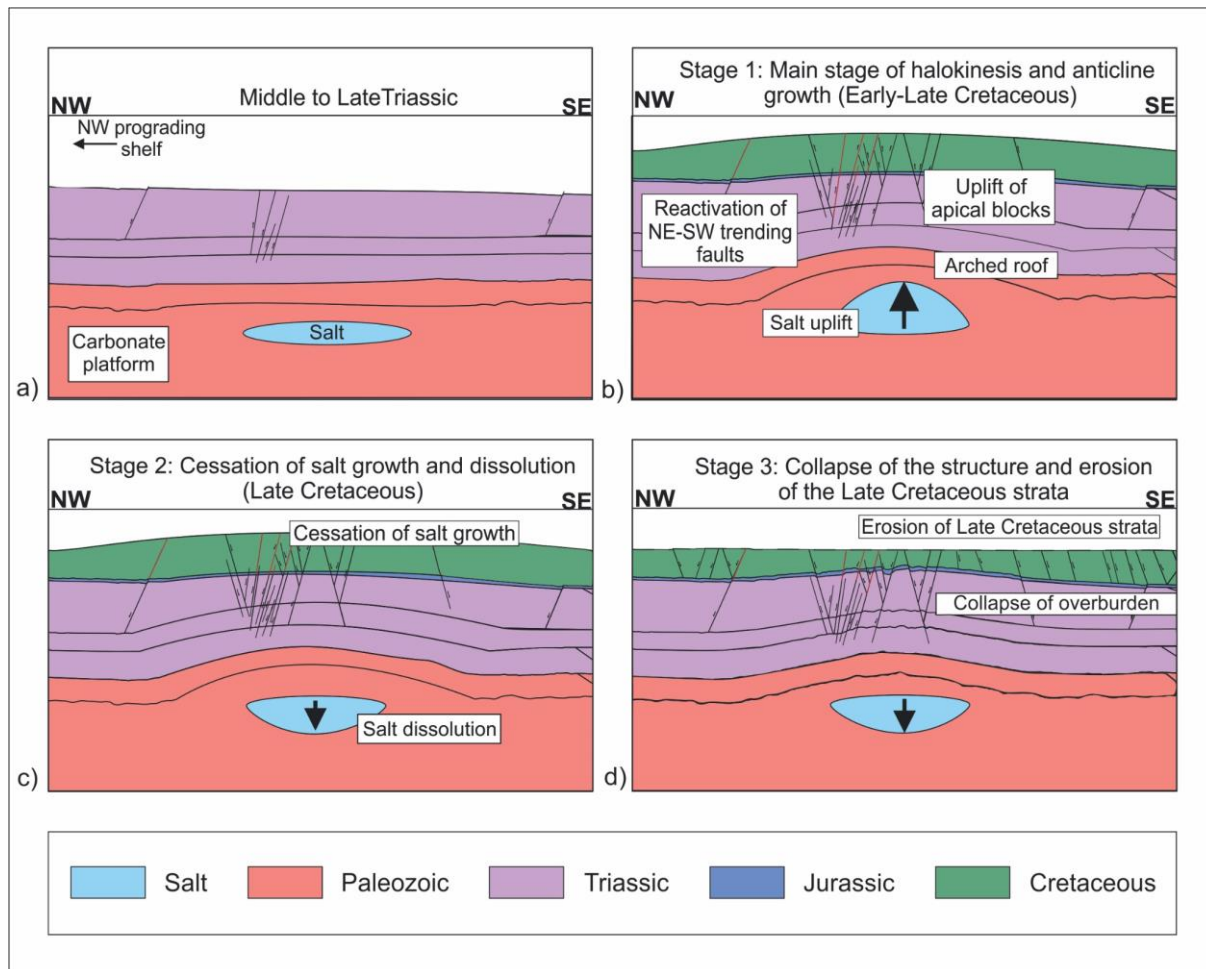


Figure 5.7: Proposed evolution of the Samson- and Norvarg Dome in the study area. Figure from Mattos et al. (2016).



## 6. Summary & Conclusion

The Paleozoic and Early-Triassic was studied in the Ottar basin by using multiple 3D seismic surveys and correlating to available wells. The focus was to map the depositional environments and processes in the Paleozoic. The Paleozoic covers an extensive time-period of marine regressions and transgressions, as well as various temperature and climate fluctuations. This has led to a transition from a lacustrine to an open marine depositional environment, and a change from siliciclastic deposition to carbonate and spiculite production, and eventually ending with the deposition of shale and suspension material from an open marine environment. The main findings of the study are:

- The Billefjorden Group (Late Devonian – Early Carboniferous) was deposited in a lacustrine environment characterized by rivers and alluvial fans prograding into a subsiding basin.
- The Gipsdalen Group (Mid Carboniferous – Early Permian) was deposited in a warm and arid climate dominated by cyclic deposition of evaporites and warm-water carbonates. Large evaporite bodies were deposited in the basinal areas of the Ottar basin, whereas carbonate production occurred along the margins.
- The Bjarmeland Group (Early Permian) signified a transition in temperature to a cooler environment and the onset of a marine regression. The sediments mainly consisted of cool-water carbonates. Carbonate production occurred along previously established carbonate buildups and evaporite bodies, along the margin as well as in the basinal areas.
- During deposition of the Tempelfjorden Group (Mid- to Late Permian), the water-level increased, while the temperature decreased further. This environmental shift favored siliciclastic deposition. Carbonate production ceased as the environmental shift favored spiculite deposition.
- At the end of the Paleozoic-era, a shift towards an open marine environment occurred. Sand, silt and shale of the Havert Formation (Early Triassic) was deposited in a low-energy setting. The period marked the formation of the stable Bjarmeland Platform.

- The Ottar basin is considered as a major evaporite basin similar in both size and evaporite quantity to the Nordkapp Basin, with two large evaporite depocenters named Norvarg- and Samson Dome.
- The absence of salt diapirs illustrate the different tectonic development of the study area compared to surrounding evaporite basins.
- The development of the Norvarg- and Samson Domes are characterized by a conformable overburden possibly haltering their evolution resulting in the development of salt pillows instead of diapirs.



## References

- Ahlborn, M., Stemmerik, L., & Kalstø, T.-K. (2014). 3D seismic analysis of karstified interbedded carbonates and evaporites, Lower Permian Gipsdalen Group, Loppa High, southwestern Barents Sea. *Marine and Petroleum Geology*, *56*, 16-33.
- Alves, T. M. (2016). Polygonal mounds in the Barents Sea reveal sustained organic productivity towards the P-T boundary. *Terra Nova*, *28*, 50-59.
- Badley, M. E. (1985). *Practical seismic interpretation*. Boston: International Human Resources Development Corporation (IHRDC).
- Bailey, W., Shannon, P. M., Walsh, J. J., & Unnithan, V. (2003). The spatial distributions of faults and deep sea carbonate mounds in the Porcupine Basin, offshore Ireland. *Marine and Petroleum Geology*, *20*, 509-522.
- Barrère, C., Ebbing, J., & Gernigon, L. (2009). Offshore prolongation of Caledonian structures and basement characterisation in the western Barents Sea from geophysical modelling. *Tectonophysics*, *470*, 71-88.
- Breivik, A., Gudlaugsson, S., & Faleide, J. (1995). Ottar Basin, SW Barents Sea: a major Upper Paleozoic rift basin containing large volumes of deeply buried salt. *Basin Res.*, *7*(4), 299-312. doi:10.1111/j.1365-2117.1995.tb00119.x
- Brown, A. R. (1999). *Interpretation of three-dimensional seismic data* (5th ed. ed. Vol. 42). Tulsa, Okla: American Association of Petroleum Geologists.
- Bubb, J. N., & Hatlelid, W. G. (1978). Seismic Stratigraphy and Global Changes of Sea Level, Part 10: Seismic Recognition of Carbonate Buildups. *The AAPG Bulletin*, *62*(5), 772-791.
- Bugge, T., Mangerud, G., Elvebakk, G., Mørk, A., Nilsson, I., Fanavoll, S., & Vigran, J. O. (1995). The Upper Paleozoic succession on the Finnmark Platform, Barents Sea. *Norsk Geologisk Tidsskrift*, *75*, 3-30.
- Bulat, J. (2005). Some considerations on the interpretation of seabed images based on commercial 3D seismic in the Faroe-Shetland Channel. *Basin Research*, *17*, 21-42.
- Catuneanu, O., Galloway, W. E., Christopher, K., Miall, A. D., Posamentier, H. W., Strasser, A., & Tucker, M. E. (2011). Sequence Stratigraphy: Methodology and Nomenclature. *Newsletter on Stratigraphy*, *44*/3, 173-245.

- Cavanagh, A. J., Di Primio, R., Scheck-Wenderoth, M., & Horsfield, B. (2006). Severity and timing of Cenozoic exhumation in the southwestern Barents Sea. *Journal of the Geological Society, London*, 163, 761-774.
- Cecchi, M. (1993). Carbonate sequence stratigraphy: application to the determination of play-models in the Upper Paleozoic succession of the Barents Sea, offshore northern Norway. *Norwegian Petroleum Society Special Publications*, 2, 419-438.
- Clark, S. A., Glorstad-Clark, E., Faleide, J. I., Schmid, D., Hartz, E. H., & Fjeldskaar, W. (2014). Southwest Barents Sea rift basin evolution: comparing results from backstripping and time-forward modeling. *Basin Research*, 26, 550-566.
- Colpaert, A., Pickard, N., Mienert, J., Henriksen, L. B., Rafaelsen, B., & Andreassen, K. (2007). 3D seismic analysis of an Upper Palaeozoic carbonate succession of the Eastern Finnmark Platform area, Norwegian Barents Sea. *Sedimentary Geology*, 197(1), 79-98. doi:<https://doi.org/10.1016/j.sedgeo.2006.09.001>
- Dalland, A., Worsley, D., & Ofstad, K. (1988). A lithostratigraphic scheme for the Mesozoic and Cenozoic succession offshore mid- and northern Norway. *NPD-Bulletin no 4*.
- Dengo, C. A., & Røssland, K. G. (1992). Extensional tectonic history of the western Barents Sea. *Norwegian Petroleum Society Special Publications*, 91-107.
- Di Lucia, M., Sayago, J., Frijia, G., Cotti, A., Sitta, A., & Mutti, M. (2017). Facies and seismic analysis of the Late Carboniferous - Early Permian Finnmark carbonate Platform (southern Norwegian Barents Sea): An assessment of the carbonate factories and depositional geometries. *Marine and Petroleum Geology*, 79, 372-393.
- Doré, A. G. (1995). Barents Sea Geology, Petroleum Resources and Commercial Potential. Retrieved from [http://www.jstor.org/stable/40511656?seq=1#page\\_scan\\_tab\\_contents](http://www.jstor.org/stable/40511656?seq=1#page_scan_tab_contents)
- Duran, E. R., Di Primio, R., Anka, Z., Stoddart, D., & Horsfield, B. (2013). 3D-basin modelling of the Hammerfest Basin (southwestern Barents Sea): A quantitative assesment of petroleum generation, migration and leakage. *Marine and Petroleum Geology*, 45, 281-303. doi:<https://doi.org/10.1016/j.marpetgeo.2013.04.023>
- Ehrenberg, S. N., Nielsen, E. B., Svånå, T. A., & Stemmerik, L. (1998). Depositional evolution of the Finnmark carbonate platform, Barents Sea: results from wells 7128/6-1 and 7128/4-1. *Norsk Geologisk Tidsskrift*, 78, 185-224.

- Ehrenberg, S. N., & Svånå, T. A. (2001). Use of spectral gamma-ray signature to interpret stratigraphic surfaces in carbonate strata: An example from the Finnmark carbonate platform (Carboniferous - Permian) Barents Sea. *AAPG Bulletin*, *85*(2), 295-308.
- Eldholm, O., Faleide, J. I., & Myhre, A. M. (1987). Continent-ocean transition at the western Barents Sea/Svalbard continental margin. *Geology*, *15*, 1118-1122. doi:[https://doi.org/10.1130/0091-7613\(1987\)15<1118:CTATWB>2.0.CO;2](https://doi.org/10.1130/0091-7613(1987)15<1118:CTATWB>2.0.CO;2)
- Elvebakk, G., Hunt, D., & Stemmerik, L. (2002). From isolated buildups to buildup mosaics: 3D seismic sheds new light on upper Carboniferous-Permian fault controlled carbonate buildups, Norwegian Barents Sea. *Sedimentary Geology*, *152*, 7-17.
- Faleide, J. I., Bjorlykke, K., & Gabrielsen, R. H. (2015). Geology of the Norwegian Continental Shelf. In K. Bjorlykke (Ed.), *Petroleum Geoscience* (pp. 603-637): Springer.
- Faleide, J. I., Gudlaugsson, S. T., Eldholm, O., Myhre, A. M., & Jackson, H. R. (1991). Deep Seismic Transects across the Sheared Western Barents Sea-Svalbard Continental-Margin. *Tectonophysics*, *189*(1-4), 73-89. doi:Doi 10.1016/0040-1951(91)90488-E
- Faleide, J. I., Gudlaugsson, S. T., & Jacquart, G. (1984). Evolution of the western Barents Sea. *Marine and Petroleum Geology*, *1*, 123-150.
- Faleide, J. I., Solheim, A., Fiedler, A., Hjelstuen, B. O., Andersen, E. S., & Vanneste, K. (1996). Late Cenozoic evolution of the western Barents Sea-Svalbard continental margin. *Global and Planetary Change*, *12*(1-4), 53-74.
- Faleide, J. I., Tsikalas, F., Breivik, A. J., Mjelde, R., Ritzman, O., Engen, Ø., . . . Eldholm, O. (2008). Structure and evolution of the continental margin off Norway and the Barents Sea. *Episodes*, *31*(1), 82-91.
- Faleide, J. I., Vågnes, E., & Gudlaugsson, S. T. (1993). Late Mesozoic-Cenozoic evolution of the south-western Barents Sea in a regional rift-shear tectonic setting. *Marine and Petroleum Geology*, *10*, 186-214.
- Fontaine, J. M., Cussey, R., Lacaze, J., Lanaud, R., & Yapaudjian, L. (1987). Seismic Interpretation of Carbonate Depositional Environments. *The AAPG Bulletin*, *71*(3), 281-297.

- Gabrielsen, R. H., Færseth, R. B., Jensen, L. N., Kalheim, J. E., & Riis, F. (1990). Structural Elements of the Norwegian continental shelf, Part 1: The Barents Sea Region. *NPD-Bulletin no 6*, 5-7.
- Ge, H., Jackson, M. P. A., & Venderville, B. C. (1997). Kinematics and Dynamics of Salt Tectonics Driven by Progradation. *AAPG Bulletin*, 81(3), 398-423.
- Gernigon, L., Brønner, M., Dumais, M., Gradmann, S., Grønlie, A., Nasuti, A., & Roberts, D. (2018). Basement inheritance and salt structures in the SE Barents Sea: Insights from new potential field data. *Journal of Geodynamics*, 1-61.
- Gernigon, L., Brønner, M., Roberts, D., Olesen, O., Nasuti, A., & Yamasaki, T. (2014). Crustal and basin evolution of the southwestern Barents Sea: From Caledonian orogeny to continental breakup. *Tectonics*, 33, 347-373.
- Glørstad-Clark, E., Faleide, J. I., Lundschie, B. A., & Nystuen, J. P. (2010). Triassic seismic sequence stratigraphy and paleogeography of the western Barents Sea area. *Marine and Petroleum Geology*, 27(7), 1448-1475.  
doi:10.1016/j.marpetgeo.2010.02.008
- Golonka, J., Bocharova, N. Y., Ford, D., Edrich, M. E., Bednarczyk, J., & Wildharber, J. (2003). Paleogeographic reconstructions and basins development of the Arctic. *Marine and Petroleum Geology*, 20(3), 211-248.  
doi:[https://doi.org/10.1016/S0264-8172\(03\)00043-6](https://doi.org/10.1016/S0264-8172(03)00043-6)
- Gudlaugsson, S. T., Faleide, J. I., Johansen, S. E., & Breivik, A. J. (1998). Late Paleozoic structural development of the South-western Barents Sea. *Marine and Petroleum Geology*, 15, 73-102.
- Henriksen, E., Ryseth, A. E., Larssen, G. B., Heide, T., Rønning, K., Sollid, K., & Stoupakova, A. V. (2011). Chapter 10 Tectonostratigraphy of the greater Barents Sea: implications for petroleum systems. *Geological Society, London, Memoirs*, 35(1), 163-195. doi:10.1144/m35.10
- Hunt, D., Elvebakk, G., Rafaelsen, B., Pajchel, J., Hogstad, K., Robak, H., & Randen, T. (2003). Palaeokarst recognition & 3D distribution - New insights from the Upper Paleozoic, Loppa High, Barents Sea. *EAGE 65th Conference & Exhibition*.
- Jensen, L. N., & Sørensen, K. (1992). Tectonic framework and halokinesis of the Nordkapp Basin, Barents Sea. *NPF Special Publication*, 1, 109-120.

- Koehl, J.-B. P., Bergh, S. G., Henningsen, T., & Faleide, J. I. (2018). Middle to Late Devonian - Carboniferous collapse basins on the Finnmark Platform and in the southwesternmost Nordkapp basin, SW Barents Sea. *Solid Earth*, 9, 341-372.
- Koyi, H., Talbot, C. J., & Tørudbakken, B. O. (1995). Salt Tectonics in the Northeastern Nordkapp Basin, SW Barents Sea. *AAPG Memoir*, 65, 437-447.
- Laberg, J. S., Andreassen, K., & Vorren, T. O. (2012). Late Cenozoic erosion of the high-latitude southwestern Barents Sea shelf revisited. *Geological Society of America Bulletin*, 124, 77-88.
- Larssen, G. B., Elvebakk, G., Henriksen, L. B., Kristensen, S. E., Nilsson, I., Samuelsen, T. J., . . . Worsley, D. (2005). Upper Palaeozoic lithostratigraphy of the southern part of the Norwegian Barents Sea. *NGU-Bulletin* 444, 3-45.
- Lawver, L. A., Gahagan, L. M., & Norton, I. (2011). Chapter 5 Palaeogeographic and tectonic evolution of the Arctic region during the Palaeozoic. *Geological Society, London, Memoirs*, 35(1), 61-77. doi:10.1144/m35.5
- Luo, G., Nikolinakou, M. A., Flemings, P. B., & Hudec, M. R. (2012). Geomechanical modeling of stresses adjacent to bodies: Part 1 - Uncoupled models. *AAPG Bulletin*, 96(1), 43-64.
- Mattos, N. H., Alves, T. M., & Osmonaya, K. O. (2016). Crestal fault geometries reveal late halokinesis and collapse of the Samson Dome, Northern Norway: Implications for petroleum systems in the Barents Sea. *Tectonophysics*, 690, 76-96.  
doi:<https://doi.org/10.1016/j.tecto.2016.04.043>
- Matysik, M., Stemmerik, L., Olaussen, S., & Brunstad, H. (2018). Diagenesis of spiculites and carbonates in a Permian temperate ramp succession - Tempelfjorden Group, Spitsbergen, Arctic Norway. *Sedimentology*, 65, 745-774.
- Mazzullo, S. J., Wilhite, B. W., & Woolsey, W. (2009). Rhythmic Carbonate Versus Spiculite Deposition in Mississippian Hydrocarbon Reservoirs in the Midcontinent USA: Causative Factors and Resulting Reservoir Petrophysical Attributes. *AAPG Annual Convention*.
- Mitchum, R. M., Vail, P. R., & Sangree, J. B. (1977). Seismic Stratigraphy and Global Changes of Sea Level: Part 6. Stratigraphic Interpretation of Seismic Reflection Patterns in Depositional Sequences. In C. E. Payton (Ed.), *Seismic Stratigraphy - Applications to Hydrocarbon Exploration* (Vol. 26, pp. 117-133): American Association of Petroleum Geologists.



- Myhre, A. M., & Eldholm, O. (1988). The Western Svalbard Margin (74-80 N). *Marine and Petroleum Geology*, 5, 134-156.
- Nichols, G. (2009). *Sedimentology and stratigraphy* (2nd ed. ed.). Chichester: Wiley-Blackwell.
- Nilsen, K. T., Hendriksen, E., & Larssen, G. B. (1993). Exploration of the Late Paleozoic carbonates in the southern Barents Sea - a seismic stratigraphic study. *Norwegian Petroleum Society Special Publications*, 2, 393-403.
- Nilsen, K. T., Vendeville, B. C., & Johansen, J. T. (1995). Influence of Regional Tectonics on Halokinesis in the Nordkapp Basin, Barents Sea. *AAPG Memoir*, 65, 413-436.
- NPDfactpages. Wellbore 7124/3-1. Retrieved from <http://factpages.npd.no/FactPages/Default.aspx?nav1=wellbore&nav2=PageView|Exploration|All&nav3=1066>
- NPDfactpages. Wellbore 7226/11-1. Retrieved from <http://factpages.npd.no/FactPages/Default.aspx?nav1=wellbore&nav2=PageView|Exploration|All&nav3=1177>
- NPDfactpages. (2014). The 2014 NPD lithostratigraphic charts. Retrieved from <http://www.npd.no/en/Topics/Geology/Lithostratigraphy/>
- Nøttvedt, A., Cecchi, M., Gjelberg, J. G., Kristensen, S. E., Lønøy, A., Rasmussen, A., . . . van Veen, P. M. (1990). Svalbard-Barents Sea correlation: a short review. In T. O. Vorren, E. Bergsager, Ø. A. Dahl-Stammes, E. Holter, B. Johansen, E. Lie, & T. B. Lund (Eds.), *Arctic Geology and Petroleum Potential* (pp. 363-376). Tromsø: Elsevier.
- Ostanin, I., Anka, Z., Di Primio, R., & Bernal, A. (2013). Hydrocarbon plumbing systems above the Snøhvit gas field: Structural control and implications for thermogenic methane leakage in the Hammerfest Basin, SW Barents Sea. *Marine and Petroleum Geology*, 43, 127-146.  
doi:<https://doi.org/10.1016/j.marpetgeo.2013.02.012>
- Rafaelsen, B., Elvebakk, G., Andreassen, K., Stemmerik, L., Colpaert, A., & Samuelsen, T. J. (2008). From detached to attached carbonate buildup complexes — 3D seismic data from the upper Palaeozoic, Finnmark Platform, southwestern Barents Sea. *Sedimentary Geology*, 206(1), 17-32.  
doi:<https://doi.org/10.1016/j.sedgeo.2008.03.001>

- Riis, F., Lundschieen, B. A., Høy, T., Mørk, A., & Mørk, M. B. E. (2008). Evolution of the Triassic shelf in the northern Barents Sea region. *Polar Research*, 27, 318-338.
- Rowan, M. G., & Lindsø, S. (2017). Salt Tectonics of the Norwegian Barents Sea and Northeast Greenland Shelf Permo-Triassic Salt Provinces of Europe, North Africa and the Atlantic Margins (pp. 265-284): Elsevier.
- Rønnevik, H., Beskow, B., & Jacobsen, H. P. (1982). Structural and stratigraphic evolution of the Barents Sea. *Canadian Society of Petroleum Geologists Memoir*, 8, 431-440.
- Samuelsberg, T. J., Elvebakk, G., & Stemmerik, L. (2003). Late Palaeozoic evolution of the Finnmark Platform, southern Norwegian Barents Sea. *Norsk Geologisk Tidsskrift*, 83(4), 351-362.
- Sangree, J. B., & Widmier, J. M. (1978). Seismic Stratigraphy and Global Changes of Sea Level, Part 9: Seismic Interpretation of Clastic Depositional Facies. *The AAPG Bulletin*, 62(5), 725-771.
- Sayago, J., Di Lucia, M., Mutti, M., Cotti, A., Sitta, A., Broberg, K., . . . Zimina, O. (2012). Characterization of a deeply buried paleokarst terrain the Loppa High using core data and multiattribute seismic facies classification. *AAPG Bulletin*, 96(10), 1843-1866.
- Schlumberger. (2010). Petrel Attribute Matrix 2010. *Interpreter's Guide to Seismic Attributes*.
- Sheriff, R. E. (1980). *Seismic stratigraphy*. Boston: International Human Resources Development Corp.
- Sheriff, R. E. (1985). Aspects of Seismic Resolution: Chapter 1 *Seismic Stratigraphy II: An Integrated Approach to Hydrocarbon Exploration* (pp. 1-10): AAPG.
- Sheriff, R. E. (2006). *Encyclopedic Dictionary of Exploration Geophysics* (5th ed.). Tulsa: Society of Exploration Geophysicists.
- Siedlecka, A., Roberts, D., Nystuen, J. P., & Olovyanishnikov, V. G. (2004). Northeastern and northwestern margins of Baltica in Neoproterozoic time: evidence from the Timanian and Caledonian Orogens. *Geological Society, London, Memoirs*, 30(1), 169-190. doi:10.1144/gsl.mem.2004.030.01.15
- Skjold, L. J., van Veen, P. M., Kristensen, S. E., & Rasmussen, A. R. (1998). Triassic sequence stratigraphy of the Southwestern Barents Sea. *SEPM Special Publication*, 60, 651-666.

- Smelror, M., Petrov, O. V., Larssen, G. B., & Werner, S. C. (2009). *Geological History of the Barents Sea*. Trondheim: Geological Survey of Norway.
- Stemmerik, L. (2000). Late Palaeozoic evolution of the North Atlantic margin of Pangea. *Palaeogeography, Palaeoclimatology, Palaeoecology*, 161(1-2), 95-126.
- Stemmerik, L., & Worsley, D. (2005). 30 years on - Arctic Upper Paleozoic stratigraphy, depositional evolution and hydrocarbon prospectivity. *Norwegian Journal of Geology*, 85, 151-168.
- Stewart, S. A. (1999). Seismic interpretation of circular geological structures. *Petroleum Geoscience*, 5, 273-285.
- Torsvik, T. H., Carlos, D., Mosar, J., Cocks, L. R. M., & Malme, T. (2002). Global reconstructions and North Atlantic paleogeography 440 Ma to recent. *BATLAS–Mid Norway plate reconstruction atlas with global and Atlantic perspectives*. Geological Survey of Norway, Trondheim, 18-39.
- Vadakkepuliymbatta, S., Bünz, S., Mienert, J., & Chand, S. (2013). Distribution of subsurface fluid-flow systems in the SW Barents Sea. *Marine and Petroleum Geology*, 43, 208-221.
- Vail, P. R. (1987). Seismic Stratigraphy Interpretation Using Sequence Stratigraphy: Part 1: Seismic Stratigraphy Interpretation Procedure. In A. W. Bally (Ed.), *Atlas of Seismic Stratigraphy* (Vol. 1, pp. 1-10): AAPG Studies in Geology No. 27.
- Veeken, P. P. (2007a). The Seismic Reflection Method and Some of Its Constraints. In K. Helbig & S. Treitel (Eds.), *Seismic Stratigraphy, Basin Analysis and Reservoir Characterisation* (Vol. 37). Oxford: Elsevier.
- Veeken, P. P. (2007b). Seismic Stratigraphy, basin analysis and reservoir characterisation *Handbook in Seismic Exploration* (pp. 111-141, 229-234, 254-263, 268-279): Elsevier.
- Veeken, P. P., & van Moerkerken, B. (2013). *Seismic Stratigraphy and Depositional Facies Models*. Burlington: Elsevier Science.
- Vorren, T. O., Richardsen, G., Knutsen, S. M., & Henriksen, E. (1991). Cenozoic erosion and sedimentation in the western Barents Sea. *Marine and Petroleum Geology*, 8, 317-340.
- Wood, R. J., Edrich, S. P., & Hutchison, I. (1989). Influence of North Atlantic tectonics on the large-scale uplift of the Stappen High and Loppa High, Western Barents Shelf

*Extensional Tectonics and Stratigraphy of the North Atlantic Margins* (pp. 559-566): AAPG.

Worsley, D. (2008). The post-Caledonian development of Svalbard and the western Barents Sea. *Polar Research*, 27(3), 298-317.